Biaxial Mechanical Evaluation of Uterosacral and Cardinal Ligaments

Adwoa Baah-Dwomoh

Dissertation submitted to the Faculty of
Virginia Polytechnic Institute and State University
in partial fulfillment of the requirements for the degree of

Doctor of Philosophy
in
Materials Science and Engineering

Raffaella De Vita, co-Chair
Rafael V. Davalos, co-Chair
Abby R. Whittington
William T. Reynolds

January 25, 2018
Blacksburg, Virginia

Keywords: Uterosacral Ligament, Cardinal Ligament, Viscoelasticity, Creep, Histology, Collagen, Smooth Muscle, Elastin

Biomechanical and Structural Analysis of Swine Uterosacral and Cardinal Ligaments

Adwoa Baah-Dwomoh

ABSTRACT

The uterosacral ligament (USL) and the cardinal ligament (CL) are two major suspensory tissues that provide structural support to the vagina/cervix/uterus complex. These ligaments have been studied mainly due for their role in the surgical repair for pelvic organ prolapse (POP). Despite their important mechanical function, little is known about the elastic and viscoelastic properties of the USL and CL due to ethical concerns with *in vivo* testing of human tissues and the lack of accepted animal models.

To help establish an appropriate animal model, the first rigorous comparison of histological and planar equi-biaxial mechanical properties of the swine and human USLs was completed. Relative collagen, smooth muscle, and elastin contents were quantified from histological sections and the USL was found to have similar components in both species, with a comparable relative collagen content. Using the digital image correlation (DIC) method to calculate the in-plane Lagrangian strain, no differences in the peak strain during preconditioning/cyclic loading tests, secant modulus of the pre-creep/elastic response, and strain at the end of creep tests were detected in the USLs from the two species along both axial loading directions (the main *in vivo* loading direction and the direction that is perpendicular to it).

Because these ligaments are subjected to repeated constant loads *in vivo*, the effect of repeated biaxial loads at three different load levels (1 N, 2 N, or 3 N) on elastic and creep properties of the swine CL was investigated. The results showed that CL was elastically anisotropic, as statistical differences were found between the mean strains along the two axial loading directions for specimens at all three different load levels. The increase in strain over time by the end of the 3rd creep test was comparable along the axial loading directions. The greatest mean normalized strain (or, equivalently, the largest increase in strain

over time) was measured at the end of the 1st creep test, regardless of the equi-biaxial load magnitude or loading direction.

Overall, these experimental findings validate the use of swine as an appropriate animal model and offer new knowledge of the mechanical properties of the USL and CL that can guide the development of better treatment methods such as surgical reconstruction for POP.

Biomechanical and Structural Analysis of Swine Uterosacral and Cardinal Ligaments

Adwoa Baah-Dwomoh

GENERAL AUDIENCE ABSTRACT

The uterosacral ligament (USL) and the cardinal ligament (CL) are two major suspensory tissues that provide structural support to the vagina/cervix/uterus complex. These ligaments have been studied mainly due for their role in the surgical repair for pelvic organ prolapse (POP). POP, which is the descent of a pelvic organ from its normal place towards the vaginal walls and into the vaginal cavity, affects an estimated 3.3 million women in the United States annually. Despite their important mechanical function, little is known about the elastic and viscoelastic properties of the USL and CL due to ethical concerns with *in vivo* testing of human tissues and the lack of accepted animal models.

The goal of this first study is to help establish an appropriate animal model for studying the mechanics of these pelvic supportive ligaments. To achieve this, the first rigorous comparison of histological and planar equi-biaxial mechanical properties of the swine and human USLs was completed. Relative collagen, smooth muscle, and elastin contents were quantified from histological sections and the USL was found to have similar components in both species, with a comparable relative collagen content. Using the digital image correlation (DIC) method to calculate the in-plane Lagrangian strain, no differences in the peak strain during preconditioning/cyclic loading tests, secant modulus of the pre-creep/elastic response, and strain at the end of creep tests were detected in the USLs from the two species along both axial loading directions (the main *in vivo* loading direction and the direction that is perpendicular to it).

Because these ligaments are subjected to repeated constant loads *in vivo*, the effect of repeated biaxial loads at three different load levels (1 N, 2 N, or 3 N) on elastic and creep properties of the swine CL was investigated. The results showed that CL was elastically

anisotropic, as statistical differences were found between the mean strains along the two axial loading directions for specimens at all three different load levels. The increase in strain over time by the end of the 3rd creep test was comparable along the axial loading directions. The greatest mean normalized strain (or, equivalently, the largest increase in strain over time) was measured at the end of the 1st creep test, regardless of the equi-biaxial load magnitude or loading direction.

Overall, these experimental findings validate the use of swine as an appropriate animal model and offer new knowledge of the mechanical properties of the USL and CL that can guide the development of better treatment methods such as surgical reconstruction for POP.

Dedication

To my parents, Joseph and Georgina Baah-Dwomoh, who instilled in me an amazing work ethic, constantly supported me, and loved me unconditionally. I love you both so much and would do anything for you.

To my siblings, Akosua, Sista Akos, Kwabena, and Kya. Thank you for always supporting me, visiting me whenever I needed to be around my loved ones, for making me laugh, and for always believing in me. I couldn't ask for better people in my life.

Last but certainly not least, to my Benjamin. I literally could not have done this degree without you. Thank you for being here from day 1. Thank you for giving me constant encouragement, love, and support and for always believing in me even in the times that I didn't believe in myself. Words can not express my gratitude to you or how important and how much of a blessing you have been to me in my life.

Acknowledgments

First and foremost, I would like to express my sincere appreciation and gratitude to my advisor, Dr. Raffaella De Vita. Thank you for welcoming me into your lab with open arms at a time when I was ready to quit. Thank you so much for your patience, constant encouragement, and persistence to help me complete this degree. I am also very grateful to my co-chair, Dr. Rafael Davalos for his continued support and guidance, not only during my graduate career but also beginning in my undergraduate studies. I would also like to thank my committee members Dr. Abby Whittington, Dr. William Reynolds, and Dr. Vincent Wang, for their continued support academically, professionally, and personally throughout my graduate education. Every single member of my graduate committee has been an influential part of my life and I would like to thank you for shaping me into the researcher I have become today.

I would like to thank all the members of the Soft Tissue Research: Experiments, Theory, and Computations by Hokies (STRETCH) Lab, particularly Jeffery McGuire, Ting Tan, and Alyssa Huntington. You all were instrumental in helping me complete these projects and I thank you all for all the suggestions, help with statistics, and friendship in the lab. I would also like to thank my other lab group, the BioElectroMechanical Systems (BEMS) lab for all of their help and suggestions throughout my graduate career.

Thank you to Dr. Catherine Amelink, who helped me create and run the VT Early Engineering Mentoring (VTEEM) program. It has been an immense pleasure and joy working with you these past few years and thank you for always being my advocate, an amazing mentor, and friend during my time here.

Thank you to Dr. Alex Aning, or "Uncle Alex" as I fondly call him. Thank you for introducing me to MSE while I was in middle school, and always being super supportive throughout all aspects of my life. You have been an amazing advocate, supporter, teacher, and friend.

Funding Acknowledgements

Funding was provided by NSF CAREER Grant No. 1150397 and VT Biotrans (formally VT MultiSTEPS).

Contents

List of Figures

List of Tables

1 Introduction

1.1 Motivation & Aims

Pelvic floor disorders (PFDs) such as urinary incontinence, fecal incontinence, and pelvic organ prolapse pose a significant health concern as well as a decrease in the quality of life to many women. Age, obesity, and parity have all been cited as factors in the development of PFDs [1–3]. In a recent study of the prevalence and trends of PFDs in women in the United states between 2005-2010, researchers found that 25% of women in the US (approximately 28.1 million) experienced one or more PFD, and this number is projected to increase from 28.1 million to 43.8 million in 2050 [4,5]. Pelvic organ prolapse (POP), the descent of a pelvic organ from its normal place towards the vaginal walls and into the vaginal cavity, affects an estimated 3.3 million women in the United States annually [6]. It is estimated that 1 in 4 women has an increased chance of experiencing POP in her lifetime, with that number increasing to 1 in 2 for women who have given birth vaginally one or more times [7].

For mild forms of POP, traditional treatment methods range from dietary or exercises such as Kegels. For more severe forms, surgical approaches, may be used which use either autologous tissue or the insertion of a synthetic mesh or even a radical hysterectomy. The high uterosacral ligament vaginal vault suspension (HUSLS) surgery, where the surgeon places three sutures through the uterosacral ligament (USL) to suspend the vaginal apex (Figure 1.1b), is an example of a repair method using autologous tissue [8, 9]. Although a commonly used technique, this surgery is not without its complications. A study conducted by Edenfield et al. that analyzed data of women who received the HUSLS surgery in the United States from December 1996 to January 2011 found that 25% of women experienced a recurrence of POP, with 15% of patients undergoing reoperations for recurrent POP [10].

In 2002, the FDA approved the first use of a mesh material to treat POP [11]. The total vaginal polypropylene mesh kit (TVM) is one of the most well-known mesh treatment options available today, being licensed by Gynecare. This transvaginal synthetic mesh is inserted without sutures around key vaginal complex ligaments, such as the uterosacral ligament (USL) (Figure 1.1c) [12]. However, several patients have experienced adverse side effects to the procedure, such as pain, mesh erosion, dyspareunia, and recurrence of urinary incontinence.

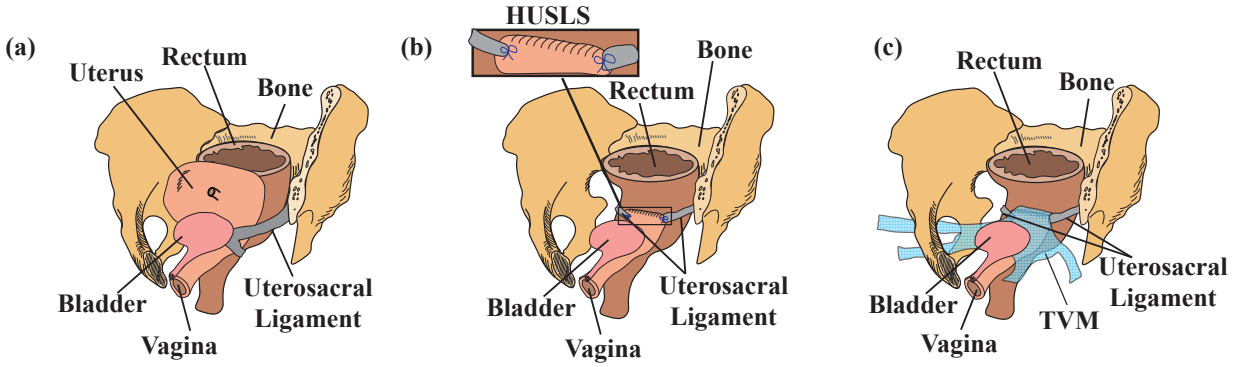

Figure 1.1: (a) Example of a normal female pelvic anatomy (b) Example of female pelvic anatomy after the high uterosacral ligament vaginal vault suspension (HUSLS) surgery. In this example, the uterus has been removed via hysterectomy. (c) Example of female pelvic anatomy after the insertion of the transvaginal mesh (TVM) In this example, the uterus has been removed via hysterectomy.

A comprehensive study by Maher et al., which collected data on surgical management of POP of approximately 6000 women, found that 14% of patients who received the TVM experienced some form of POP recurrence [13]. The study also found that 18% of patients who received the TVM experienced mesh erosion and 11% of patients underwent reoperation [13]. A more recent retrospective analysis of the TVM in 2016 found that 23% of patients had mesh exposure into the adjacent organs and through the vaginal epithelium, and that 16.2% of patients had a reoperation due to POP [14].

Most of these surgical techniques and mesh materials were developed without taking into account the structural and biomechanical properties of the tissues they interact with. Surgical meshes used for PFDs were developed initially to treat abdominal hernia repairs in the 1950's and, due to their success, in the 1970's gynecologists started using these meshes for

abdominal repair of POP [15]. Medical devices such as these meshes are cleared for use by the FDA through the 510k process [16]. Once a device is cleared, a modified device only has to be deemed substantially equivalent to a comparable device that is currently available [16]. This means that no clinical human trials are required for the new device and the manufacturer is not required to show success rates or adverse effects [17]. Due to this FDA approval procedure, surgical meshes for hernia repairs were used for the treatment of POP, causing significant complications. These complications are likely triggered by the mismatch in mechanical properties between the native tissue and the synthetic mesh material.

Studies have shown that structural changes and damage to pelvic supportive ligaments, such as the USL and the cardinal ligament (CL), contributes to the development of PFDs [1,18,19]. Further studies have also tried to elucidate the role of the different components of these tissues, such as smooth muscle cells within these ligaments [20–23]. The amount and organization of these different components of the tissues may vary the mechanical behavior of these ligaments. Therefore, it is essential to have a clear understanding and knowledge of the underlying structure. It is also imperative to understand if and how the biomechanical behavior of these pelvic supportive ligaments is affected by its structure. With this knowledge, researchers will have a better grasp on the pathogenesis of PFDs with regards to the pelvic ligaments' structure and mechanical behavior. When treating PFDs through surgery, researchers will be able to develop better surgical techniques and mesh materials by taking into account the structure and time-dependent behavior of these ligaments.

This dissertation aims to study the elastic and viscoelastic behavior of the USL and CL to aid in the creation of more robust surgical techniques and mesh materials for the treatment of PFDs. Specifically, the objectives of this dissertation are to:

- Characterize and quantify the structural components of the USL.
- Understand the elastic and viscoelastic behavior, specifically the creep behavior, of the USL.

- Establish swine as an appropriate animal model for studying the mechanical behavior of pelvic supportive ligaments.
- Study the effect of repeated biaxial loads on the creep properties of the CL.

1.2 Summary of Chapters

Chapter 2 covers the previously published work related to structural analysis and mechanical testing of pelvic supportive ligaments. An exploration of histological techniques used to characterize the USL and CL are presented. Mechanical characterization of these ligaments explores both *ex vivo* testing and *in vivo* testing of both human and chosen animal models. While some work has been done, it is clear that there are still gaps in the knowledge that need to be filled.

In chapter 3, a direct histological and biomechanical comparison of swine USL and human USL is presented. Both swine and human USL are stained using two different histological techniques, the Masson's trichrome (MT) protocol and the Verhoff van Geison (VVG) method to identify the components of the tissue. For mechanical testing, both swine and human USL are subjected to planar equi-biaixal cyclic loading tests to 2 N then subjected to planar equi-biaxial creep tests at 2 N. The results from this study indicate that swine and human USL contain a similar structural composition and comparable planar equi-biaxial cyclic, elastic, and creep properties. This study helps validate the use of swine as an appropriate animal model for mechanical characterization of the USL.

In chapter 4, the effect of repeated biaxial loads on the creep properties of the CL is presented. CL specimens are subjected to three consecutive planar equi-biaxial tests at different load levels (1 N, 2 N, and 3 N). Elastic properties of the CL are presented through pre-creep mean stress-strain data, showing that the CL exhibits anisotropic elastic behavior. Corresponding mean normalized strain vs. time (creep) data indicate that these CL specimens always creep the most during the first test, regardless of the load magnitude and direction.

2 Literature Review

2.1 Function and Structural Analysis of USL and CL

2.1.a Anatomical Relationship

The USL and CL are two visceral ligaments that connect the upper vagina/cervix to the sacrum and pelvic sidewall, respectively, and provide support to the vagina, cervix, and uterus [24]. The USL was first recognized in the early 1900's and was quickly identified as a major supportive structure of the uterus [25, 26]. By the 1950's, surgeons and scientists such as Campbell et al. noted that the USL is very useful for pelvic surgeries [27]. Described as fan shaped, the USL is connected distally to the CL and originates from the S2 to S4 sacral vertebrae, where it narrows to its smallest width just proximal to the cervix [24, 28]. The USL is typically 12-14 cm in length and is often divided into three regions: the distal region that is approximately 2-3 cm long and 5 cm wide, the intermediate region that is approximately 5 cm long and 2.7 cm wide, and the proximal portion which is approximately 5-6 cm long and 2 cm wide [24].

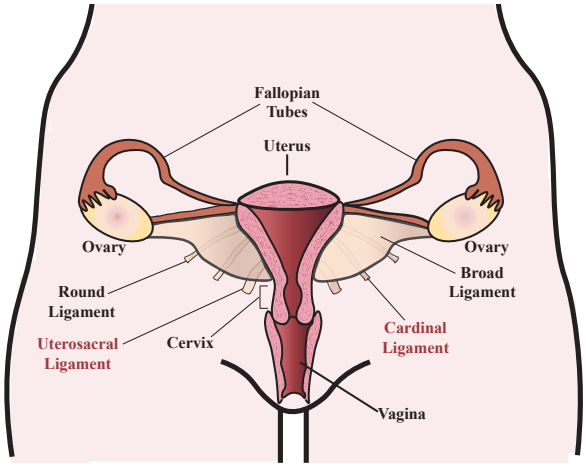

Figure 2.1: Female reproductive organs and supportive tissues

The CL was first identified in the late 1890's by Mackenrodt who described the CL as a transverse cervical ligament that is the chief supporting structure of the uterus [29]. By the 1960's, Range et al. conducted an anatomical analysis of the CL, finding that it is

mostly made of blood vessels, nerves, lymphatic vessels, and loose connective tissue with collagen and smooth muscle fiber bundles [30]. The CL is described as a perivascular sheath with a distal insertion at the cervix and laterally attaches the pelvic organs to the pelvic sidewalls [31]. With an approximate length of 10 cm, the CL is also typically divided into 3 regions: the distal region which is approximately 2.1 cm long and is attached laterally to the cervix, the intermediate section which is approximately 3.4 cm long, and the pelvic section which is approximately 4.6 cm and is attached to the pelvic sidewall [31]. The distal region of the CL forms the attachment point to the USL, which is why the two ligaments are often characterized together and termed the USL-CL complex [24, 31].

2.1.b Histology

Histological stains have been used to study the structure of the USL and CL. Campbell et al. were the first investigators to conduct histology on USL from female cadavers and observed that these ligaments were mainly comprised of smooth muscle bundles, blood vessels, nerve bundles, and connective tissue [27]. Campbell et al. also noted that composition varied along the different sections of the ligament. The distal region contained the majority of the smooth muscle found within the ligament and the intermediate and sacral regions were mostly comprised of connective tissue [27]. A much later histological study conducted by Cole et al. confirmed Campbell et al. analysis, finding that the USL in fresh cadavers was mostly comprised of poorly organized connective tissue, with few collagen fibers, elastin fibers, and smooth muscle in a disorganized condensed structure [32]. Range et al. were the first to conduct investigative histological studies on the CL and observed that blood vessels and loose areolar connective tissue made up the bulk of the CL, with the smooth muscle fibers mostly associated with these blood vessels [30]. The CL was also characterized as having loose areolar connective tissue, comprised of collagen and elastin fibers [30]. Kato et al. investigated nerve distribution in the CL by myelin staining and noted that the inferior hypogastric plexus, which is formed by sacral nerve roots that are joined by sympathetic fibers, forms a small plexus plate-like structure in the CL and extends into the USL [33].

Some studies have been conducted to quantify the the structural components of the USL and CL that have been identified through histology [34–39]. Butler-Manuel et al. quantified and compared the nerve content of USL and CL in women undergoing radical hysterectomy vs women undergoing a simple hysterectomy by measuring the percentage area of immunoreactivity [34]. Specimens from women who underwent a radical hysterectomy had a significantly higher nerve content in both the USL and CL compared to specimens from women who underwent a simple hysterectomy. For radical hysterectomy patients, the CL contained a lower nerve content than the USL, where the majority of the nerves were concentrated in large bundles [34]. In a later study, Butler-Manuel et al. also concluded that there was a higher percentage of nerve content in the deep USL compared to the superficial USL [35]. Gabriel et al. quantified the structural components of USL in women with and without POP [36]. The authors determined that the USL contained approximately 20% smooth muscle and that collagen III expression was significantly higher in women with POP [36]. While analyzing the extracellular matrix components of USL in relation to POP, Gabriel et al. discovered that women with POP had an increased expression of matrix metalloproteinase 2, which is an enzyme associated with the degradation of collagen and other extracellular matrix proteins [37]. In the CL, Ewies et al. explored the changes in extracellular matrix proteins of post-menopausal women with or without POP and saw a higher expression of collagen III and tenascin and lower expression of elastin in women with POP [38]. Upon further analysis, the authors noted that women with POP had higher levels of estrogen alpha, androgen, and progesterone receptors in the CL [39].

Studying animal models provide an alternative to studying human tissue, as tissues from animals are more readily available, can be obtained ethically, and can be cost efficient. While there have been some studies of the mechanical behavior of pelvic ligaments from animals, which will be discussed in a later section, very few histological studies have been conducted on animal pelvic supportive ligaments. Gruber et al. conducted an anatomical and histological study of the vagina and supportive ligaments of the swine in order to establish swine as an appropriate animal model for pelvic floor disorder evaluation and management [40]. Using

a 5 point scale to evaluate the presence of collagen, smooth muscle, and elastin, Gruber et al. determined that the swine vagina and the adjacent supportive structures, particularly the USL and CL, were similar in both composition and anatomy to that of human [40]. Tan et al. also performed histological analysis of swine USL and CL and discovered that the swine ligaments contain similar composition to that of human [41]. In an effort to directly compare animal models to human specimens, Iwanaga et al. compared the structural components of mouse and rat USL, CL, and round ligament (RL) to human USL, CL, and RL [42]. The authors confirmed that mice and rats have a similar composition and histological structure to human USL and RL, but noted that mouse USL and RL contained significantly more smooth muscle and less connective tissue compared to human and rat ligaments [42]. These studies strengthen the case for using animal models to study female human pelvic health. However, more analysis needs to be performed to confirm if these species are appropriate animal models to study women's pelvic health issues.

2.2 Mechanical Properties of Pelvic Supportive Ligaments

2.2.a *Ex Vivo* Tests

The mechanical properties of pelvic supportive ligaments have mainly been investigated *ex vivo* via uniaxial tensile tests [41, 43–49] and planar biaxial tests [50, 51]. Cosson et al. were the first to test the strength of pelvic ligaments, specifically the illiopectineal, sacrospinus and the arcus tendineus of pelvic fascia taken from female cadavers [43]. A suture was attached to each ligament and the force required to induce tearing of the tissue was recorded. Cosson et al. discovered that such force varied greatly, ranging between 20 N and 200 N [43]. The authors also noted variance in strength between individuals. Within the same individual, variances were noted between the type of ligament and the side of the body it resided, suggesting that a pre-operative strength evaluation of these ligaments should be conducted for each individual case [43]. Focusing on the USL, the broad ligament (BL), and the RL,

Rivaux et al. conducted a study to compare the biomechanics of these ligaments from female cadavers without POP [47]. All of the ligaments were found to be nonlinear elastic and their mean tensile strengths were measured to be 4 MPa for the USL, 1.5MPa for the BL, and 4.1 MPa for the RL [47]. Using the Mooney-Rivlin model parameters as a measure of elasticity, where C_0 represents mechanical behavior at small deformations and C_1 represents mechanical behavior at large deformations, the USL was the stiffest of all the ligaments at both small and large deformations, while the BL was determined to be the least stiff of the three ligaments [47]. The authors deduced that, due to the fact that the USL is the most rigid of the three ligaments, it provides the best option as an anchoring point for pelvic reconstructive surgery, and plays an important role in supporting pelvic organs [47].

Some studies have tried to investigate the effect of different factors on the biomechanical properties of pelvic support ligaments. A study conducted by Reay Jones et al. analyzed the effect of vaginal delivery, menopause, age, and uterine prolapse on uterosacral resilience from female hysterectomy patients [44]. Uterosacral resilience is defined as the area under the force vs displacement curve up until the plastic limit [44]. Reay Jones et al. determined that USL resilience was significantly reduced in patients that experienced symptomatic uterovaginal prolapse, at least one vaginal delivery, with menopause, and in older patients [44]. The authors concluded that the decrease in USL resilience may be a contributing factor to the development of symptomatic POP. Martins et al. investigated the tensile biomechanical properties of the USL and RL, taking into considerations certain factors such as age, parity, body mass index (BMI), and menopause [48]. The stiffness and maximum stress of these two ligaments were determined. The stiffness and the maximum stress of the RL did not vary significantly due to age, parity, BMI, or menopause [48]. For the USL, it was determined that parous women had a significantly higher stiffness (15.5 MPa vs. 10.0 MPa) and maximum stress (8.2 MPa vs 4.2 MPa) compared to nulliparous women [48]. However, no other significant differences were determined for the factors of age, BMI, or menopause for the USL [48]. When comparing the two ligaments, the USL was found to be significantly stiffer (14.1 MPa vs 9.1 MPa) and had a significantly higher maximum stress (6.3 MPa vs

4.3 MPa) than the RL [48]. The authors attributed the increased stiffness in the USL to parturition and speculate biomechanical alterations occur to the tissue after vaginal delivery so that the tissue can adapt to the higher mechanical loads acting on the tissue during childbirth [48]. Chantereau et al. performed a study to look at the influence of aging on the tensile properties of the USL, RL, and BL [49]. Using the Mooney-Rivlin model parameters C_0 and C_1 as a measure of elasticity, the authors discovered that the USL and RL were significantly stiffer for older patients than for young female cadavers at both small and large deformations [49]. However, no significant differences were determined for the BL between young and old patients. Chantereau et al. speculate that these pelvic ligaments may become naturally stiffer over time due to tissue remodeling [49]. The authors also concluded that, due to the ligaments becoming stiffer over time, they may no longer be able to stabilize the pelvic floor, giving rise to various pelvic floor disorders [49].

While studying human tissue would be most ideal, sample sizes tend to be small and due to ethical concerns, it is extremely hard to obtain the most optimal tissue for testing. Many of these tissues are obtained either from cadavers or from women who are undergoing pelvic surgeries such as a hysterectomy due to some pelvic disorder. Animal models provide a reasonable alternative to human subjects in this regard. Couri et al. conducted an extensive review of animal models for the study of female POP [52]. Using the rat as an animal model, Moalli et al. examined the structural and mechanical properties of the vagina and its supportive structures by pulling the vagina and measuring the failure of the vaginal wall and supportive ligaments as a complex [45]. The supportive ligaments failed at a lower elongation than the vagina, and the mean stiffness of the complex was found to be 2.9 N/mm and the mean energy absorbed at failure was found to be 49.4 J [45]. Vardy et al. studied the effect of hormone treatment on the mechanical properties of the USL and round ligaments in post-menopausal monkeys [46]. Each monkey had their ovaries removed (a procedure known as ovariectomy), and received no treatment for 12 months (OVX) or were exposed to conjugated equine estrogens plus continuous medroxyprogesterone acetate (CEE/MPA), or ethinyl estradiol plus norethindrone acetate (EE/NA) for 12 months [46]. Repeated step

stress-relaxation tests were first performed on these ligaments at strains ranging from 5% to 30%, and then specimens were pulled to failure. The tensile moduli were calculated from the pre-relaxation. For OVX monkeys, the mean failure stress and mean tensile modulus at 30% strain for the USL was reported to be 0.6 MPa and 0.75 MPa, respectively [46]. Significant differences in the tensile modulus of the USL were found between OVX, CEE/MPA, and EE/NA monkeys only at strains lower than 15%, with OVX monkeys having the lowest tensile modulus [46]. For the RL, the mean failure stress and mean tensile modulus at 30% strain was reported to be 2.1 MPa and 14 MPa, respectively [46]. Significant differences in the tensile modulus for the RL were reported between OVX, CEE/MPA, and EE/NA monkeys for strains greater than 12%, with OVX monkeys having the highest tensile modulus [46]. The two hormone treatments were selected to simulate hormones that are prevalent in pre-menopausal women. The increased stiffness of the hormone treated USL may be attributed to need for the USL to bear the increased mechanical load experienced on the body during pregnancy. Also during pregnancy, the RL increases in size to allow for the growing fetus, which may also explain why hormone treated specimens experienced lower stiffness than non hormone treated specimens. Overall, the authors concluded that hormonal status of a patient has an effect on pelvic support and draw a potential link between menopause and the occurrence of POP [46]. Vardy et al. also speculated that hormonal treatment after menopause may have a positive effect on pelvic supportive function [46].

Swine has shown to have similarities to humans in the histological and structural components of the USL and CL, as described in a previous section [40,41]. Tan et al. conducted structural characterization as well as uniaxial tensile testing of swine USL and CL. The USL exhibited a significantly higher mean ultimate tensile stress (2.767 MPa) compared to the left CL (2.767 MPa) and the right CL (1.278 MPa) [41]. A mean tangent modulus of 29.819 MPa was found for the USL and 3.449 MPa and 5.385 MPa for the left and right CLs, respectively [41]. Tan et al. also noted that these mechanical properties varied based on the location of the specimens relative to the uterus, cervix, vagina, and rectum.

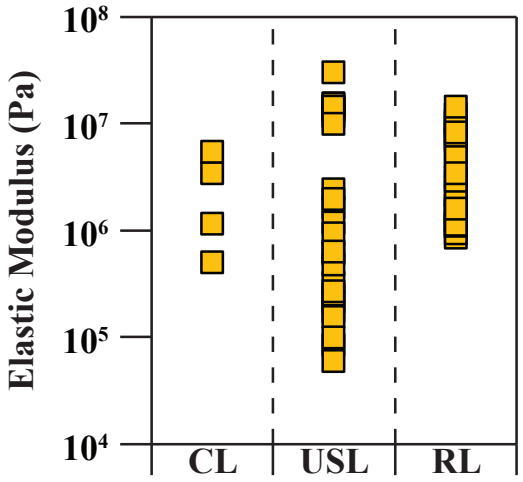

Figure 2.2: Comparison of mean values of the elastic moduli for the uterosacral ligament (USL) [41, 46, 48], cardinal ligament (CL) [41], and round ligament (RL) [46, 48] determined using uniaxial testing methods.

Figure 2.2 presents a summary of the range of elastic moduli data obtained from the literature, organized by the different pelvic supportive ligaments, specifically the CL, USL, RL. All of these elastic moduli have been calculated using data obtained from uniaxial tensile tests. No elastic moduli are reported for the BL in the literature. Since the elastic modulus was the most reported value, it was provided in order to compare these ligaments. The elastic moduli ranges were reported as 0.5 - 5.4 MPa for the CL, 0.75 - 29.8 MPa for the USL, and 9.1-14.0MPa for the RL.

Planar biaxial tests were performed both by Becker et al. [50] and Tan et al. [51] to study the viscoelastic behavior of the swine USL and CL. Specimens were loaded into a planar biaxial system with the axial loading directions selected to be the main *in vivo* loading direction and the directional perpendicular to the main *in vivo* loading direction. While studying the biaxial elastic behavior, it was observed that these ligaments undergo large deformations under biaxial load and are orthotropic [50]. When studying the viscoelastic behavior from the stress relaxation data, Becker et al. noted that these ligaments relaxed equally in both loading directions, with higher relaxation of the ligaments when they are stretched less [50]. Tan et al. performed planar biaxial creep tests on both the USL and CL at two different load levels, 2N and 4N [51]. Over a 120 min period, the mean strain increased by 20%-34% along the main *in vivo* loading direction and by 33%-41% along the perpendicular loading direction [51]. No statistical differences were found between the two loading directions for the 2N load or the 4N load [51]. However, it was noted that the higher applied equi-biaxial load produced lower creep [51].

2.2.b *In Vivo* Tests

While studying mechanical properties of biological tissues *ex vivo* provides a great deal of information, studying these tissues *in vivo* whenever possible is ideal. Very few studies have been conducted on the *in vivo* mechanical properties of the pelvic supportive ligaments. A study conducted by Smith et al. developed a system to measure the *in vivo* uterine suspensory ligament stiffness in women with normal uterine support to those suffering from POP [53]. Using a computer controlled linear servo-actuator, Smith et al. applied a tensile force to the cervix and the resulting displacement of the cervix and supportive ligaments was measured. The mean stiffness of the complex was reported to be 0.49 N/mm and no statistical differences were noted between women with normal uterine support and women who experienced different degrees of POP [53].

Similar to the Smith et al.'s study, Luo et al. studied the *in vivo* viscoelastic properties of uterine suspensory tissue, which include the USL and CL, of women suffering from POP by performing multiple tensile and stress relaxation tests [54]. After a total of three ramp and hold test trials, the uterine suspensory tissue was determined to be viscoelastic. More specifically, the mean stiffness of the complex was found to be 0.49 N/mm, 0.61 N/mm and 0.59 N/mm for the 1st, 2nd, and 3rd trial, respectively [54]. The mean energy absorbed during the ramping of the tissue was reported to be 0.27 J, 0.23 J, and 0.22 J for the 1st, 2nd, and 3rd trial, respectively, while the mean normalized final relaxation force obtained was 0.57 N, 0.64 N, and 0.70 N for the 1st, 2nd, and 3rd trial, respectively [54]. Using a simplified four cable model, Luo et al. computed the stiffness of the USL to be 0.12 N/mm and the stiffness of the CL to be 0.2 N/mm. Due to the increase of the mean stiffness and final relaxation force and the decrease in the mean absorbed energy across the three trials, the authors concluded that the rest time was not adequate for fully tissue recovery [54].

3

Mechanical Analysis of the Uterosacral Ligament: Swine vs Human

3.1 Abstract

The uterosacral ligament (USL) is a major suspensory structure of the female pelvic floor, providing support to the cervix and/or upper vagina. It plays a pivotal role in surgical procedures for pelvic organ prolapse (POP), aimed at restoring apical support. Despite its important mechanical function, little is known about the mechanical properties of the USL due to the constraints associated with in vivo testing of human USL and the lack of validated large animal models that enable such investigations. In this study, we provide the first comparison of the mechanical properties of the swine and human USLs. Preconditioning and pre-creep data up to a 2 N load and creep data under a 2 N load over 1200 s were obtained on swine (n=9) and human (n=9) USL specimens by performing planar equi-biaxial tensile tests and using the digital image correlation (DIC) method. No differences in the peak strain during preconditioning tests, secant modulus of the pre-creep response, and strain at the end of creep tests were detected in the USLs from the two species along both axial loading directions (the main in vivo loading direction and the direction that is perpendicular to it). These findings suggest that the swine is an appropriate large animal model for studying the mechanical role of the USL in apical vaginal support and treatment of POP.

3.2 Introduction

Pelvic organ prolapse (POP) is a very common pelvic floor disorder, affecting half of all women over the age of 50 [55]. The number of affected women is expected to increase by 46% in 2050 due to the growing older population [56]. This disorder is characterized by an

abnormal descent of the female pelvic organs that causes the protrusion of the vagina and/or uterus. It adversely affects women's quality of life, including social, psychological, occupational, physical, and sexual well-being [57, 58]. Although the etiology is unknown, vaginal delivery, obesity, and aging have long been linked to the development of POP. Treatment options may vary based upon patient symptoms and preferences but, in severe cases, surgery is recommended. Unfortunately, the current success rate of POP surgeries is low, with 30% of women requiring reoperation for recurrence [59].

The goal of pelvic reconstructive surgeries is to restore the pelvic floor support so that the patient can maintain a normal quality of life. For many years, surgeons have used endogenous materials in these procedures. The most used endogenous material for two forms of prolapse, the vaginal vault prolapse and the uterine prolapse, is the uterosacral ligament (USL). The name "uterosacral ligament" is a misnomer since this is not a ligament in any traditional sense [24]. It is primarily composed of collagen fibers and smooth muscle cells with an autonomic nerve supply and a network of blood vessels. The USL connects the cervix to the sacrum, providing apical support to the uterus/cervix/vagina complex. In USL suspension surgeries, the length and tension of this ligament are adjusted in an ad-hoc manner to re-establish the support of the uterus or the vault of the vagina (after hysterectomy).

Since the early 2000s, surgeons have started to augment traditional POP repairs with synthetic mesh grafts. The mesh grafts, originally developed for the treatment of hernias, were marketed for POP repair without undergoing rigorous clinical trials, under the Food and Drug Administration (FDA) 510(k) exemption process [60]. Not surprisingly, over the years, these grafts have been found to have an unacceptably high rate of complications that include pain, infection, bleeding, mesh erosion, and organ perforation [61]. The FDA issued a Public Health Notification in 2008 with an update in 2011 regarding the increased rate of complications associated with the use of meshes in reconstructive surgeries for POP. To date, the potential benefits of synthetic meshes in prolapse repair are unclear. Only when the native tissues have poor mechanical properties, the mesh repair is recommended since the potential

benefits of mesh repair may outweigh the risks. Given the very important role played by the USL in the normal support function of the pelvic organs and in reconstructive surgeries (with and without mesh implants), fundamental engineering research is needed to advance our limited knowledge about the mechanical properties of the USL. Indeed, the success of USL suspension surgeries relies heavily on the mechanical properties of this ligament and the ideal mesh grafts must be developed by considering as target the mechanical properties of these native tissues.

The mechanical properties of the USL are determined by its constituents and their organization. Several histological studies have been conducted to identify and sometimes quantify the components of the USL [27,32,34–37,40,42]. In one of the earliest histological studies on cadaveric USL, Campbell et al. [27] identified but did not quantified the predominant components of the USL in the cervical, intermediate, and posterior regions using hematoxylin and eosin stain. Smooth muscle was the most prominent component in the cervical portion, dense connective tissue in the intermediate portion, and loose connective tissue and fat in the posterior portion [27]. Using the Movat stain, Cole et al. [32] detected disorganized collagen and interspersed elastin in cadaveric USLs. Butler-Manuel et al. [34] quantified the nerve content of the USL and determined that USLs from women undergoing radical hysterectomy had a higher nerve density than USLs from women undergoing a simple hysterectomy. Moreover, the deep portion of the USL contained a higher nerve content than the superficial portion of the USL [35]. Using immunohistochemistry techniques, Gabriel et al. [36] detected collagen type I, collagen type III, and smooth muscle in USLs of postmenopausal women with or without POP. While the above mentioned studies were on human USL, a few studies have been carried out on USL from other species. Gruber et al. [40] conducted the first histological studies of the USL from swine using hematoxylin and eosin, Van Gieson, and Masson's trichrome stains and determined the presence of collagen, elastin, smooth muscle, adipose tissue, and neural tissue. The content of USL was not quantified but, using a 5 point scale, it was graded and compared to the content of the vagina and cardinal ligament. The USL was found to contain a moderate amount of collagen and an extensive amount

of elastin while the presence of smooth muscle was only identified and not graded on this scale. Recently, Iwanaga et al. [42] conducted an histological study comparing human, rat, and mouse USLs. Using the Masson's trichrome staining method, the human USL and rat USL were found to have comparable collagen and smooth muscle content, while mouse USL had a significantly lower collagen content than human USL and significantly higher smooth muscle content than human and rat USL [42].

Ex vivo uniaxial tests have been conducted to characterize the mechanical behavior of the human USL [44, 47–49]. In a study by Reay Jones et al. [44], the resilience of USLs from women undergoing hysterectomy for a benign disorder was evaluated. Martins et al. [48] computed the stiffness and maximum stress of USLs obtained from female cadavers while Rivaux et al. [47] measured their nonlinear elasticity by computing the parameters of the Mooney-Rivlin model. Chantereau et al. [49] investigated the effect of age on the stiffness of USL from female cadavers. While these *ex vivo* studies have provided valuable information with regards to the mechanical behavior of the USL, *in vivo* mechanical tests of the USL, whenever possible, are ideal. Smith et al. [53] measured the stiffness of the USL by applying a tensile force to the cervix in women with normal uterine support and varying degrees of POP. Luo et al. [54] performed multiple tensile and stress relaxation tests on uterine suspensory tissue. Both of these studies were conducted over a very short period of time due to the ethical concerns associated with subjecting the patients to mechanical testing for extended periods of time. Thus, with the exception of two studies [53, 54], mechanical data on human USL were collected either using cadaveric tissue or fresh tissue collected from women undergoing hysterectomy. The medical history, age, and parity of the donor may affect the mechanical properties of the USLs. For example, the support function of USLs from patients undergoing hysterectomy is compromised and, therefore, the properties that are measured by mechanically testing these ligaments are the properties in a diseased rather than healthy state.

The use of animal models for studying the mechanical function of the USL for the prevention

and treatment of POP is crucial since the health state, age, and parity of the animals can be controlled. Using the monkey, Vardy et al. [46] measured the uniaxial elastic and stress relaxation response of USLs while, more recently, we have characterized the elastic, stress relaxation and creep properties of the USL (and cardinal ligament) using the swine as animal model [41, 50, 51, 62, 63]. In addition to uniaxial tensile tests [41], planar biaxial tensile tests, which better emulate the complex *in vivo* loading conditions of the USL, were performed [50, 51, 62].

This study presents a direct comparison of the histological and mechanical properties of swine and human USLs in order to establish the swine as an animal model for POP. Toward this end, the relative contents of collagen, smooth muscle, and elastin in both swine and human USL sections are quantified following Masson's trichrome (MT) and Verhoeff-van Giesson (VVG) staining. Planar biaxial testing and digital image correlation methods are also used to measure the preconditioning/cyclic, pre-creep/elastic, and creep properties of the USL from the two species along the main *in vivo* loading direction and the direction that is perpendicular to it. To our knowledge, there are no published studies that directly compare the mechanical properties of human USL to those of USL from other species. Additionally, there are no studies that present the biaxial preconditioning/cyclic, pre-creep/elastic, and creep data of the human USL. The findings of this novel research will not only serve to establish the swine as animal model for mechanical testing of the USL but will offer new mechanical data on the human USL, ultimately leading to new prevention and treatment methods for POP.

3.3 Materials and Methods

3.3.a Swine Specimen Preparation

This study was conducted with the approval of the Institutional Animal Care and Use Committee (IACUC) at Virginia Tech. Eleven adult (3-4 year-old, approximately 450 lbs) domestic swine were obtained from a slaughterhouse (Gunnoe Sausage Co, Goode, VA). Nine

swine were used for mechanical testing and two for histology. The USLs were harvested from the swine using previously detailed techniques [41] in the region extending from the cervix to and around the rectum. Given the size of the USL, only one square specimen was selected from each swine for mechanical testing. The specimens (n=9) were hydrated in phosphate-buffered saline solution (PBS, pH 7.4, Fisher Scientific, USA) and stored at -20° C until testing. For histological analysis, n=4 specimens (2 from each swine) were harvested from the USLs and immediately placed in 10% buffered formalin solution.

3.3.b Human Specimen Preparation

Human fresh cadaveric bilateral USLs were procured from 4 unpreserved female donors, whose medical records were available for review, through collaboration with the Bequest Body Donation Program at the University of Minnesota. Donors with history of symptomatic POP, pelvic reconstructive surgeries, hysterectomy, pelvic malignancy, pelvic radiation, connective tissue disorders, myopathy, or POP distal to the hymen on post-mortem examination, facilitated by the Credé's Maneuver were executed. The study was exempt from the Institutional Review Board approval, as it did not include living human subjects. The average age and body mass index of the cadaveric donors were 65.5±12.3 years and 23.2±5.5 kg/m^2, respectively. Out of four donors, three were nulliparous and one was parous, with history of 3 vaginal deliveries. Bilateral USLs were identified by tracking each ligament along its length from origin to insertion, and harvested in their entirety within 96 hours post-mortem. The proximal ends of the ligaments were tagged with a single suture to guide specimen orientation during subsequent mechanical testing. The USLs were stored in PBS solution at 4°C and shipped overnight on ice to Virginia Tech. Given the size of the individual USLs, one specimen/ligament was isolated from seven out of eight USL

Once received, due to size limitations, seven USL square specimens were isolated from seven of the eight USLs and two USL square specimens were isolated from one USL for mechanical testing. These specimens (n=9) were stored in PBS at -20° C until testing. Specimens intended for histological analysis (n=4) were collected from the remaining portions of the

USL that included the mid to distal regions (n=2) and mid to proximal regions (n=2). They were placed in 10% buffered formalin and stored in 70% ethanol until testing at room temperature.

3.3.c Histology

Both swine and human USL specimens were fixed in 10% buffered formalin and then stored in 70% ethanol for 48 hours. Specimens were then gradually dehydrated in a graded ethanol and xylol series before being embedded in paraffin wax. Once in paraffin wax, specimens were cut into 4 μm sections with a microtome. Four sections from swine USLs and four sections from human USLs were stained with the Masson's trichrome (MT) stain. Similarly, four sections from swine USLs and four sections from human USLs were stained with the Verhoeff-van Giesson (VVG) stain. Under the MT protocol, collagen and smooth muscle were stained blue and red, respectively. For the VVG protocol, collagen was stained pink, elastin and nuclei were stained black, and smooth muscle was stained purple. The histological slides were examined under a light microscope (DMI6000B, Leica Microsystems, Bannockburn, IL, USA) equipped with a scanning stage (LMT260, Leica Microsystems, Bannockburn, IL, USA) at 40× magnification and images were collected using a digital microscope camera (DMC4500, Leica Microsystems, Bannockburn, IL, USA). More specifically, a random area of 1160×870 μm^2 was divided into 4×4 tiles, each of 290×218 μm^2 for analysis. Five randomly selected areas of this size (1160×870 μm^2) on each histological slide were captured for quantification of the components of the USL. Quantification of USL components was performed using a color deconvolution plug-in (http://4n6site.com) of Adobe Photoshop software and ImageJ (NIH, MD). Smooth muscle and collagen contents were determined from the MT-stained slides while smooth muscle, elastin, and collagen contents were quantified from the VVG-strained slides. Techniques for the selection of colors for color deconvolution were modified from Lehr et al. [64] and Iwanaga et al. [42], who have completed similar analysis on digital histological images. Briefly, the color representing one component (e.g., blue for collagen using the MT protocol) was selected while all other colors were eliminated from the image

using Adobe Photoshop software. Then, using ImageJ, the number of pixel that remained in that color were counted and divided by the total number of colored pixels (excluding white pixels) in the entire image. This was performed for each of the five random 1160×870 μm^2 areas on a given slide for a total of eight (MT-stained or VVG-stained) slides.

3.3.d Mechanical Testing

The ligaments were thawed at room temperature and cut into squares ranging from approximately 2.3×2.3 cm^2 to 3×3 cm^2 specimens. The thickness of each specimen was measured in 4 different locations using a digital caliper (accuracy ± 0.05 mm, Series 573, Mitutoyo, Japan) under a 50 g compressive load and the average was then computed to calculate the thickness of each specimen. The specimen was gripped with 4 safety pins on each of the four sides and mounted into an Instron planar biaxial testing system equipped with four 20 N load cells (accuracy ± 0.02 N, Instron, UK). The two axial loading directions were selected to be the main *in vivo* loading direction of the USL and the direction perpendicular to this one. For each specimen, the distances between the two closest safety pins on opposite sides of the specimen along each direction were used to compute the two side lengths of the specimens using ImageJ (NIH, Bethesda, MD). Each of those lengths were then multiplied by the specimen's average thickness to determine the specimen's undeformed cross-sectional area along the main *in vivo* and perpendicular loading directions. The specimen was then lowered into a bath made of acrylic glass (Perspex, UK) which was filled with PBS at room temperature (21 °C). A cover, also made of acrylic glass, was placed over the bath, making complete contact with the PBS to avoid subtle fluid movements that could influence the strain measurement.

The 3D digital image correlation (DIC) technique was employed for non-contact strain measurement. The DIC system consisted of two CCD cameras (Prosilica GX 1660, Allied Vision Technologies, Exton, Pennsylvania, USA) equipped with macro lenses (AT-X 100 mm F2.8 AT-X M100 Pro D Macro Lens, Tokina, Tokyo, Japan) that were utilized to capture high resolution (1600×1200 pixels) images of each specimen during testing.

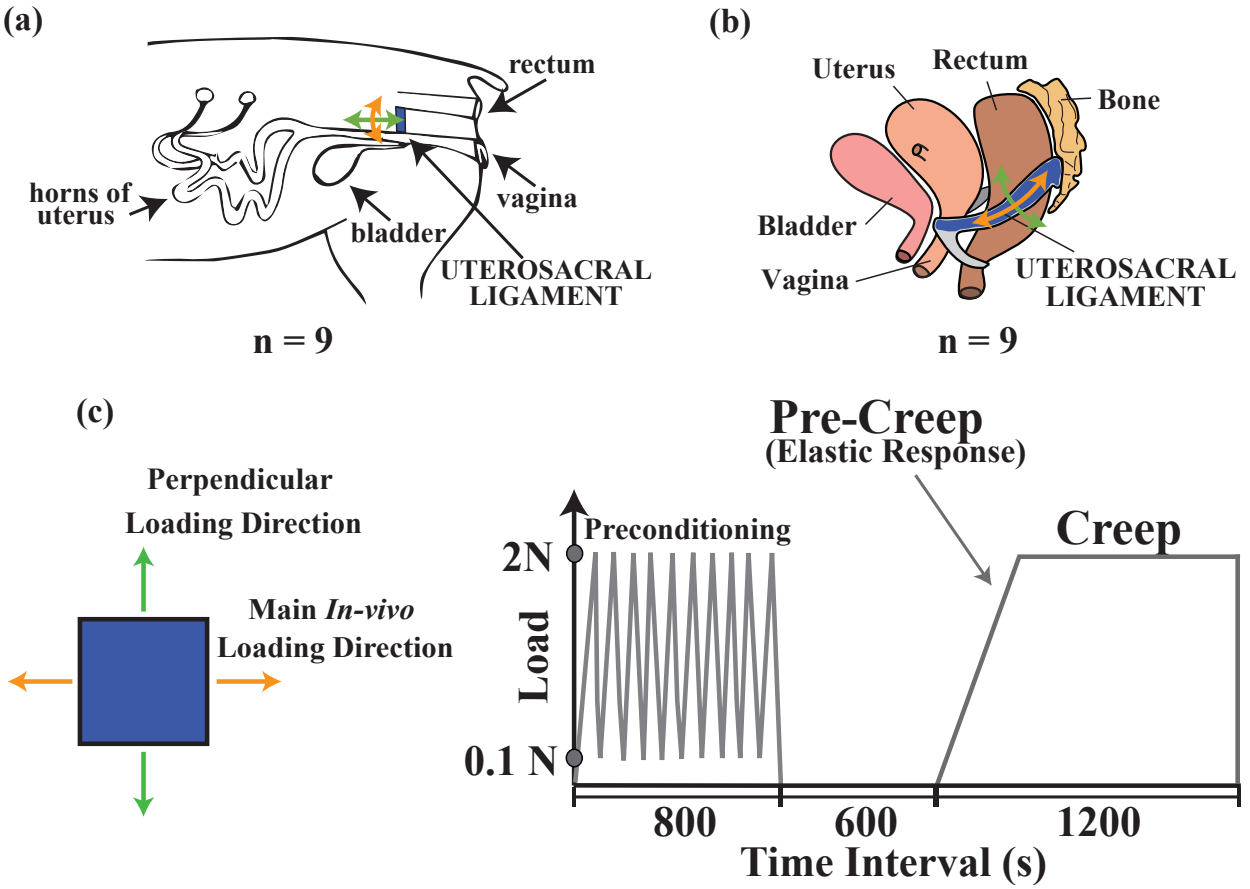

Figure 3.1: Location of the uterosacral ligament (USL) in the (a) swine and (b) human with marked main *in vivo* (orange arrows) and perpendicular (green arrows) loading directions (c) Square specimens ranging from approximately 2.3×2.3 cm^2 to 3×3 cm^2 s were oriented along the main *in vivo* and perpendicular loading directions and the load vs time protocol used for both swine and human at 2 N equi-biaxial loads.

Before each test, images of a 12×9 mm^2 plastic grid with 4 mm spacing were taken in order to calibrate the system. Each specimen was immersed in a solution of PBS and methylene blue, 1% aqueous solution (Fisher Science Education, USA) and a speckle pattern was created on the surface of the specimen using an aerosol fast dry gloss white paint (McMaster-Carr, USA) [65].

As shown in Figure 3.1c, both swine specimens (n=9) and human specimens (n=9) were preloaded to 0.1 N and preconditioned by loading/unloading them from 0.1 N to 2 N ten

times at 0.05 N/s loading rate in both axial loading directions. Following preconditioning, the specimens were unloaded and allowed to recover for 600 s (=10 min). They were then stretched along the two loading directions at 0.05 N/s loading rate until an equi-biaxial load of 2 N was reached. The equi-biaxial load of 2 N was held constant for 1200 s (=20 min). Thus, for each specimen, preconditioning/cyclic, pre-creep/elastic, and creep data were collected in the main *in vivo* loading direction and in the perpendicular direction.

For the preconditioning/cyclic, pre-creep/elastic, and creep portions of the test, the nominal normal stress in the main *in vivo* or perpendicular loading direction for each specimen was calculated by dividing the axial load in that direction by the specimen's undeformed cross sectional area that was perpendicular to such direction. This quantity will be referred simply as "stress" hereafter. Using the DIC method, the Lagrangian strain of each tested specimen was calculated. More specifically, a square region was selected in the center of each specimen and the local normal Lagrangian strain in both axial loading directions at every second for the entire duration of each test (preconditioning/cyclic, pre-creep/elastic, and creep tests) was recorded. These local normal Lagrangian strains were then averaged over this square region, resulting, at every second, in a single average normal Lagrangian strain value along the main *in vivo* loading direction and a single average normal Lagrangian strain value along the perpendicular direction for a given specimen. The average normal Lagrangian strain calculated for one specimen in each of the axial loading directions will be further referred simply as "strain" in such direction.

The secant modulus for each specimen in each loading direction was computed as the slope of a secant line drawn from the first and last point of the pre-creep/elastic stress-strain curve in such direction. In each loading direction, the strain during creep was also normalized by dividing it, at each second, by the corresponding pre-creep peak strain. Moreover, the creep rate in the main *in vivo* or perpendicular loading direction was calculated for each specimen as the slope of the linear regression line of the normalized strain vs. time data in the corresponding direction using logarithmic scales [66].

3.3.e Statistical Analysis

For histological analysis, the relative fractional area of each component of the (swine or human) USL was averaged over the five random areas selected from a given (MT or VVG) histological slide. This relative fractional area was then averaged over the total number of slides (n=4 swine USLs or n=4 human USLs) obtained from each staining protocol and simply termed "relative content." The Student's t test was used to compare the mean relative contents of a given component between swine and human USLs from histological slides obtained using the MT or VVG protocol (α=0.05). For biaxial mechanical analysis, an analysis of variance followed by Fishers LSD post hoc analysis (α=0.05) was performed to compare the mean peak strains recorded during preconditioning, the mean secant moduli of the pre-creep stress-strain curve, and the mean creep rates across directions (main *in vivo* and perpendicular directions) and species (swine and human). It must be noted that these means were computed over the number of specimens (n=9 swine USL specimens and n=9 human USL specimens). This statistical test was also used to compare the mean over the number of specimens of the minimum, average (over the square region selected for strain measurement), and maximum Lagrangian strains at the end of the creep test (t = 1200 s) across directions and species. The Student's t test (α=0.05) was used to compare the mean peak strain during preconditioning and the mean peak strain during creep (i.e., the mean strain at the end of creep at t=1200 s) for human or swine USLs in each loading direction. Mean and standard error of the mean (S.E.M.) were reported for all the data and statistical analysis was conducted using Minitab statistical software (Minitab 17, Minitab Inc.).

3.4 Results

3.4.a Histology

Figure 3.2 shows representative images of swine and human USLs stained using the MT protocol, which is used to identify collagen and smooth muscle contents. Collagen bundles, smooth muscle fibers, arteries, nerve fibers, and veins are found in both swine and human

USLs. The smooth muscle content appears to be more dispersed within the human USL compared to the swine USL. This figure also presents a comparison of the relative contents of collagen and smooth muscle in the USL of both species. No significant differences were found in relative collagen content (83.3 ± 2.13% for swine vs 78.3 ± 1.97% for human, $p > 0.05$) and in relative smooth muscle content (16.7 ± 2.13 % for swine vs 21.7 ± 1.97% for human, $p > 0.05$).

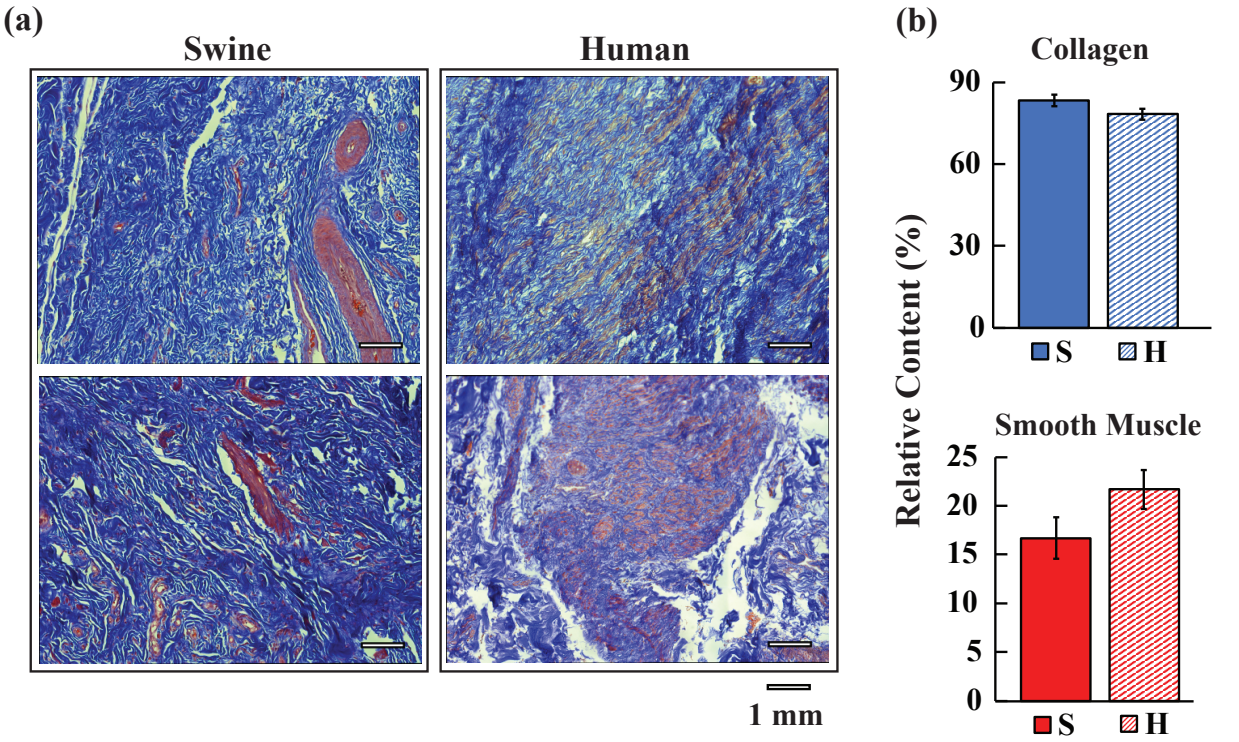

Figure 3.2: (a) Swine and human USL histological slides with MT stain. Both swine and human USLs were composed of collagen bundles, smooth muscle, arteries, and veins. (b) Swine and human USLs have comparable relative collagen content and comparable smooth muscle content ($p>0.05$).

Figure 3.3 shows representative images of swine and human USLs stained using the VVG protocol, which is used for detecting collagen, smooth muscle, and elastin contents. Similar to the MT stain, both swine and human USL contained collagen bundles, smooth muscle fibers, arteries, veins, and nerve fibers. Additionally, both swine and human USL contained elastin. The collagen fiber bundles appeared more loose and wavy in the human USL compared to the swine USL. Under the VVG protocol, swine USL contained a similar relative collagen

content as human USL (59.7 ± 3.33 % for swine vs 62.7 ± 3.15 % for human, $p > 0.05$). Swine USL showed a higher relative smooth muscle content when compared to human USL (33.4 ± 3.32 % for swine vs 24.4 ± 1.61 % for human, $p<0.05$). Human USL had a significantly higher relative elastin content than swine USL (5.91 ± 0.69 % for swine vs 7.01 ± 0.87 % for human, $p<0.05$).

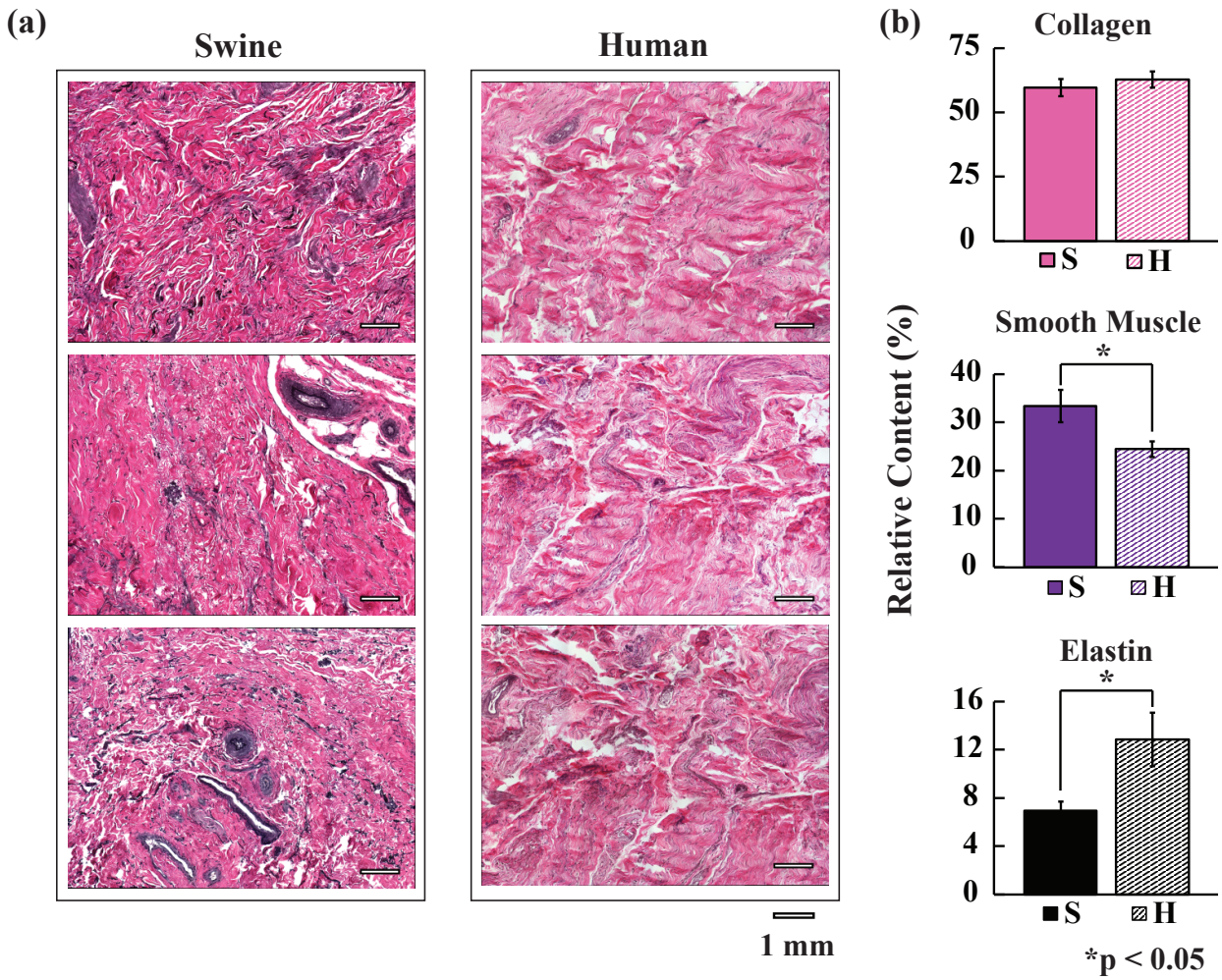

Figure 3.3: (a) Swine and human USL histological slides with VVG stain. As was seen using the MT stain, both swine and human USL were composed of collagen bundles, smooth muscle, arteries, and veins. In addition to these components, both swine and human USL contained elastin (b) Swine and human USLs have comparable relative collagen content ($p>0.05$) while swine USLs has a significantly higher relative smooth muscle content and a significantly lower relative elastin content than human USLs ($p<0.05$).

3.4.b Mechanical Testing

Both swine and human USL specimens experienced lower strains in the main *in vivo* loading direction compared to the perpendicular loading direction during preconditioning (Figure 3.4(a)). However, when comparing the mean peak strain during preconditioning across loading directions and species, no significant differences were found ($p > 0.05$) (Figure 3.4(b)).

The mean stress-strain data computed from both swine and human USL specimens during the pre-creep tests are reported in Figure 3.5(a). From the mean stress-strain curves, the human USL appeared to be stiffer than the swine USL. The mean secant moduli of the stress-strain curves are reported in Figure 3.5(b). For human USL specimens, the mean ($\pm$ S.E.M.) secant moduli in the main *in vivo* and perpendicular loading directions were 7.755$\pm$1.648 MPa and 5.996$\pm$1.354 MPa, respectively. For swine USL specimens, the mean ($\pm$ S.E.M.) secant moduli in the main *in vivo* and perpendicular loading directions were 3.512$\pm$0.611 MPa and 4.872$\pm$1.936 MPa, respectively. No significant differences were found when comparing the secant moduli of the stress-strain curves across loading directions and species ($p>0.05$).

The mean stresses for human USL specimens (n=9) subjected to creep tests at 2 N equi-biaxial load were found to be 0.1553 MPa and 0.1699 MPa in the main *in vivo* and perpendicular loading directions, respectively (Table 3.1). The mean stresses for swine USL specimens (n=9) subjected to creep tests at 2 N equi-biaxial load were found to be 0.0949 MPa and 0.0936 MPa in the main *in vivo* and perpendicular loading directions, respectively (Table 3.1). The mean initial creep strain (i.e. the mean strain at the beginning of creep at t=0) was lower, but not significantly lower, in the main *in vivo* loading direction compared to the perpendicular loading direction for both swine and human USL specimens. No significant differences were found when comparing the mean initial creep strains across loading directions and species ($p>0.05$).

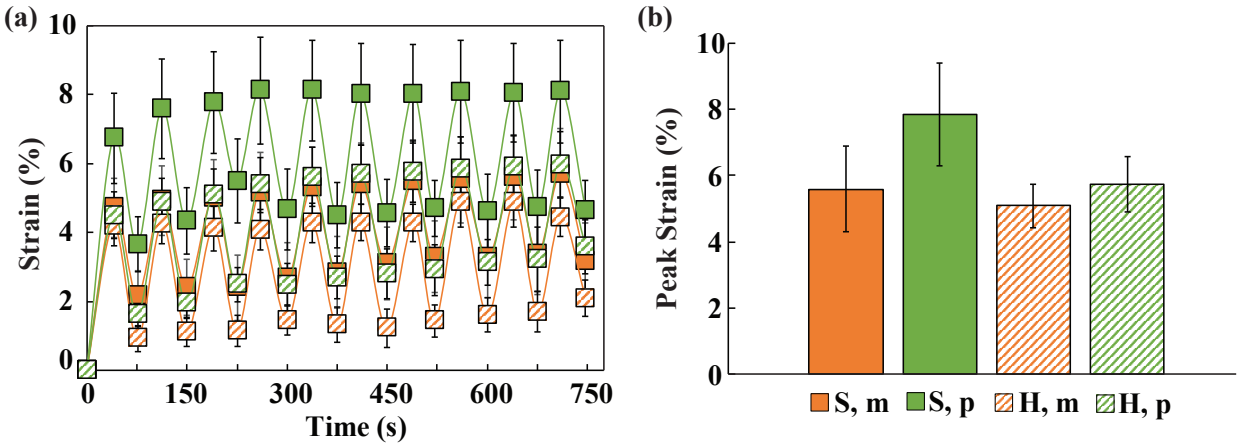

Figure 3.4: (a) Mean (± S.E.M.) strain vs time and (b) mean (± S.E.M.) peak strain in the main *in vivo* and perpendicular loading directions of human USL specimens (n=9) and swine USL (n=9) specimens subjected to ten preconditioning cycles from 0.1 N to 2 N equi-biaxial loads. The mean strain over time and mean peak strain were higher, but not significantly higher, in the perpendicular loading direction than in the main *in vivo* loading direction for both swine and human USLs ($p>0.05$). (**S** denotes data from swine USL, **H** data from human USL, **m** data in the main *in vivo* loading direction, and **p** data in the perpendicular loading direction).

During creep, the mean strain over time always remained lower in the main *in vivo* loading direction compared to the perpendicular loading direction for both swine and human USL specimens (Figure 3.6). Specifically, at the end of the creep test (t=1200 s), the minimum, average, and maximum of the axial Lagrangian strains for both swine and human USL

Table 3.1: Creep test parameters for human USL specimens (n=9) (thickness: 0.779 ± 0.328 mm) and swine USL specimens (n=9) (thickness: 0.922 ± 0.293 mm).

Species	**Mechanical Quantity**	**Loading Direction**	**Value (Mean ± S.E.M)**
Human	Stress (MPa)	Main *In vivo*	0.1553 ± 0.024
		Perpendicular	0.1699 ± 0.026
	Initial Creep Strain (%)	Main *In vivo*	2.780 ± 0.470
		Perpendicular	3.274 ± 0.408
Swine	Stress (MPa)	Main *In vivo*	0.0949 ± 0.010
		Perpendicular	0.0936 ± 0.009
	Initial Creep Strain (%)	Main *In vivo*	3.214 ± 0.400
		Perpendicular	3.688 ± 0.755

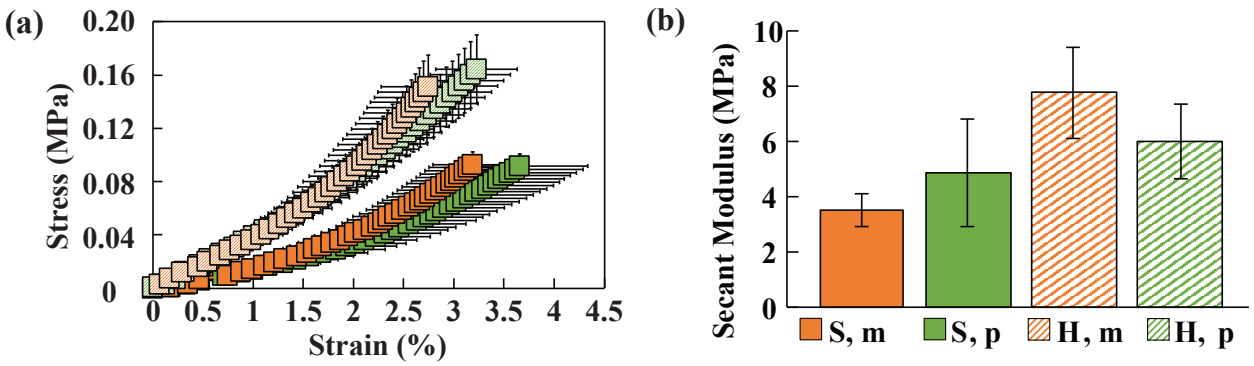

Figure 3.5: Mean (±S.E.M.) of (a) pre-creep stress-strain curves and (b) secant moduli of the pre-creep stress-strain curves in the main *in vivo* and perpendicular loading directions for swine USL specimens (n=9) and human USL specimens (n=9) equi-biaxially loaded up to 2 N. The mean secant modulus of the swine USL was lower, but not significantly lower, than that of the human USL ($p>0.05$). (**S** denotes data from swine USL, **H** data from human USL, **m** data in the main *in vivo* loading direction, and **p** data in the perpendicular loading direction).

specimens along both loading directions were compared (Figure 3.7). No significant differences were found for both swine and human USL specimens along both loading directions ($p > 0.05$).

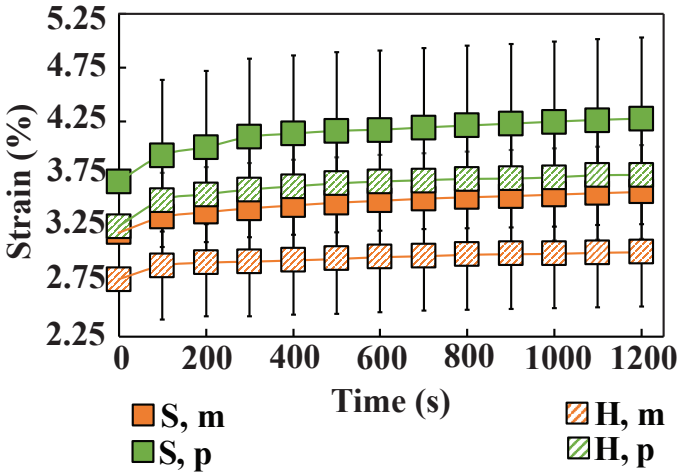

Figure 3.6: Mean (±S.E.M.) strain vs time for human USL specimens (n=9) and swine USL (n=9) specimens in the main *in vivo* and perpendicular loading directions subjected to 2 N equi-biaxial load. The mean strain over time is higher in the perpendicular loading direction than in the main *in vivo* loading direction for both swine and human USLs. (**S** denotes data from swine USL, **H** data from human USL, **m** data in the main *in vivo* loading direction, and **p** data in the perpendicular loading direction).

The mean normalized strains vs time data obtained during creep tests and the corresponding creep rates are shown in Figure 3.8. For human USL specimens, the mean peak strain during creep strain (or equivalently, the mean strain at the end of creep) was found to be 1.093 and 1.155 times the mean initial creep strain in the main *in vivo* and perpendicular loading directions, respectively. For swine USL specimens, the mean peak strain during creep was found to be 1.124 and 1.163 times the mean initial creep strain in the main *in vivo* and perpendicular loading directions, respectively. For both swine and human specimens, the mean normalized strain over time was larger in the perpendicular loading direction compared to the main *in vivo* loading direction. For human USL specimens, the mean ($\pm$S.E.M.) creep rate was 0.0200$\pm$0.003 1/sec and 0.0282$\pm$0.006 1/sec in the main *in vivo* and perpendicular loading directions, respectively, and, for swine USL specimens, it was 0.0289$\pm$0.008 1/sec and 0.0308$\pm$0.008 1/sec in the main *in vivo* and perpendicular loading directions, respectively. No significant differences were found when comparing the mean creep rates across loading directions and species ($p>0.05$).

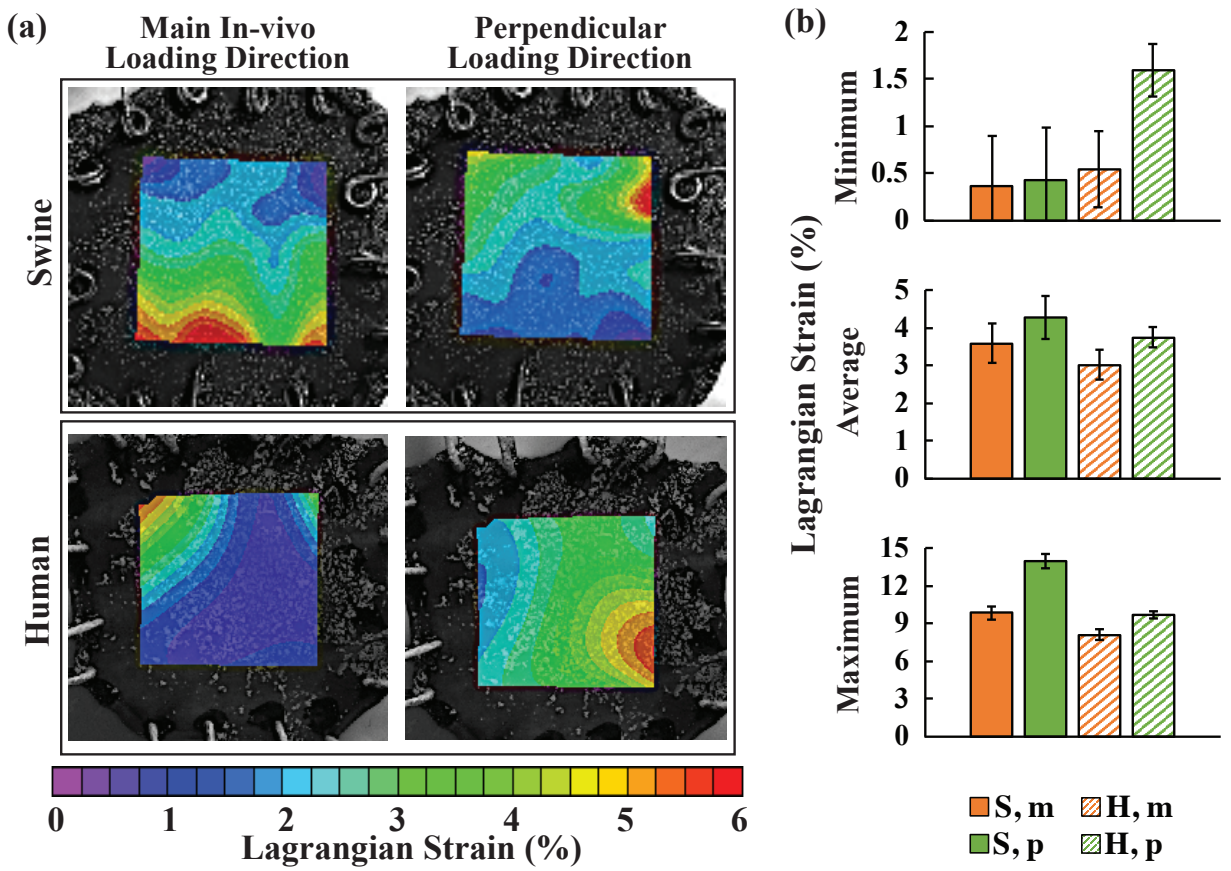

Figure 3.7: (a) Local axial Lagrangian strain map of representative swine and human USL specimens in the main *in vivo* and perpendicular loading directions at the end of creep at t=1200 s. (b) Mean (±S.E.M.) of the minimum, average, and maximum axial Lagrangian strains in the main *in vivo* and perpendicular loading directions for swine USL specimens (n=9) and human USL specimens (n=9). The mean minimum, average, and maximum axial Lagrangian strain in the perpendicular loading direction was higher, but not significantly higher, than in the main *in vivo* loading direction for both swine and human USLs. (**S** denotes data from swine USL, **H** data from human USL, **m** data in the main *in vivo* loading direction, and **p** data in the perpendicular loading direction).

In Figure 3.9, the comparison of the mean peak strains computed during preconditioning with the mean peak strains computed during creep, that is at the end of the creep test, for swine and human USL specimens for each loading direction is shown. Both swine and human USL specimens showed higher mean peak strains during preconditioning than during creep for both loading directions ($p=0.0341$ for the preconditioning vs creep comparison for human USL specimens in the main *in vivo* loading direction, $p>0.05$ for all other comparisons).

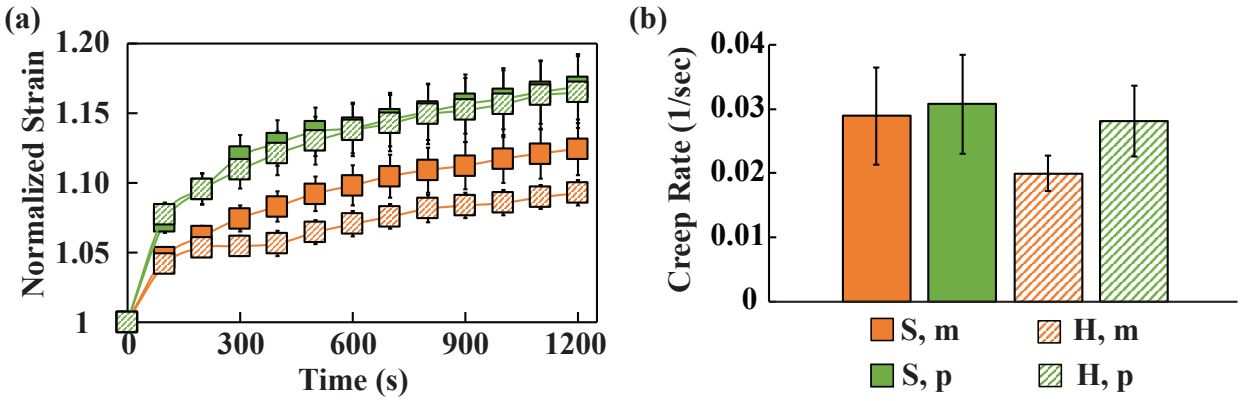

Figure 3.8: Mean (±S.E.M) of (a) normalized strain vs time and (b) creep rates in the main *in vivo* and perpendicular loading directions during creep at 2 N equi-biaxial load for swine USL specimens (n=9) and human USL specimens (n=9). The mean normalized strain in the perpendicular loading direction was higher, but not significantly higher, than in the main *in vivo* loading direction for both swine and human USLs. The mean creep rate of the USL is no significantly different across species and loading directions. (**S** denotes data from swine USL, **H** data from human USL, **m** data in the main *in vivo* loading direction, and **p** data in the perpendicular loading direction).

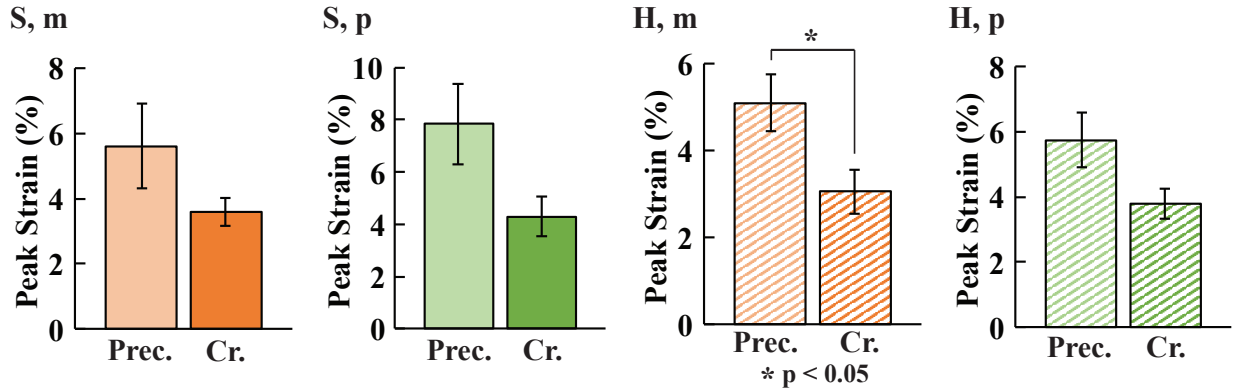

Figure 3.9: Mean (±S.E.M.) peak strains calculated during preconditioning and creep (at the end of creep at t=1200 s) in the main *in vivo* and perpendicular loading directions for swine USL specimens (n=9) and human USL specimens (n=9). The mean peak strain during preconditioning was higher than the mean peak strain during creep for swine and human USLs in both loading directions. Only for human USLs in the main *in vivo* loading direction, the mean peak strain during preconditioning was significantly higher than the mean peak strain during creep (p=0.0345). (**S** denotes data from swine USL, **H** data from human USL, **m** data in the main *in vivo* loading direction, and **p** data in the perpendicular loading direction).

3.5 Discussion

This study compared the composition and mechanical behavior of the swine and human USLs. Our quantitative analysis of MT-stained and VVG-stained histological sections indicated that swine and human USLs have comparable relative collagen content (Figures 3.2-3.3). Under cyclic equi-biaxial loads to 2 N, during preconditioning, the swine USL appeared to achieve higher mean peak strains (5.7% and 8.1% in the main *in vivo* and perpendicular loading directions, respectively) than human USL (4.9% and 6.0% in the main *in vivo* and the perpendicular loading directions, respectively) (Figure 3.4). However, no statistical differences were found amongst the mean peak strains across species and directions. Similarly, no statistical differences were found in the mean secant modulus of the pre-creep stress-strain curve across species and directions (Figure 3.5) although the mean secant modulus was higher for the human USL. During equi-biaxial creep tests at 2 N, the swine USL achieved higher mean strain (and normalized strain) over time in each loading direction than the human USL but, again, no statistical differences were found when comparing the mean peak strain during creep and the mean creep rates across species and loading directions (Figures 3.6-3.8). Overall the swine USL is comparable both structurally and mechanically to the human USL, suggesting that the swine is a good animal model for testing the mechanical properties of the USL.

Several studies have been conducted to identify the main components of the USL but only a few have quantified their contents in human USLs or swine USLs [36, 40, 42]. Gabriel et al. [36] analyzed the composition of the USLs in postmenopausal women with or without POP via immunohistochemistry techniques with antibodies that stained specifically for collagen type I, collagen type III, and smooth muscle. The USL from women without prolapse exhibited approximately 25% smooth muscle content [36], which is comparable to the results obtained in this study for human USL using both the MT protocol and VVG protocol, as our human specimens were also from women without POP. Recently, Iwanaga et al. [42] performed a comparative histological study of human, rat, and mouse USLs using the MT

staining method. Both our study and the study by Iwanaga et al. found that the collagen content was higher than the smooth muscle content in human USLs, as expected given the support function of these ligaments. The first histological study on the USL from swine was published by Gruber et al [40]. These authors evaluated the collagen and elastin content with a subjective 1- to 5-point scale, where 1 indicated no collagen or elastin content and 5 indicating extensive collagen or elastin content. The collagen content was rated 2.5 and the elastin content was rated 5 for the USL in comparison to the elastin content of the vagina and cardinal ligament. Given the large amount of elastin reported by Gruber et al. [40], we also employed the VVG staining method to detect the relative amount of elastin in swine and human USLs. Our analysis of the VVG stained histological slides confirmed that swine and human USLs have a comparable collagen content but showed that the swine USL had a significantly higher smooth muscle content and lower elastin content than human USL.

The histological analysis conducted in this study is not without its limitations. Random sections of the USL were evaluated to measure the collagen, smooth muscle, and elastin relative contents. These sections do not necessarily represent the entire ligament, which has been shown to have three distinct histological regions [27]. Moreover, for the MT protocol, it is generally accepted that anything dyed blue is typically collagen and anything dyed red is typical muscle. In reality, collagen, mucous, cartilage, and nuclei can be stained blue while cytoplasm, keratin, red muscle fibers, red blood cells, and fibrin can be stained red. [67] Therefore, while we report 83% and 78% relative collagen contents in swine and human USLs, respectively, and 17% and 22% relative smooth muscle contents in swine and human USLs, respectively, using the MT protocol, these quantities are not exclusively representing the relative collagen and smooth muscle contents. Similar considerations apply to the results obtained using the VVG protocol. The VVG stain is a combination of two stains: the van Geison stain and Verhoff's stain. The van Geison portion stains collagen deep red/pink, muscle yellow, nuclei blue/blackish, while the Verhoff portion stains nuclei and elastin fibers blue/blackish, with the resulting mix turning smooth muscle purple. In addition, for the VVG protocol, the time of differentiation of the stain is dependent on the amount of elastin

fibers that are present in the specimen [67]. Therefore, depending on the amount of elastin in the specimen at the time of staining, which is unknown before staining, some specimens may be under or even over differentiated even when they are allowed the same staining time. This would alter the amount of elastin that would be stained. Within these limitations, under the VVG protocol, it was determined that human USL had a significantly higher elastin content than swine USL. In general, elastin in connective tissues allows for long range deformability and resilience and, specifically in the human USL, large amount of elastin may be needed to allow a wide range of movements of the pelvic organs [40, 68]. The anatomical differences between the human pelvis and swine pelvis may explain this difference as well as possible differences in smooth muscle contents detected only using the VVG protocol. In women, the skeletal muscles of the pelvic floor also provide support of the pelvic organs from below while in the swine these muscles provide little support and are mainly used to move the tail. It is thus possible that a larger content of smooth muscle is needed in the swine USL to make up for the lack of support from the skeletal muscles of the pelvis.

In this study, we preconditioned swine and human USL specimens by applying cyclic loading at a constant magnitude and loading rate. Preconditioning reduces residual stresses in soft tissues and provides a repeatable no-load reference configuration [69]. The strain was found to increase slightly over time and reached a steady state after ten cycles (Figure 3.4). In early studies by Fung on mesenteric membranes [70, 71], which are similar to the USLs [24], the loading and unloading curves obtained by cyclically loading the membranes at a constant amplitude and elongation rate never reached a steady state, even after several cycles. However, the differences in load recorded in successive cycles was observed to decrease with the number of cycles as in our study. Over the past years, a variety of preconditioning protocols have been proposed for soft tissues [72–76] but no consensus has been reached on the ideal protocol. More recently, some investigators have suggested that preconditioning protocols must be selected based on the mechanical tests that are performed. More specifically, a preconditioning protocol that includes both cyclic loading and stress relaxation tests with long recovery periods should be employed for characterizing the stress relaxation response [75,76].

In our study, the protocol recommended by Carew et al. [75, 76] would have been infeasible. We had to limit the overall testing time since the quality of the speckle pattern created for the DIC strain measurement was compromised with time.

Overall, swine and human USLs exhibited a comparable elastic and creep response (Figures 3.5-3.8). However, the human USL appeared to be slightly stiffer than the swine USL. This is confirmed by the slightly higher mean secant modulus of the stress-strain curve in both loading directions for the human USL when compared to the swine USL (Figure 3.5). Moreover, the swine USLs deformed more, but not significantly more, than the human USLs during creep (Figures 3.6-3.7). These difference may be attributed, in part, to the differences in how the swine and human tissues were handled post mortem. Before mechanical testing, the swine USLs were dissected within 4 hours of death and then placed in PBS at -20°C while the human USLs were dissected 96 hours post mortem and then preserved in PBS at -20°C. The onset of rigor mortis, which is marked by a shortening of muscle fibers and an increase in the rates of glycolysis, lactic acid levels, and adenosine diphosphate levels in tissues, has been shown to be delayed by a decrease in temperature [77–82]. The human USL was thus able to achieve higher levels of rigor mortis than the swine USL. This may have contributed to the increase in stiffness measured during pre-creep tests and decrease in strain measured during creep tests for the human USL.

While no studies report the secant moduli of the USL computed via biaxial testing, some studies have reported the elastic modulus of the USL computed from the linear region of the stress-strain curve collected along the main *in vivo* loading direction via uniaxial tests [41, 46, 48]. In the study by Vardy et al. [46], elastic moduli of postmenopausal monkey USLs were determined at different strain levels from incremental pre-relaxation stress-strain curves, reaching a value of 1.00 MPa at 30% strain. By testing USLs up to failure, Martins et al. [48] reported a mean value of 14.1 MPa, ranging from 5.7 to 26.1 MPa, for human USL while Tan et al. [41] reported values that ranged from 0.46 MPa to 2.99 MPa for the toe region and from 20.1 MPa to 38.9 MPa for the linear region for swine USLs. These values

are comparable to the secant moduli that are reported for swine and human USLs in our study (Figure 3.5). In our study, the stress-strain curves were collected during pre-creep tests by equi-biaxially loading the USL specimens only up to 2 N. Therefore, we obtained lower stresses (Table 3.1) that those reported in previous studies [41, 48] and, consequently, lower values of the secant moduli.

The biaxial creep response of both swine and human USLs was consistent with our previous study on the swine USL/cardinal ligament complexes [51]. In our previous study, the mean normalized strain at 1200 s was approximately 1.2 and 1.3 times the initial creep strain in the main *in vivo* and perpendicular loading directions, respectively, whereas in this study the mean normalized strain for the swine USL was approximately 1.16 and 1.09 times the initial creep strain in the main *in vivo* and perpendicular loading directions, respectively (Figure 3.8). These differences can be not only determined by the difference in the tested specimens but also by the differences in the experimental protocols. More specifically, in this study we performed tests by controlling the load rate but in our previous study we controlled the displacement rate. Load controlled deformation and displacement controlled deformation can lead to different results: for the same value of stress, soft tissue specimens under load controlled deformations were found to deform less than tissue specimens subjected to displacement controlled deformations [83].

The DIC method was used throughout the preconditioning/cyclic loading, pre-creep/elastic, and creep tests for non-contact strain measurements. As shown in Figure 3.7(a), the measured Lagrangian strain was not uniform across the specimens. The non-homogeneous deformation may be the result of inherent inhomogeneities of the specimens but it may be also determined by the clamping technique. Indeed, several studies have shown that clamping techniques affect the strain fields in planar biaxial testing of soft tissues [84–88]. For nonlinear materials, Eilaghi et al. [87] concluded that having the attachment points span a wide zone along each edge of the specimen leads to a more uniform strain field. These investigators also noted that any shifts in the alignment of the attachment points along one

edge of the specimen can significantly distort the strain field. Precautions were taken in our study to ensure the alignment of the pins along each side of the specimens by using a stamp to mark the points where the safety pins were to be inserted and a plastic grid to guide the safety pin placement. However, misalignment of the attachment points was inevitable due to the soft nature of the specimens, and this likely affected the strain field uniformity.

Preconditioning data are rarely published since, as discussed above, preconditioning is only used to establish a repeatable no-load reference configuration. Many investigators in biomechanics have questioned the benefits of preconditioning and they have excluded it from their protocols. We opted to present the mechanical data we collected during preconditioning since, if preconditioning is not deemed necessary, these data can be interpreted as cyclic loading data. We then compared the mean peak strain during preconditioning/cyclic loading to the mean peak strain during creep for both the swine and human USL specimens (Figure 3.9). Our goal was to determine differences in strain of the USL under cyclic equi-biaxial loads of 2 N at constant loading rate and under constant equi-biaxial loads of 2 N over time. From our results, strains achieved during cyclic loading were higher than those achieved during creep for both species in both loading directions. Specifically for human tissue, the mean peak strain achieved during cyclic loading was significantly higher than the mean peak strain achieved during creep along the main *in vivo* loading direction (Figure 3.9). Even though both cyclic loading and creep tests were performed up to the same load magnitude, USL specimens experienced higher loading rates during cyclic loading than during creep. This explains why higher strains were experienced by the USL specimens during cyclic loading. These findings may suggest that certain exercises, such as exercises where the USL are under constant loads over time (e.g., a squat or a wall sit for a prolonged amount of time) may cause less damage to the pelvic supportive ligaments than exercises where the loads are oscillating at a constant load rate (e.g., a high rep of squats or leg lunges).

Although the etiology of POP is unknown and likely multifactorial, alterations in the mechanical properties of the female reproductive organs and supportive tissues are, without

doubt, contributing factors [62]. Due to limited sample size and ethical concerns with examining human tissue, the selection of appropriate animal models for mechanical testing of pelvic organs and tissues is crucial not only to explore the etiology of POP but also to develop new surgical techniques and mesh materials before being applied to humans. Different animal models such as mice, rats, rabbits, sheep, swine, and nonhuman primates have been used to study POP [52]. Through this novel study, we have demonstrated the remarkable histological and mechanical similarities between swine and human USLs. Our results together with the low cost and ease of breeding of swine and the fact that the swine naturally develop POP suggest that the swine is an ideal model for testing the mechanical properties of the USL.

3.6 Conclusions

Through comparative histological and mechanical studies, we have shown that the swine is a good animal model for testing the elastic and creep properties of the USL. Swine and human USLs are composed primarily of collagen, smooth muscle, and elastin. They have a comparable amount of collagen, the main structural protein of connective tissues, and exhibit similar preconditioning/cyclic loading, pre-creep/elastic, and creep properties measured via planar biaxial testing in combination with DIC. The findings of this study will hopefully prompt future research on the support function of the USL to assess novel therapies for POP.

4

Effects of Repeated Biaxial Loads on the Creep Properties of Cardinal Ligaments

This chapter was originally published as a journal article in the Journal of the Mechanical Behavior of Biomedical Materials.

It is available at https://doi.org/10.1016/j.jmbbm.2017.05.038.

4.1 Abstract

The cardinal ligament (CL) is one of the major pelvic ligaments providing structural support to the vagina/cervix/uterus complex. This ligament has been studied mainly with regards to its important function in the treatment of different diseases such as surgical repair for pelvic organ prolapse and radical hysterectomy for cervical cancer. However, the mechanical properties of the CL have not been fully determined, despite the important *in vivo* supportive role of this ligament within the pelvic floor. To advance our limited knowledge about the elastic and viscoelastic properties of the CL, we conducted three consecutive planar equi-biaxial tests on CL specimens isolated from swine. Specifically, the CL specimens were divided into three groups: specimens in group 1 ($n = 7$) were loaded equi-biaxially to 1 N, specimens in group 2 ($n = 8$) were loaded equi-biaxially to 2 N, and specimens in group 3 ($n = 7$) were loaded equi-biaxially to 3 N. In each group, the equi-biaxial loads of 1 N, 2 N, or 3 N were applied and kept constant for 1200 s three times. The two axial loading directions were selected to be the main *in-vivo* loading direction of the CL and the direction that is perpendicular to it. Using digital image correlation (DIC) methods, the in-plane Lagrangian

strains in these two loading directions were measured throughout the tests. The results showed that CL was elastically anisotropic, as statistical differences were found between the mean strains along the two axial loading directions for specimens in group 1, 2, or 3 when the equi-biaxial load reached 1 N, 2 N, or 3 N, respectively. For specimens in group 1 and 2, no statistical differences were detected in the mean normalized strains (or, equivalently, the increase in strain over time) between the two axial loading directions for each creep test. For specimens in group 3, some differences were noted but, by the end of the 3rd creep test, there were no statistical differences in the mean normalized strains between the two axial loading directions. These findings indicated that the increase in strain over time by the end of the 3rd creep test were comparable along these directions. The greatest mean normalized strain (or, equivalently, the largest increase in strain over time) was measured at the end of the 1st creep test (t = 1200 s), regardless of the equi-biaxial load magnitude or loading direction. Mean normalized strains during the 2nd and 3rd creep tests (t = 100, 600, and 1200 s), along each loading direction, were not statistically different. Isochronal data collected at 1 N, 2 N, or 3 N equi-biaxial loads indicated that the CL may be a nonlinear viscoelastic material. Overall, this experimental study offers new knowledge of the mechanical properties of the CL that can guide the development of better treatment methods such as surgical reconstruction for pelvic organ prolapse and radical hysterectomy for cervical cancer.

4.2 Introduction

Pelvic floor disorders (PFDs), such as urinary incontinence, fecal incontinence, and pelvic organ prolapse (POP) are a growing component of women's health issues in the United States. It has been estimated that in 2010 over 28 million women had at least one PFD and this number is expected to increase to 44 million by 2050 [56]. In particular, POP, the descent of a pelvic organ from its normal place towards the vaginal walls and into the vaginal cavity, is one of the most common form of PFDs. As of 2010, it is estimated that POP affects 3.3 million women in the United States, annually [6]. The onset of POP can be attributed to several factors, with the most common being age, labor, parity, menopause, and weight gain [1,2,89].

For mild cases of POP, lifestyle changes such as a change in diet and exercise or muscle strengthening exercises such as Kegel exercises can help alleviate some of the symptoms. For more severe or extreme cases, the recommended course of treatment for the most common type of POP, the uterine prolapse, is typically a pelvic reconstructive surgery.The number of women who will undergo surgery to treat POP continues to dramatically increase, and it has been estimated that this number will increase from 166,000 in 2010 to approximately 250,000 in 2050 [90].

Traditionally, native tissue repairs have been adopted to treat POP but mesh augmented repairs have become more common over the past years. However, many women experienced adverse side effects to mesh augmented procedures, such as pain, mesh erosion, dyspareunia, and recurrence of POP. A comprehensive study by Maher et al., which collected data on surgical management of POP of approximately 6,000 women, found that 14% of patients who received a transvaginal mesh experienced some form of POP recurrence [13]. The study also found that 18% of patients who received a transvaginal mesh experienced mesh erosion and 11% of patients underwent reoperation. Surgical meshes used for PFDs were developed in the 1950's initially to treat abdominal hernia repairs and, due to their success, in the 1970's gynecologists started using these abdominal meshes for repair of POP [15]. However, women experienced many of the complications outlined above and these were, most likely, triggered by the mismatch in properties between the native tissue and the synthetic mesh.

Damage to pelvic supportive ligaments, such as uterosacral ligament (USL) and cardinal ligament (CL), contributes significantly to the development of PFDs [1, 18, 19]. The USL and CL are visceral ligaments that connect the upper vagina/cervix to the sacrum and pelvic sidewall, respectively, and provide support to the vagina, cervix, and uterus [24] (Figure 4.1). These ligaments are often characterized together and are commonly referred to as the USL/CL complex [91–93]. They are, however, quite different and, for this reason, they deserve to be studied also independently. The CL is parallel to the body axis and is vertically oriented when a woman is an upright position, while the USL is dorsally directed

toward the sacrum. Using an MRI based 3D technique, the CL was found to be much longer and more curved than the USL [93].

One of the first studies to investigate the existence of the CL was conducted by Mackenrodt who described the CL as a transverse cervical ligament that is the chief supporting structure of the uterus [29]. By the 1960's, Range et al. conducted an anatomical analysis of the CL, finding that it is mostly made of blood vessels, nerves, lymphatic vessels, and loose connective tissue with collagen and smooth muscle fibers [30]. Through a more recent structural characterization of the CL, Samaan et al. suggested the CL may be a suitable attachment point for a synthetic mesh in surgical repair of POP [31]. The CL has also been found to play a pivotal role in the treatment of cervical cancer via radical hysterectomy. Historically, the CL and its surrounding connective tissue were removed in radical hysterectomy, following a procedure that was established by Latzko and Okabayashi [94, 95]. However, studies conducted by Yabuki et al. in the 1990's and 2000's determined that preservation of the CL is crucial in order to prevent neurogenic bladder and excessive bleeding given the proximity of the CL to the neural pathway responsible for the control of bladder function [96–98].

Investigating the effect of repeated constant loading on the time-dependent mechanical behavior of the CL and other supportive ligaments is essential since these ligaments are constantly under tension and experience large changes in length and curvature *in vivo* [99]. Recently, Chen et al. used geometrical data collected via an MRI based 3D technique and developed a four-cable mechanical model in order to quantify the geometrical and mechanical characteristics of CL and USL in living healthy women [93]. After reconstructing the pelvic anatomy of 20 healthy women, the authors deduced that the CL is parallel to the body axis and, as a woman stands upright, the CL becomes vertically oriented. Due to its alignment, the CL experiences greater tension than the USL and its curvature allows the apical support to have a large range of motion. In everyday life, the CL undergoes changes in tension as a woman sits and stands upright but, over time, these changes are exacerbated with fluctuations in weight and during pregnancy when the growing fetus exerts additional tension on

the pelvic organs. The CL is subjected to repeated loads over time *in vivo*, especially after the levator ani muscle are damaged during vaginal delivery. These loads are likely to cause an increase in the tissue's length over time, compromising the support function of the CL and contributing to the development of POP.

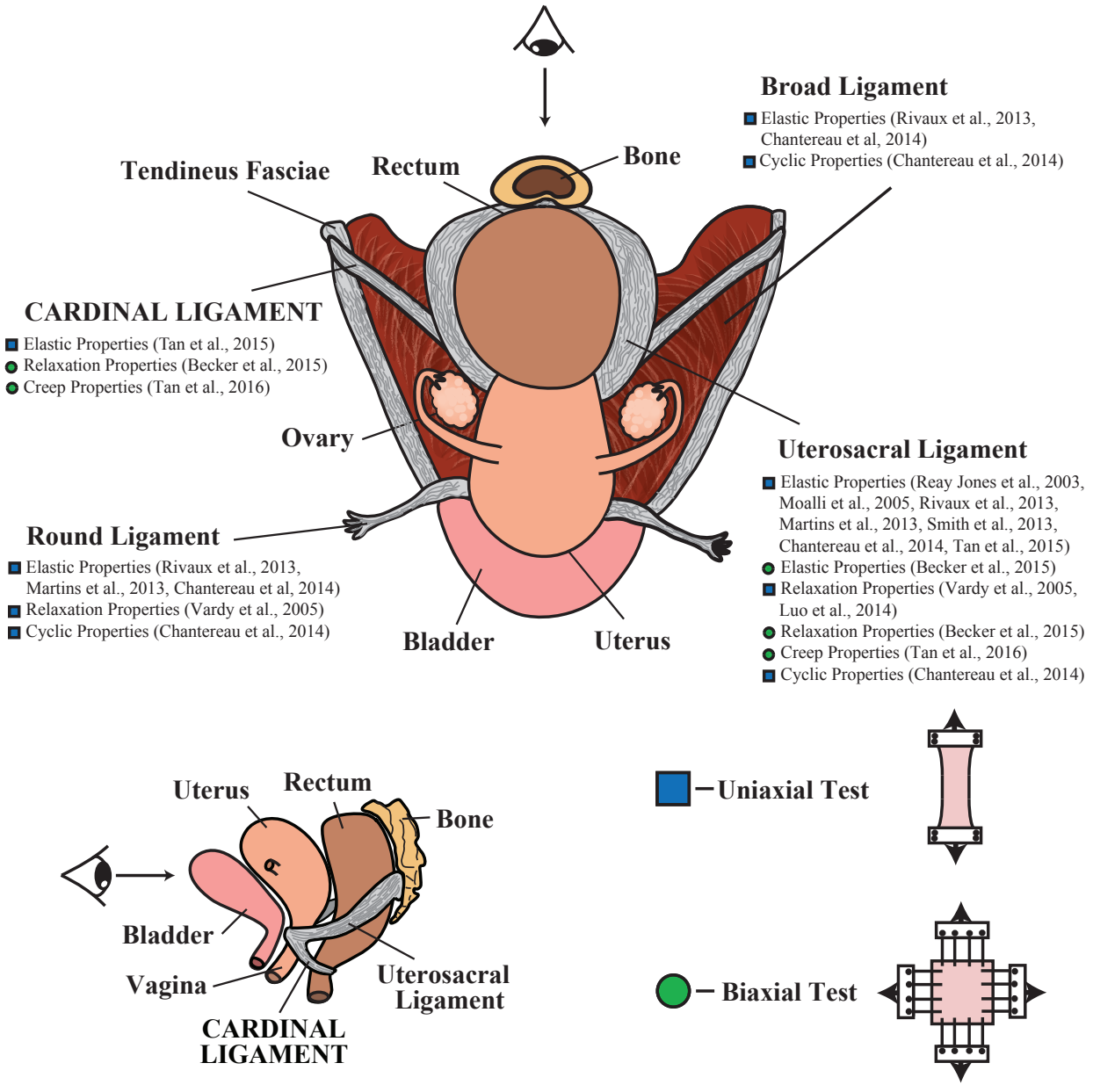

Figure 4.1: Relative position of female pelvic organs and ligaments (top-down view and side view) with a list of published uniaxial and biaxial elastic and viscoelastic studies on pelvic ligaments.

In a recent review article, we summarized the current knowledge of the mechanical properties of female reproductive organs and supporting connective tissues, presenting the results of experimental studies that characterized the nonlinear elastic and viscoelastic responses of these tissues [62]. *Ex vivo* uniaxial tensile tests of supportive ligaments were conducted [44–49] and mechanical quantities, such as the ultimate strength and tensile modulus were reported for the CL [41]. *In vivo* uniaxial tests were also performed to measure stiffness and repeated force-relaxation of USL/CL complexes in women affected by POP [53, 54]. Clearly, the *in vivo* tests produced the most physiologically relevant mechanical data but, due to ethical considerations and limited time in the operating room during testing, the tests only lasted a few minutes. Both the USL and CL are membrane-like and experience loads in multiple directions over long time intervals and thus *ex vivo* planar biaxial tests can offer a more complete description of their mechanical behavior. Using *ex vivo* planar biaxial methods, more recently, the Authors characterized the elastic, stress relaxation [50], and creep [51] properties of the USL/CL complex (Figure 4.1).

In this study, we investigate the effects of repeated equi-biaxial loads on the mechanical properties of swine CLs. The swine is selected as animal model due to histological similarities that exist between the CL in swine and the CL in humans [40, 41, 51]. *Ex vivo* testing is a valuable alternative method to *in vivo* testing for exploring the time dependent behavior of CL since changes in mechanical properties can be assessed over longer time intervals. More specifically, the creep properties are evaluated after three 1200 s long equi-biaxial loads are applied along the main *in vivo* loading direction of the CL and the direction perpendicular to this one. While the CL specimens are loaded, accurate strain maps are obtained using the Digital Image Correlation (DIC) method. This study extends our limited knowledge about the time-dependent mechanical behavior of the CL, providing insight into the effect of repeated loading on the supportive function of CL within the pelvic floor and suggesting new treatment strategies for PFDs and cervical cancer.

4.3 Materials and Methods

4.3.a Specimen Preparation

This study was conducted with the approval of the Institutional Animal Care and Use Committee (IACUC) at Virginia Tech. Four adult (3 to 4 year-old, approximately 450 lbs) domestic swine were obtained from a slaughterhouse (Gunnoe Sausage Co, Goode, VA). The CLs were harvested from the swine using techniques detailed in our previous study [41]. They were hydrated with phosphate-buffered saline solution (PBS, pH 7.4, Fisher Scientific, USA) and then frozen at -20°C. They were thawed at room temperature and cut into approximately 3×3 cm^2 specimens (Figure 4.2(a)-(b)). A total of 24 specimens were used for mechanical testing.

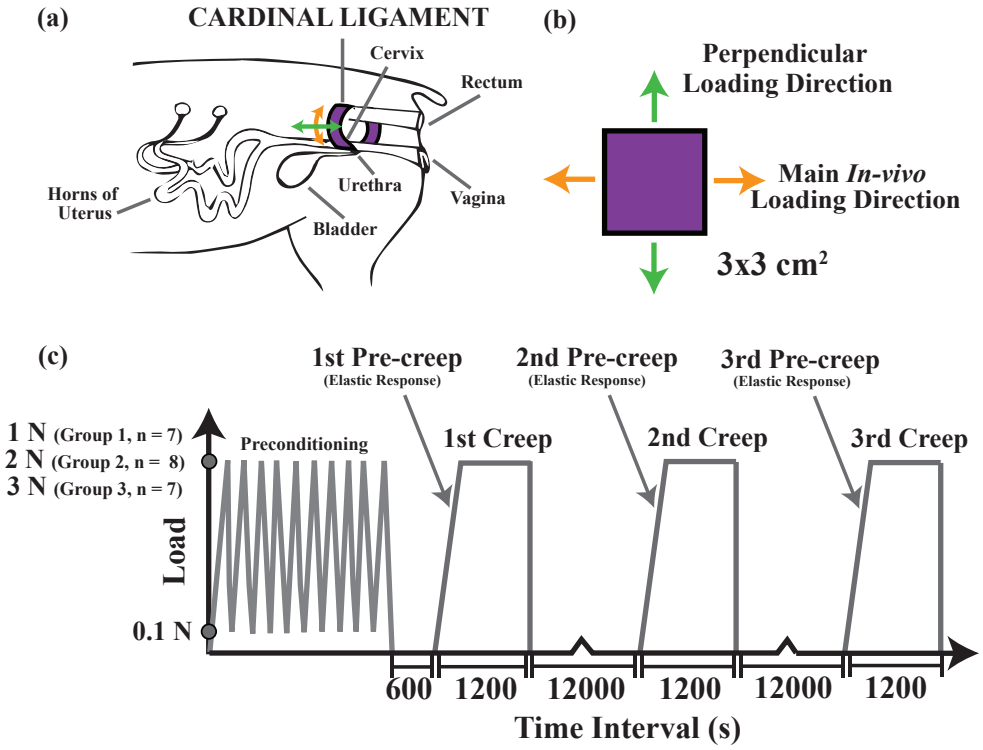

Figure 4.2: (a) Location of the cardinal ligament (CL) in the swine with marked main *in vivo* (orange arrow) and perpendicular (green arrow) loading directions. (b) 3×3 cm^2 size square specimens with sides that were oriented along the main *in vivo* (orange arrow) and perpendicular (green arrow) loading directions. (c) Load versus time protocol along each (main *in vivo* or perpendicular) axis used to test specimens at 1 N, 2 N, and 3 N equi-biaxial loads.

4.3.b Planar Biaxial Creep Testing

Before mechanical testing, the thickness of each specimen was measured in 4 different locations using a digital caliper (accuracy ± 0.05 mm, Series 573, Mitutoyo, Japan) under a 50 g compressive load. The average thickness of each specimen was then computed and used for stress measurements. Following the methods described by Lionello et al. [65], each specimen was immersed in a solution of PBS and methylene blue, 1% aqueous solution (Fisher Science Education, USA) and a speckle pattern was created on each specimen using an aerosol fast dry gloss white paint (McMaster-Carr, USA). Two CCD cameras (Prosilica GX 1660, Allied Vision Technologies, Exton, Pennsylvania, USA) equipped with macro lenses (AT-X 100mm F2.8 AT-X M100 Pro D Macro Lens, Tokina, Tokyo, Japan) were employed to capture high resolution (1600×1200 pixel) images of each specimen during testing. The cameras were an integral part of the 3D digital image correlation (DIC) system (VIC-3D, Correlated Solutions, Columbia, South Carolina, USA) that was used to perform non-contact strain measurement. Before each test, images of a 12 × 9 mm^2 plastic grid with 4 mm spacing were taken in order to calibrate the DIC system. After calibration, each specimen was gripped with 4 safety pins on each of the four sides and mounted into an Instron planar biaxial testing system equipped with four 20 N load cells (accuracy ± 0.02 N, Instron, UK). The two axial loading directions were selected to be the main *in vivo* loading direction of the CL and the direction perpendicular to this one (Figure 4.2(a)-(b)). For each specimen, the distances between the two closest safety pins on opposite sides of the specimen were used to compute the two side lengths of the specimens using ImageJ (NIH, Bethesda, MD). Each of those lengths were then multiplied by the specimen's average thickness to determine the specimen's undeformed cross-sectional area along the main *in vivo* and perpendicular loading directions. The specimen was then placed in a bath made of acrylic glass (Perspex, UK) which was filled with PBS at room temperature (21°C). The bath was then enclosed with a cover also made of acrylic glass. The acrylic glass cover came into complete contact with the PBS to create a flat planar surface for DIC measurements and ensure that subtle fluid movements did not influence the measurements of the motion of the specimen.

Specimens ($n = 24$) were split into three groups, group 1, group 2, and group 3, based on their thicknesses and, consequently, magnitude of the equi-biaxial load applied during creep testing (Figure 4.2(c)). The specimens in each group were randomly collected from the four different swine. Thinner specimens were subjected to lower equi-biaxial loads to avoid their premature damage and failure during testing. Specimens in group 1 ($n = 8$) were preloaded to 0.1 N and preconditioned by loading/unloading them from 0.1 N to 1 N ten times at 0.05 N/s loading rate. Following preconditioning, the specimens were unloaded and allowed to recover for 600 s (=10 min). They were then stretched at a 0.05 N/s loading rate until an equi-biaxial load of 1 N was reached. The equi-biaxial load of 1 N was held constant for 1200 s (=20 min). Then the specimens were unloaded and allowed to recover for 12,000 s (=200 min). The recovery time was selected to be 10 times longer than the duration of the creep test [100, 101]. After recovery, the specimens were again stretched at a 0.05 N/s loading rate until an equi-biaxial load of 1 N was reached. This equi-biaxial load was held constant for 1200 s (=20 min) and then the specimens were unloaded again and allowed to recover for 12,000 s (=200 min). Next, the specimens were stretched a final time at a 0.05 N/s loading rate until an equi-biaxial load of 1 N was reached. Again, the equi-biaxial load was held constant for 1200 s (=20 min) and subsequently the specimens were unloaded. Specimens in group 2 ($n = 8$) and group 3 ($n = 8$) followed the same protocol but the maximum equi-biaxial loads achieved during preconditioning and held after the 600 s long recovery interval and the two 12000 s long recovery intervals were 2 N and 3 N, respectively (Figure 4.2(c)).

4.3.c Data and Statistical Analysis

Nominal normal stress in the main *in vivo* or perpendicular loading direction was calculated by dividing the axial load (1 N, 2 N , or 3 N) in the corresponding direction by the specimen's undeformed cross-sectional area in that particular direction. This quantity will be referred simply as "stress" hereafter. Using the DIC method, the local Lagrangian strain in both axial loading directions over a square region in the center of the specimen was recorded

every second for the entire duration of the test. These local axial Lagrangian strains were then averaged, resulting, at every second, in a single average Lagrangian strain value along the main *in vivo* loading direction and a single average Lagrangian strain value along the perpendicular direction. The average axial Lagrangian strain calculated for one specimen in each of the axial directions will be further referred simply as "strain" along such direction. Figures 4.3, 4.4, and 4.5 show the axial Lagrangian strain map and the corresponding average values for three representative specimens at four selected times (t = 0, 100, 600, and 1200 s) during the 1st creep test at 1 N, 2 N, and 3 N equi-biaxial loads, respectively. The strain (average axial Lagrangian strain) during the creep test was also normalized by dividing it, at each second, by the corresponding pre-creep strain (pre-creep average axial Lagrangian strain), that is by the strain at the beginning of the creep test. This was done for each tested specimen.

Within each specimen group (group 1, group 2, or group 3), the stresses in each direction were averaged, resulting in a mean stress in the main *in vivo* loading direction and a mean stress in the perpendicular loading direction. In each specimen group, the strains along both loading directions were also averaged resulting in a mean strain in the main *in vivo* loading direction and a mean strain in the perpendicular loading direction. Next, the normalized strains in both loading directions were also analyzed at every 50 s for the entire duration (1200 s) of each creep test, that is at twenty-five time points: 0, 50, 100, 150, $\cdots$, 1200 s. A Grubb's test with $\alpha = 0.1$ was utilized to remove outliers in each specimen group based on these normalized strains. Specifically, a specimen was considered to be an outlier amongst its group if it was an outlier for over half of the twenty-five time points. By applying this test, one specimen from group 1 and one from group 3 were excluded. A Tukey's HSD test using $\alpha = 0.1$ for statistical significance was performed to compare the pre-creep strains (strains at the beginning of the creep test, that is at $t = 0$ s) and peak strains (strains at the end of the creep test, that is at $t = 1200$ s) between the two loading directions at each creep test (1st, 2nd, or 3rd creep test) and at each equi-biaxial load (1 N, 2 N, or 3 N equi-biaxial load). The same test was employed to compare the normalized strains at t = 100, 600,

and 1200 s *a*) between the two loading directions (main *in vivo* and perpendicular loading directions) at each creep test (1st, 2nd, or 3rd creep test) and at each equi-biaxial load (1 N, 2 N, or 3 N equi-biaxial load), *b*) among creep tests (1st, 2nd, and 3rd creep tests) at each equi-biaxial load (1 N, 2 N, or 3 N equi-biaxial load) and at each loading direction (main *in vivo* or perpendicular loading direction). Isochronal mean stress-strain data along the main *in vivo* and perpendicular loading directions were computed from the 1st, 2nd, and 3rd creep tests. This was done by taking the mean strains during the 1st, 2nd, and 3rd creep tests at $t = 0$, 100, 600, and 1200 s and their corresponding constant mean stresses for each specimen group. All data were analyzed using Minitab statistical software (Minitab 17, Minitab Inc.). Mean stresses, strains, and normalized strains in loading directions were reported together with the standard error of the mean (S.E.M.).

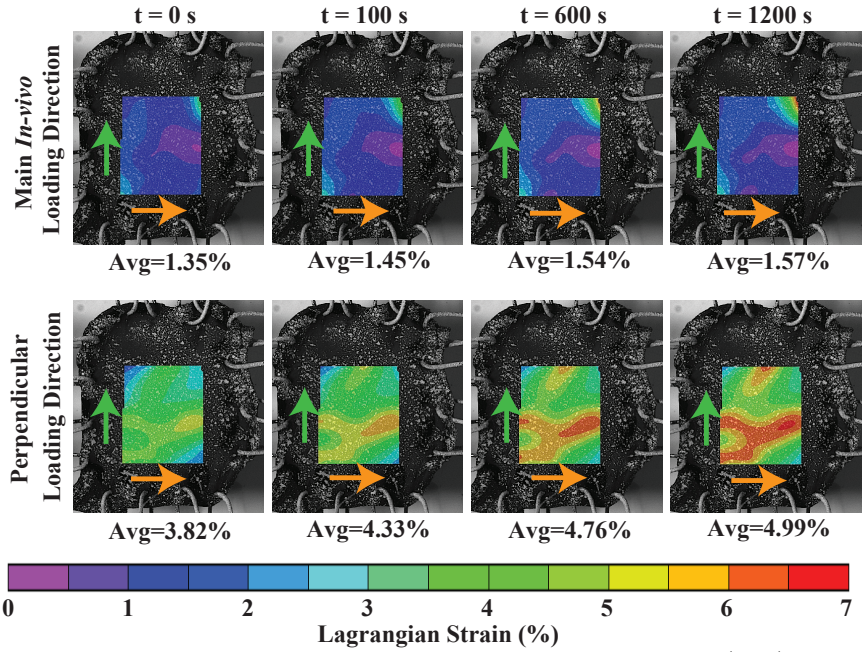

Figure 4.3: Local Lagrangian strain map and corresponding average (avg) Lagrangian strain in the main *in vivo* and perpendicular loading directions at t = 0, 100, 600, and 1200 s during the 1st creep test of a representative specimen subjected to a constant 1 N equi-biaxial load. The main *in vivo* and perpendicular loading directions are denoted with orange and green arrows, respectively.

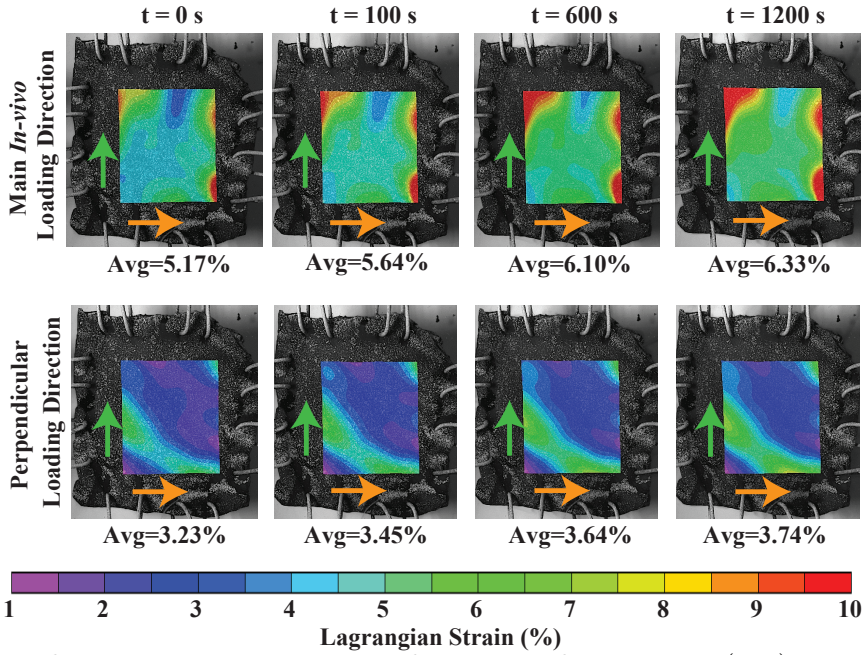

Figure 4.4: Local Lagrangian strain map and corresponding average (avg) Lagrangian strain in the main *in vivo* and perpendicular loading directions at t = 0, 100, 600, and 1200 s during the 1st creep test of a representative specimen subjected to a constant 2 N equi-biaxial load. The main *in vivo* and perpendicular loading directions are denoted with orange and green arrows, respectively.

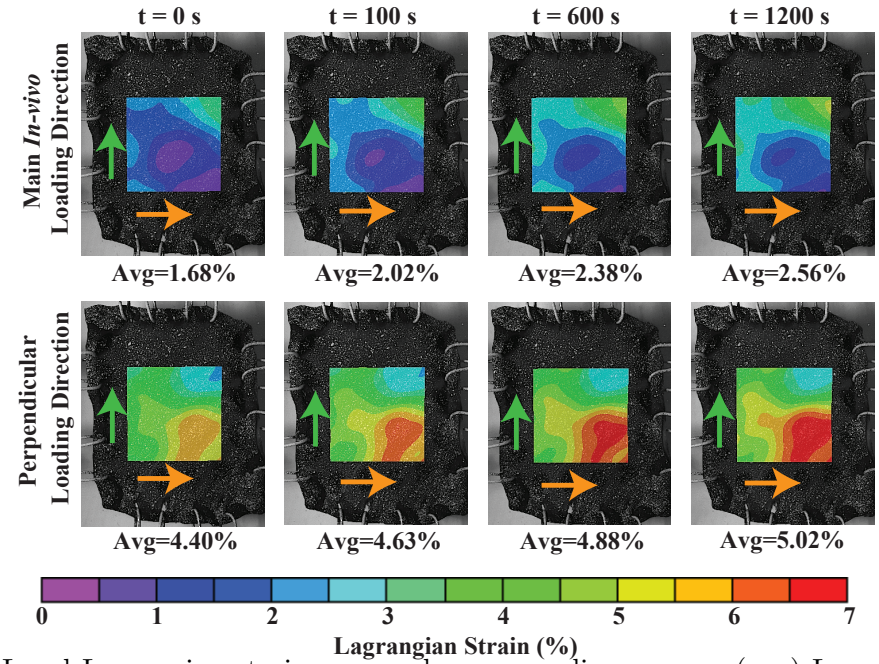

Figure 4.5: Local Lagrangian strain map and corresponding average (avg) Lagrangian strain in the main *in vivo* and perpendicular loading directions at t = 0, 100, 600, and 1200 s during the 1st creep test of a representative specimen subjected to a constant 3 N equi-biaxial load. Main *in vivo* and perpendicular loading directions are denoted with orange and green arrows, respectively.

4.4 Results

4.4.a Specimen Group 1: Pre-creep and Creep Tests at 1 N Equi-Biaxial Load

Table 4.1: Creep test parameters for group 1 specimens (n = 7, 1 N equi-biaxial load, thickness: 0.51 ± 0.07 mm, mean ± S.D.)

Mechanical Quantity	Test Order	Loading Direction	Value (Mean ± S.E.M.)
Stress (MPa)		Main *In vivo*	0.0686 ± 0.004
		Perpendicular	0.0648 ± 0.003
Pre-creep Strain (%)	1st Creep	Main *In vivo*	2.738 ± 0.757
		Perpendicular	4.909 ± 0.726
	2nd Creep	Main *In vivo*	2.283 ± 0.522
		Perpendicular	5.701 ± 1.099
	3rd Creep	Main *In vivo*	2.351 ± 0.586
		Perpendicular	5.372 ± 0.843

The mean stresses for specimens in group 1 (n = 7) subjected to creep tests at 1 N equi-biaxial load were found to be 0.0686 MPa and 0.0648 MPa in the main *in vivo* and perpendicular loading directions, respectively (Table 4.1). The mean pre-creep strain (i.e. the mean strain at the beginning of the 1st, 2nd or 3rd creep test) in the main *in vivo* loading direction was always lower than the mean pre-creep strain in the perpendicular loading direction for the 1st, 2nd or 3rd creep tests ($0.018 \leq p \leq 0.079$) (Table 4.1). The mean strain over time remained always lower in the main *in vivo* loading direction compared to the perpendicular loading direction (Figure 4.6(a)). However, for two specimens the strain was higher along the main *in vivo* loading direction during the 1st creep test and for another specimen was higher along the main *in vivo* loading direction during the 2nd creep test (Figure 4.7). As shown in Figure 4.6(a), when comparing the mean peak strains (i.e. the mean strains at the end of the creep test) between the two loading directions at the 1st, 2nd or 3rd creep test, the mean peak strain in the perpendicular loading direction was found to be always higher than the mean peak strain in the main *in vivo* loading direction ($0.016 \leq p \leq 0.077$).

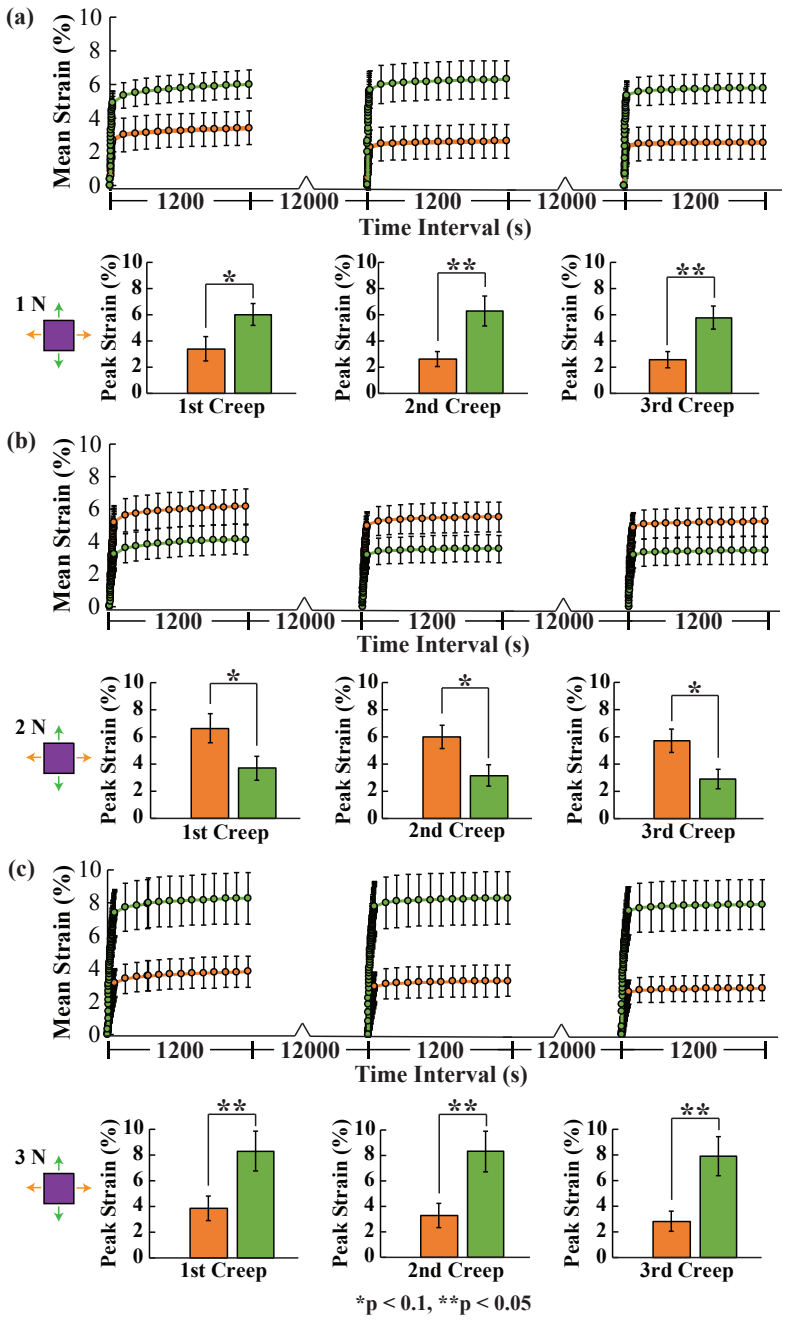

Figure 4.6: Mean strain with S.E.M. vs. time curves and box plots of peak strains for (a) specimens in group 1 subjected to 1 N equi-biaxial loads during the 1st, 2nd, and 3rd creep tests (n = 7 specimens), (b) specimens in group 2 subjected to 2 N equi-biaxial loads during the 1st, 2nd, and 3rd creep tests (n = 8 specimens), and (c) specimens in group 3 subjected to 3 N equi-biaxial loads during the 1st, 2nd, and 3rd creep tests (n = 7 specimens). The data along the main *in vivo* and the perpendicular loading directions are reported in orange and green, respectively. Specimens experienced lower strains in the main in vivo loading direction at 1 N and 3 N equi-biaxial loads, but higher strains in such direction at 2 N equi-biaxial loads.

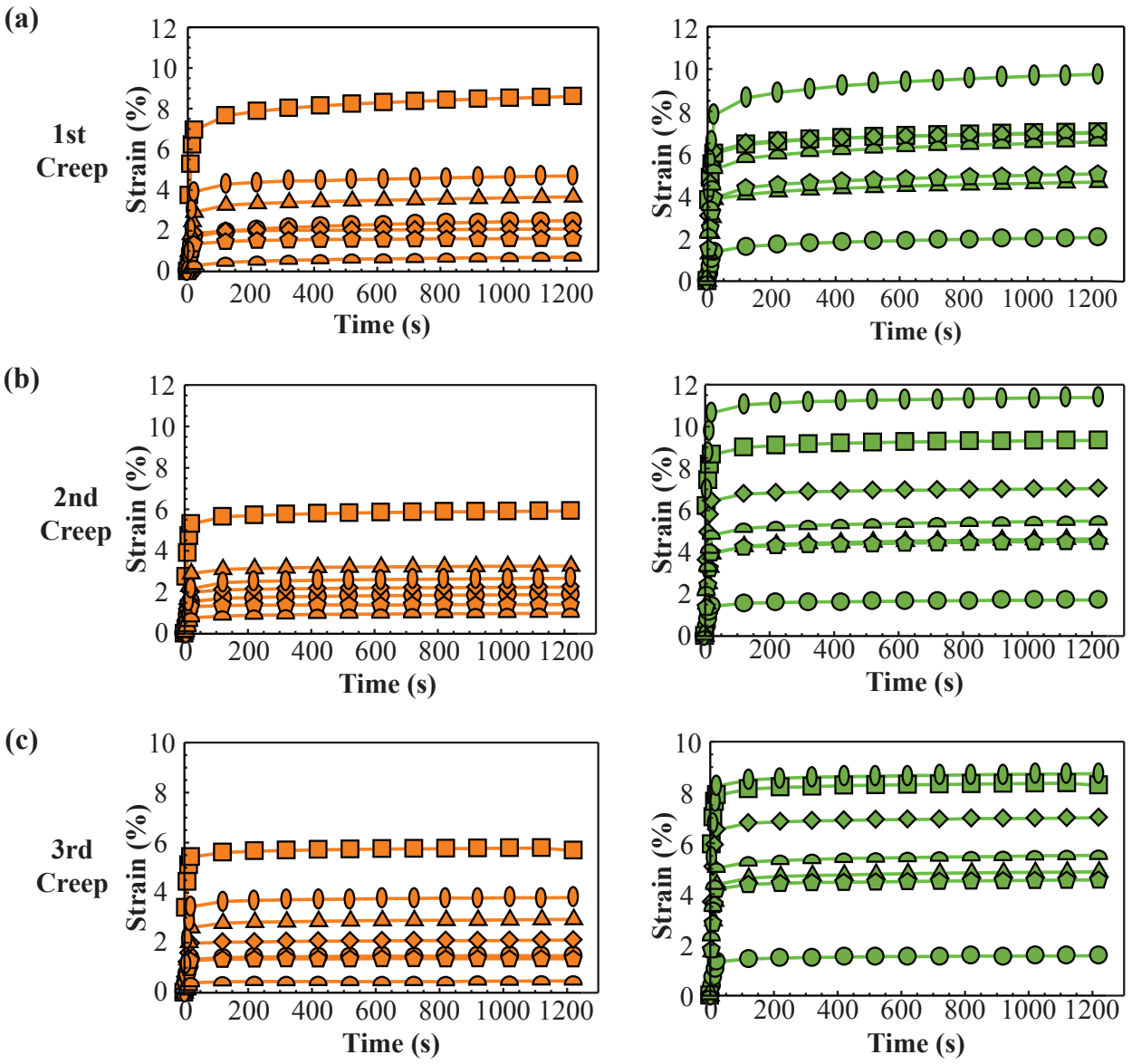

Figure 4.7: Strain vs. time curves for specimens (n = 7) in group 1 subjected to 1 N equi-biaxial loads during the (a) 1st creep test, (b) 2nd creep test, and (c) 3rd creep test. The data for each specimen are reported using the same symbol. These symbols are orange for data collected along the main *in vivo* direction and green for data collected along the perpendicular loading direction. While specimens, on average, exhibited higher strains in the perpendicular loading direction compared to the main *in vivo* loading direction (please refer to Figure 4.6(a)), this was not the case for all specimens. The specimens denoted by the circle and the square symbols exhibited higher strains in the main *in vivo* loading direction com- pared to the perpendicular loading direction for the 1st creep. For the 2nd creep, the specimen denoted by the circle symbols exhibited higher strains in the main *in vivo* loading direction compared to the perpendicular loading direction.

However, when comparing the mean peak strains among the 1st, 2nd, 3rd creep tests along the main *in vivo* loading direction or the perpendicular loading direction, no statistical differences were found ($p = 0.706$ for the main *in vivo* loading direction comparison and $p = 0.940$ for the perpendicular loading direction comparison).

The mean stress-strain data computed from specimens in group 1 during each of the three pre-creep tests are reported in Figure 4.9(a). From these mean pre-creep stress-strain curves, the CL tissue appeared to be stiffer and experienced lower strain in the main *in vivo* loading direction than in the perpendicular loading direction. The corresponding mean normalized strain vs. time data obtained during the three creep tests are shown in Figure 4.9(b). The mean normalized strains at $t = 100$, 600, 1200 s between the two loading directions were found to be not statistically different during the 1st, 2nd, or 3rd creep test ($0.293 \leq p \leq 0.989$) (Figure 4.9(b)).

While comparing the mean normalized strains across the three creep tests in the main *in vivo* or perpendicular loading direction, the mean normalized strain during the 1st creep test was greater than the mean normalized strain during the 2nd and 3rd creep tests at $t = 100$, 600, and 1200 s ($0.008 \leq p \leq 0.018$). Under constant equi-biaxial loads of 1 N, the mean normalized strain at $t = 1200$ s was approximately 1.26 times greater than the mean pre-creep strain for both the main *in vivo* and perpendicular loading directions. The 2nd creep test yielded a mean normalized strain at $t = 1200$ s approximately 1.17 and 1.31 times higher than the mean pre-creep strain in the main *in vivo* and perpendicular loading directions, respectively. After the 3rd creep test, the mean normalized strain at $t = 1200$ s was approximately 1.10 and 1.09 times higher than the mean pre-creep strain in the main *in vivo* and perpendicular loading directions, respectively. Moreover, the mean normalized strains during the 2nd and 3rd creep tests along each loading direction were not significantly different at $t = 100$, 600, and 1200 s.

4.4.b Specimen Group 2: Pre-creep and Creep Tests at 2 N Equi-Biaxial Load

Table 4.2: Creep test parameters for group 2 specimens (n = 8, 2 N equi-biaxial load, thickness (0.69 ± 0.15 mm, mean ± S.D.)

Mechanical Quantity	Test Order	Loading Direction	Value (Mean ± S.E.M.)
Stress (MPa)		Main *In vivo*	0.0924 ± 0.005
		Perpendicular	0.0898 ± 0.006
Pre-creep Strain (%)	1st Creep	Main *In vivo*	5.213 ± 0.996
		Perpendicular	2.986 ± 0.928
	2nd Creep	Main *In vivo*	4.999 ± 0.870
		Perpendicular	3.197 ± 0.767
	3rd Creep	Main *In vivo*	4.894 ± 0.869
		Perpendicular	3.172 ± 0.788

For specimens in group 2 ($n = 8$) subjected to 2 N equi-biaxial loads, the mean stresses in the main *in vivo* and perpendicular loading directions during creep were found to be 0.0924 MPa and 0.0898 MPa, respectively (Table 4.2). Unlike specimens in group 1, the mean pre-creep strain in the main *in vivo* loading direction was always higher, but not significantly higher, than the mean pre-creep strain in the perpendicular loading direction for each of the three creep tests (Table 4.2) ($0.168 \leq p \leq 0.190$). The mean strain over time continued to be higher in the main *in vivo* loading direction compared to the perpendicular loading direction (Figure 4.6(b)). This was in contrast with the findings for specimens in group 1. However, for two specimens, the strain over time was higher in the perpendicular loading direction during the three creep tests (Figure 4.8). Moreover, when comparing the mean peak strains between the two loading directions, the mean peak strain in the main *in vivo* loading direction was found to always be higher than the mean peak strain in the perpendicular loading direction for the three creep tests ($0.053 \leq p \leq 0.09$) (Figure 4.6(b)). No statistical differences were noted when the mean peak strains along the main *in vivo* or perpendicular loading direction were compared among the three creep tests at 2 N equi-biaxial loads ($p = 0.830$ for the main *in vivo* loading direction comparison and $p = 0.876$ for the perpendicular loading direction

comparison).

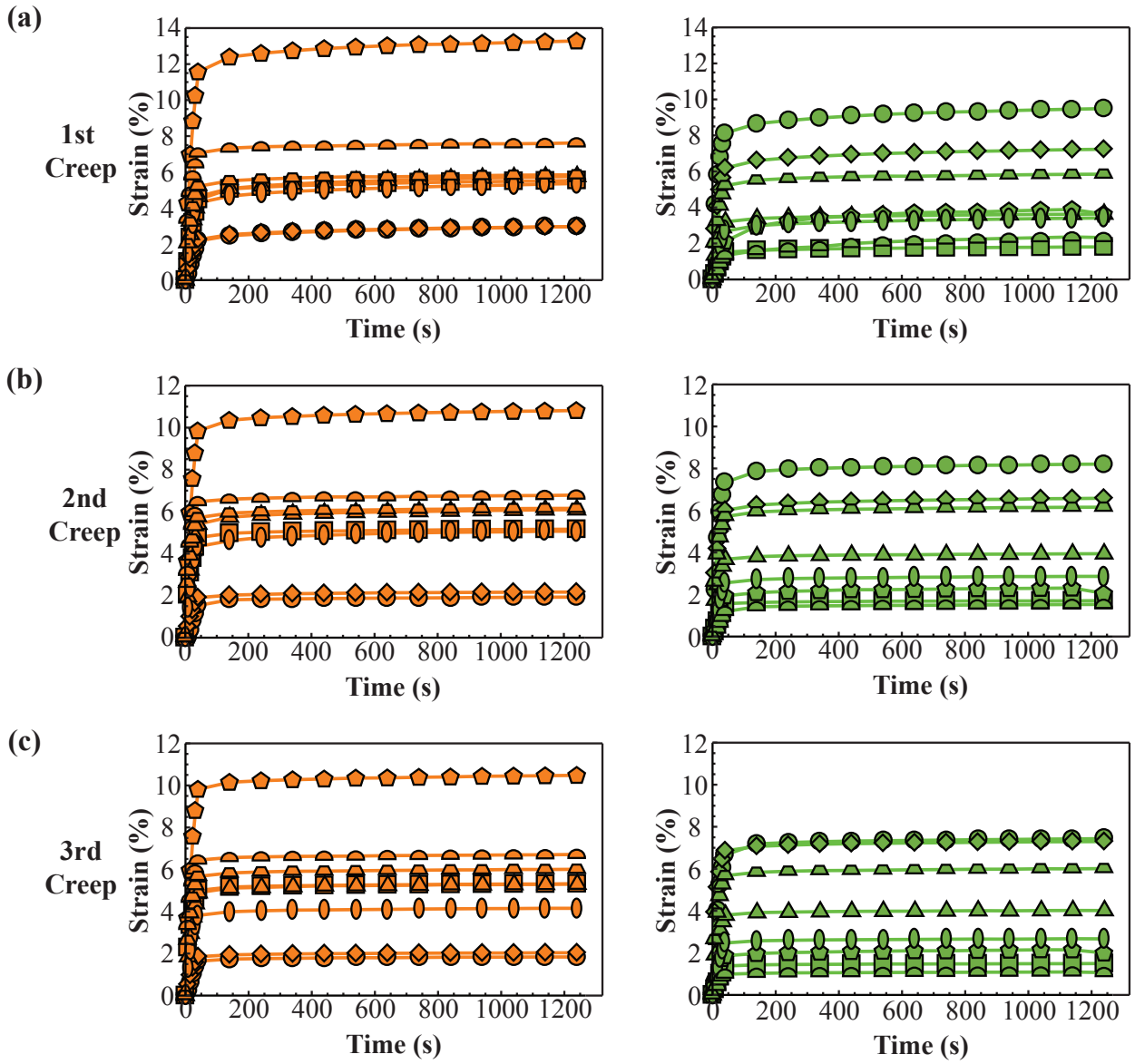

Figure 4.8: Strain vs. time curves for specimens (n = 8) in group 2 subjected to 2 N equi-biaxial loads during the (a) 1st creep test, (b) 2nd creep test, and (c) 3rd creep test. The data for each specimen are reported using the same symbol. These symbols are orange for data collected along the main *in vivo* direction and green for data collected along the perpendicular loading direction. While specimens, on average, exhibited higher strains in the main *in vivo* loading direction compared to the perpendicular loading direction (please refer to Figure 4.6(b))), this was not the case for all specimens. The specimens denoted by the circle and the diamond symbols exhibited higher strains in the perpendicular loading direction com- pared to the main in vivo loading direction for the 1st, 2nd, and 3rd creep tests.

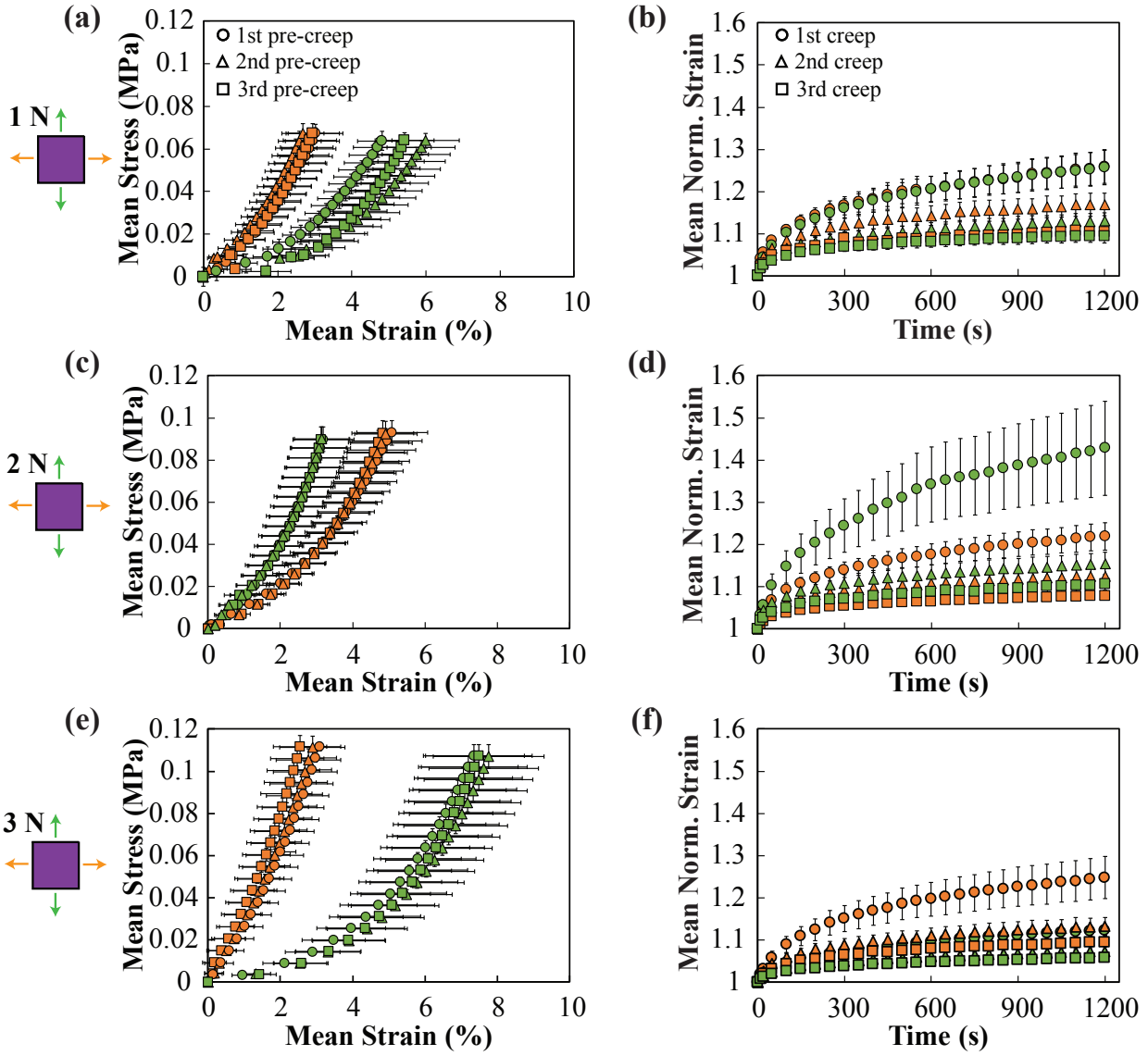

Figure 4.9: Pre-creep mean stress-strain data and corresponding mean normalized strain vs. time for (a)-(b) group 1 specimens subjected to 1 N equi-biaxial loads (mean computed over $n = 7$ specimens), (c)-(d) group 2 specimens subjected to 2 N equi-biaxial loads (mean computed over $n = 8$ specimens), and (e)-(f) group 3 specimens subjected to 3 N equi-biaxial loads (mean computed over $n = 7$ specimens). During each pre-creep test, the CL appears to be stiffer in the main *in vivo* loading direction at 1 N and 3 N equi-biaxial loads and in the perpendicular direction at 2 N equi-biaxial loads. The mean normalized strain during the 1st creep tests at any equi-biaxial load appears to be always the greatest, regardless of loading direction.

The mean stress-strain data calculated from specimens in group 2 before the creep tests are shown in Figure 4.9(c). As the stress increased, higher strains were recorded along the main *in vivo* loading direction compared to the perpendicular loading direction during each of the pre-creep tests. The corresponding mean normalized strain vs. time data recorded during the creep tests are shown in Figure 4.9(d). When comparing the mean normalized strains at $t = 100$, 600, and 1200 s as recorded during the 1st, 2nd, or 3rd creep test, no statistical differences were found between the two loading directions ($0.114 \leq p \leq 0.764$).

In each loading direction at $t = 100$ s, the mean normalized strain calculated from the 1st creep tests was not significantly different from the mean normalized strain computed from the 2nd creep tests but were greater than the mean normalized strain obtained from the 3rd creep tests ($p = 0.020$ for main *in vivo* loading direction comparison and $p = 0.046$ for perpendicular loading direction comparison). At $t = 600$ and 1200 s, the mean normalized strain calculated from the 1st creep tests was greater than both the mean normalized strains from the 2nd and 3rd creep tests ($0.002 \leq p \leq 0.005$). Thus, at constant equi-biaxial loads of 2 N, the specimens experienced always the highest increase in mean strain by the end of the 1st creep test, regardless of the loading direction. For the 1st creep tests, the mean normalized strain at $t = 1200$ s was approximately 1.22 and 1.43 times higher than the mean pre-creep strain in the main *in vivo* and perpendicular loading directions, respectively. The mean normalized strain at $t = 1200$ s for the 2nd creep tests was approximately 1.12 and 1.15 times higher than the mean pre-creep strain in the main *in vivo* and perpendicular loading directions, respectively. For the 3rd creep tests, the mean normalized strain at $t = 1200$ s was approximately 1.08 and 1.11 times higher than the mean pre-creep strain along the main *in vivo* and perpendicular loading direction, respectively. Finally, the mean normalized strains recorded during the 2nd and 3rd creep tests along the main *in vivo* or the perpendicular loading direction were not statistically different at $t = 100$, 600, and 1200 s.

4.4.c Specimen Group 3: Pre-creep and Creep Tests at 3 N Equi-Biaxial Load

Table 4.3: Creep test parameters for group 3 specimens (n = 7, 3 N equi-biaxial load, thickness: 0.98 ± 0.16 mm, mean ± S.D.)

Mechanical Quantity	Test Order	Loading Direction	Value (Mean ± S.E.M.)
Stress (MPa)		Main *In vivo*	0.112 ± 0.006
		Perpendicular	0.107 ± 0.005
Pre-creep Strain (%)	1st Creep	Main *In vivo*	3.149 ± 0.843
		Perpendicular	7.410 ± 1.400
	2nd Creep	Main *In vivo*	2.916 ± 0.899
		Perpendicular	7.798 ± 1.537
	3rd Creep	Main *In vivo*	2.587 ± 0.743
		Perpendicular	7.531 ± 1.478

For specimens in group 3 (n = 7) subjected to 3 N equi-biaxial loads, the mean stresses were determined to be 0.112 MPa and 0.107 MPa in the main *in vivo* and perpendicular loading directions, respectively (Table 4.3). As seen for specimens in group 1, the mean pre-creep strain along the main *in vivo* loading direction was also always lower than the mean pre-creep strain in the perpendicular loading direction for the 1st, 2nd, or 3rd creep tests ($0.017 \leq p \leq 0.032$) (Table 4.3). Similarly, over the duration of the creep tests, the mean strain along the main *in vivo* loading direction remained lower than the mean strain along the perpendicular loading direction (Figure 4.6(c)). However, for one specimen, the strain over time was higher in the main *in vivo* loading direction during the three creep tests (Figure 4.10). As shown in Figure 4.6(c), the mean peak strain in the perpendicular loading direction was found to always be significantly higher than the mean peak strain in the main *in vivo* loading direction for the 1st, 2nd, or 3rd creep tests ($0.018 \leq p \leq 0.043$). Again no statistical differences in the mean peak strains among the three creep tests were noted along the main *in vivo* or perpendicular loading direction ($p = 0.766$ for the main *in vivo* loading direction comparison and $p = 0.983$ for the perpendicular loading direction comparison).

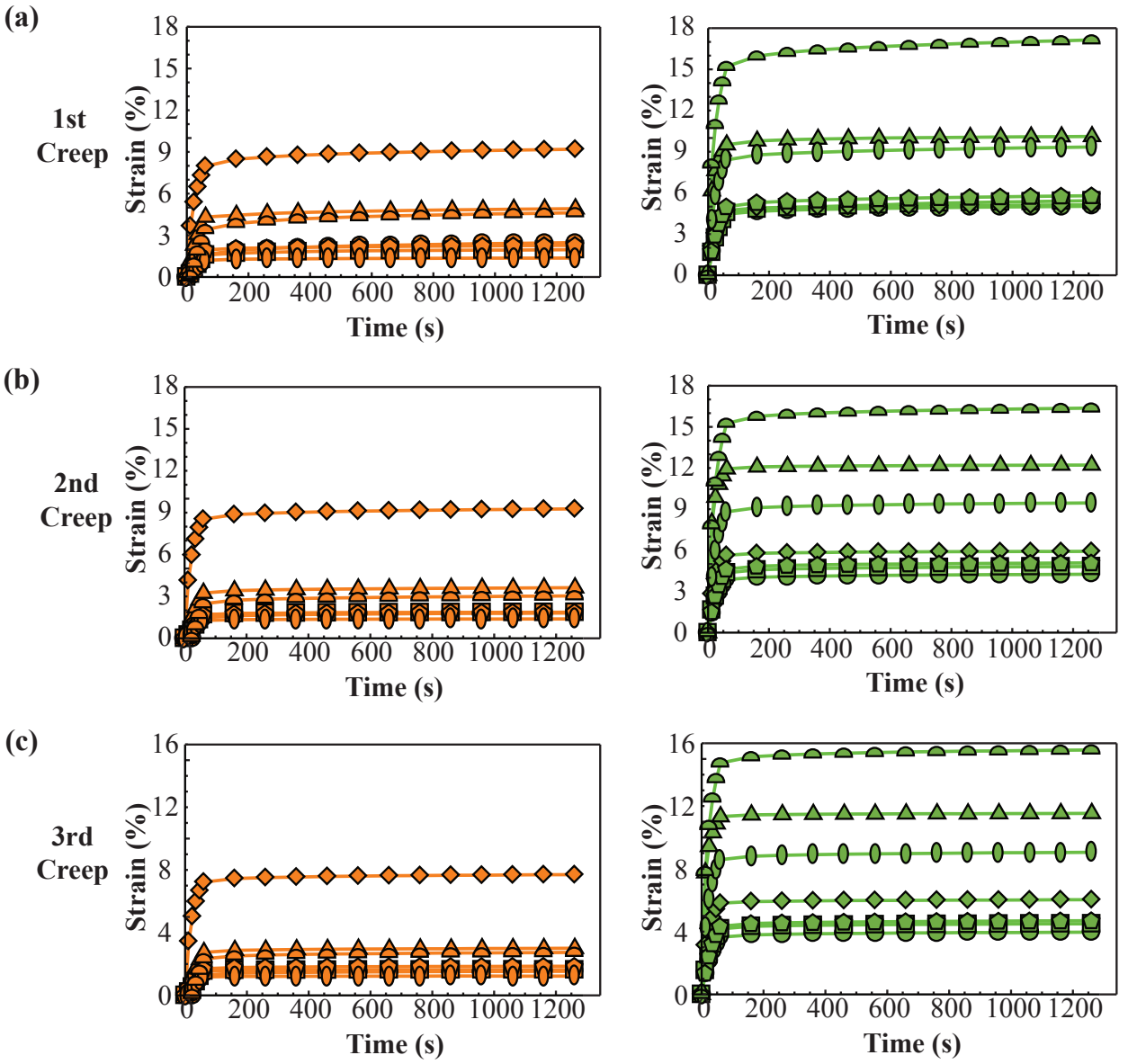

Figure 4.10: Strain vs. time curves for specimens (n = 7) in group 3 subjected to 3 N equi-biaxial loads during the (a) 1st creep test, (b) 2nd creep test, and (c) 3rd creep test. The data for each specimen are reported using the same symbol. These symbols are orange for data collected along the main *in vivo* direction and green for data collected along the perpendicular loading direction. While specimens, on average, exhibited higher strains in the perpendicular loading direction compared to the main *in vivo* loading direction (please refer to Figure 4.6(c)), this was not the case for all specimens. The specimen denoted by the diamond symbols exhibited higher strains in the main *in vivo* loading direction during the 1st, 2nd, and 3rd creep tests.

The mean stress-strain curves obtained from the data collected during the pre-creep tests for specimens in group 3 are shown in Figure 4.9(e). At equal stresses, lower strains were observed along the main *in vivo* loading direction compared to the perpendicular loading direction during each of the three pre-creep tests. The corresponding mean normalized strain vs. time data recorded during the creep tests are reported in Figure 4.9(f). Some statistical differences were found in the mean normalized strain between the two loading directions. For the 1st and 2nd creep test, statistical differences were found between the main *in vivo* and perpendicular loading directions at $t = 100$, 600, and 1200 s, with the mean normalized strain in the main *in vivo* loading direction being higher than the mean normalized strain in the perpendicular loading direction ($0.038 \leq p \leq 0.076$). For the 3rd creep test, the mean normalized strain was found to only be significantly different at $t = 100$ s ($p = 0.063$) between these directions and not statistically different at $t = 600$ and 1200 s ($0.107 \leq p \leq 0.112$).

In the main *in vivo* loading direction at $t = 100$ s, the mean normalized strains recorded during the 1st, 2nd, and 3rd creep tests were not statistically different ($p = 0.110$). At $t = 600$ and 1200 s, the mean normalized strain of the 1st creep was not significantly different than the mean normalized strain of the 2nd creep but was greater than the mean normalized strain of the 3rd creep ($0.028 \leq p \leq 0.038$). In the perpendicular direction at $t = 100$ s, the mean normalized strain of the 1st creep was not statistically different than the mean normalized strain of the 2nd creep but was greater than the mean normalized strain of the 3rd creep ($p = 0.012$). In this direction, at $t = 600$ and 1200 s, the mean normalized strain of the 1st creep test was significantly greater than the mean normalized strains of the 2nd and 3rd creep tests ($0.004 \leq p \leq 0.012$). Specifically, under constant 3 N equi-biaxial loads, the increase in strain during the 1st creep was always greater (although not always significantly greater) than the increase in strain during the 2nd or 3rd creep, regardless of the loading direction, as observed for specimens in group 1 and 2. During the 1st creep tests, the mean normalized strain at $t = 1200$ s was approximately 1.25 and 1.12 times higher than the mean pre-creep strain in the main *in vivo* and perpendicular loading directions, respectively.

For the 2nd creep test, the mean normalized strain at $t = 1200$ s was approximately 1.13 and 1.07 times higher than the mean pre-creep strain in the main *in vivo* and perpendicular loading directions, respectively. Finally, for the 3rd creep test, the mean normalized strain at $t = 1200$ s was approximately 1.09 and 1.06 times higher than the mean pre-creep strain in the main *in vivo* and perpendicular loading directions, respectively. Along each loading direction, the mean normalized strains at $t = 100$, 600, and 1200 s for the 2nd and 3rd creep tests were not statistically different.

4.4.d Isochronal Data

Isochronal mean stress-strain curves were also generated (Figure 4.11). Toward this end, the stresses in the main *in vivo* loading direction and in the perpendicular loading direction were assumed to remain constant during the 1st, 2nd, and 3rd creep tests for each tested specimen. The values of these constants are reported in Tables 4.1, 4.2, and 4.3. The mean strain values during the 1st, 2nd, and 3rd creep tests at $t = 0$, 100, 600, and 1200 s were then plotted with the corresponding constant stresses along each loading direction. The isochronal data obtained from the 1st, 2nd, and 3rd creep tests for both the main *in vivo* and perpendicular loading directions are shown in Figure 4.11(a) and 4.11(b), Figure 4.11(c) and 4.11(d), and Figure 4.11(e) and 4.11(f), respectively. It is evident from the nonlinearities of these preliminary curves that tissues exhibited a nonlinear viscoelastic behavior.

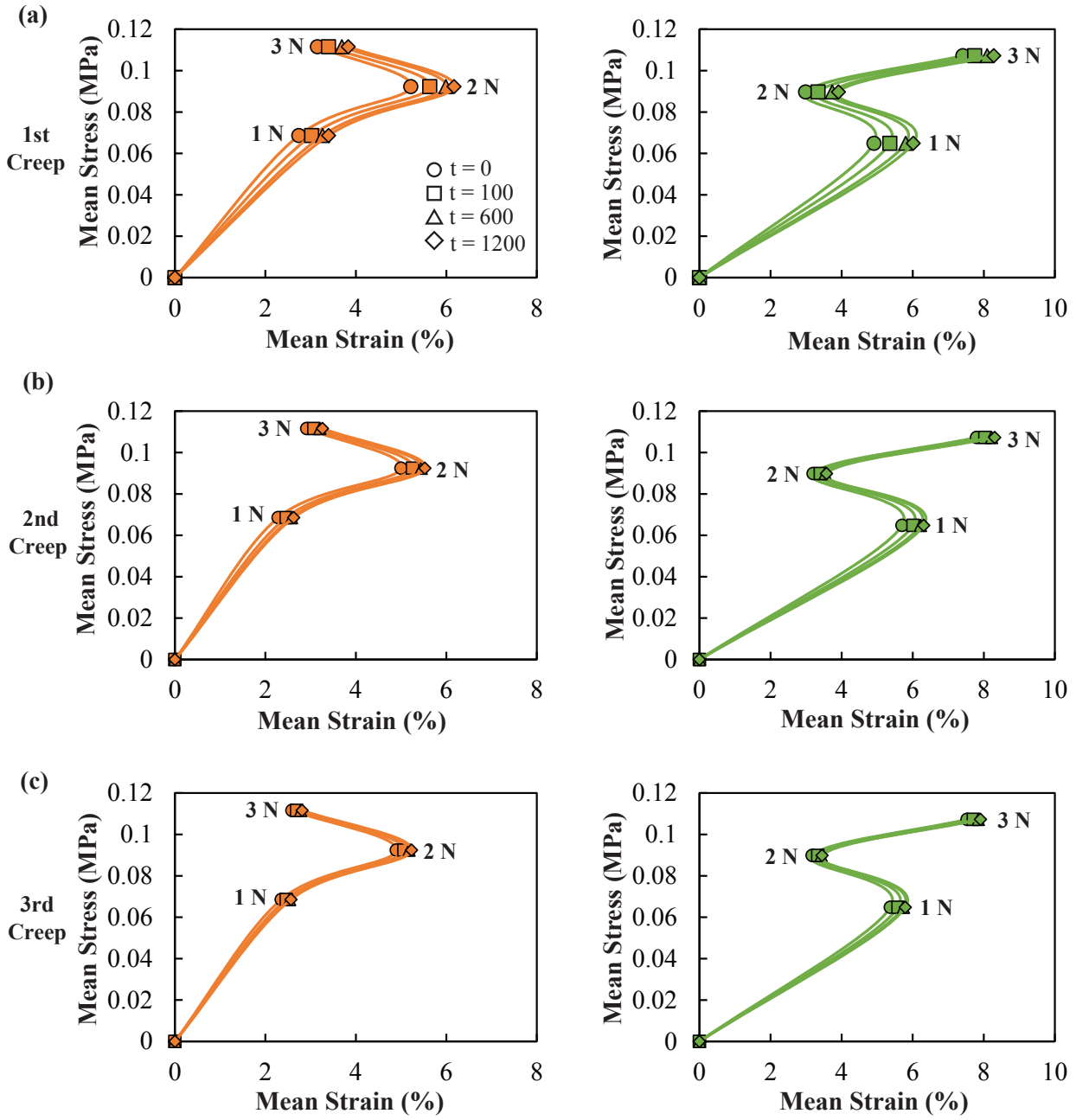

Figure 4.11: Mean isochronal stress-strain curves along the main *in vivo* loading direction (orange) and perpendicular to the main *in vivo* loading direction (green) computed from stress-strain data from specimens ($n = 22$) subjected to (a) the 1st creep tests, (b) 2nd creep tests, and (c) 3rd creep tests. The nonlinearities of these curves demonstrate the nonlinear creep behavior of the CL.

4.5 Discussion

This study focuses on characterizing the mechanical behavior of the swine CL under repeated planar biaxial loads. By subjecting the ligaments to three equi-biaxial loads, the elastic and creep properties were determined in two loading directions: the main *in vivo* and perpendicular loading directions as defined in Figure 4.2. The elastic response of the CL was found to be anisotropic, as in our previous study on the USL/CL complex [50]. On average, specimens in groups 1 and 3 were stiffer in the main in main *in vivo* loading direction while specimens in groups 2 were more compliant (although not significantly more compliant) in such direction (Figures 4.6-4.9). The peak strains, which are the strains at the end of each creep test, were also different in the two loading directions for specimens in groups 1, 2, and 3. For specimens in groups 1 and 3, the mean peak strain was higher in the perpendicular direction but, for specimens in group 2, the mean peak strain was lower in such direction (Figure 4.6). This anisotropy was most likely determined by the micro-structural organization of the ligament. SEM and histological analyses indicated that the collagen fibers in the CL were loosely organized, although they seemed to be primarily oriented in the main *in vivo* loading direction [41]. The presence of more fibers in one loading direction could have caused the specimen to be stiffer and creep less in that direction.

Clearly, the differences in results between groups 1 and 3 and group 2 on the elastic and creep properties of the CL were determined by large inter-specimen variation as discussed in detail below but, in addition to such variation, they are likely caused by large intra-specimen variation.

Figure 4.12 shows three micrographs that are obtained using a confocal microscope from the same planar section of one CL. The collagen fibers within the specimen have different organization, waviness, and orientation. Specifically, in Figure 4.12(a), collagen fibers are oriented almost along the main *in vivo* loading direction while, in Figure 4.12(b), collagen fibers are oriented along the perpendicular loading direction. Collagen fibers are also oriented

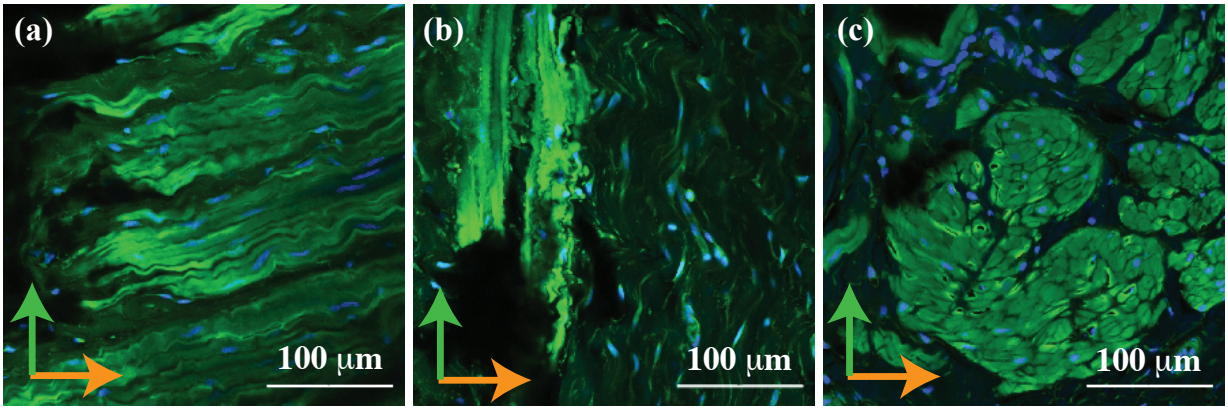

Figure 4.12: Confocal microscopy images of CL stained for collagen (in green) and nuclei (in blue) taken from the planar section of one CL in three locations, clearly showing the difference in collagen alignment and orientation. Main *in vivo* and perpendicular loading directions are denoted with orange and green arrows, respectively.

perpendicular to the planar section, as cross sections of collagen fiber bundles can be detected in Figure 4.12(c). Based on these preliminary images and our previous studies [51], although for several specimens the majority of the collagen fibers may have been oriented along the main *in vivo* loading direction, there may have been a large variation in the microstructure of the CL that led to conflicting results between groups 1 and 3 and group 2 as presented in Figure 4.9. Specimens in group 1 and 2 did not always creep less along the main *in vivo* loading direction (Figures 4.7 and 4.10) and specimens in group 2 did not always creep more in the main *in vivo* loading direction (Figure 4.8).

The mean relative increase in strain, which was measured by the mean normalized strain, was comparable during the 1st, 2nd, or 3rd creep test in the two axial loading directions for specimens in groups 1 and 2. Some differences in mean normalized strains between the loading directions were found only for specimens in group 3 during the 1st or 2nd creep test and at the beginning (t = 100 s) of the 3rd creep test. By the end of the 3rd creep test, there was no significant difference in the mean relative increase in strain between the two axial loading directions for all specimens. Other studies on relaxation and creep conducted in our lab, where the swine USL/CL complexes were subjected to single relaxation or creep tests, confirmed these findings [50, 51].

The mean relative increase in strain at the end (i.e., the mean normalized strain at $t = 1200$ s) of the 1st creep was always greater than the mean relative increase in strain at the end of the 3rd creep, regardless of the axial loading direction (main *in vivo* or perpendicular loading direction) and equi-biaxial load magnitude (1 N, 2 N, or 3 N) (Figure 4.9). This was likely due either to the exudation of water from the specimens or the occurrence of permanent deformation during the 1st or 2nd creep test. When the equi-biaxial load was applied and held constant over time during the 1st or 2nd creep test, it is possible that water was forced out of the specimen. Even though the specimen was allowed to recover before the 2nd and 3rd creep tests, the water did not fully re-enter into the specimen. This decrease in water content may have reduced the relative movement of collagen fibers within the specimen, limiting the increase in strain during the 3rd creep test. This speculation is supported by a study conducted by Thornton et al. [102] on the effect of altering water content on the creep behavior of articular ligaments. The authors found that a decrease in hydration of these ligaments led to a decrease in creep and they deduced that a less hydrated tissue had a greater resistance to creep. In our study, we may have mechanically dehydrated the tissue during the 1st or 2nd creep test and, for this reason, we obtained results that are in agreement with those by Thornton et al. during the 3rd creep tests. In another study, Thornton et al. [102–104] theorized that recruitment and straightening of the collagen fibers occurred during creep and further confirmed that collagen fiber recruitment affected the creep behavior in articular ligaments. Thus, the collagen fibers within the CL specimen may have been recruited and straightened out during the 1st or 2nd creep, inducing permanent deformation of the specimen. Once the collagen fibers were straightened, they deformed much less during the 3rd creep and, for this reason, the relative increase in strain was lower.

Overall, there was a large variability in the measured elastic and viscoelastic properties. The difference in the thickness of the specimens was a major contributing factor. Specimens were divided into three groups based on their thicknesses, with thinner specimens being tested at 1 N equi-biaxial loads and thicker specimens being tested at 2 N or 3 N equi-biaxial loads.

Thicker specimens were placed in groups 2 and 3 because they had to withstand higher loads compared to thinner specimens. It must be noted that, among the three groups, specimens in group 2 exhibited the largest amount of variability with regards to specimen thickness (Table 4.2). This variability may have accounted for the different results between specimens in groups 1, 2, and 3 along the two axial loading directions, with specimens in group 2, unlike specimens in groups 1 and 3, experiencing higher pre-creep and peak strains in the main *in vivo* loading direction and specimens in group 3 experiencing higher normalized strain in the main *in vivo* loading direction. Furthermore, the large variability could be also attributed to the collection of specimens from different swine. Indeed, the swine were not fully matched with regards to age, weight, litter size, and parity. We attempted to reduce this variability by collecting as many specimens from each sow as possible and by selecting swine that were approximately the same age (3 to 4 years old) and weight (425 to 475 lbs). However, even with this large variability, some statistical differences were detected when the mean pre-creep and peak strains between the two loading directions were compared for the 1st, 2nd, or 3rd test.

One limitation of our experimental methods was the use of safety pins to clamp the specimens. Inevitably, the pins caused local stress concentration and inhomogeneities in strain. Several experimental and numerical studies investigated boundary effects due to clamping techniques on the strain and stress fields in planar biaxial testing of soft tissues [84–88]. According to Sun et al. [86], using sutured based gripping methods, as done in our study, for biological soft tissues reduced boundary effects. Eilaghi et al. [87] found that the number of attachment points and the spacing of such attachment points greatly affected the strain uniformity within a specimen. In our study, we carefully attempted to place safety pins equidistantly on each side of the squared specimens. However, when working with thin, small, and soft specimens, ensuring that the safety pins were equidistant every time was impossible. It was also difficult to ensure that the safety pins were aligned along each edge of the specimen and were aligned on opposite sides of the specimen. Precautions were taken to minimize these effects, mainly by using a plastic grid as a guide to puncture the tissue

with the safety pins.

After the 1st or 2nd creep test, each specimen was allowed to recover for a time interval that was ten times the time interval of the creep test, that is 1200×10 s (= 200 m), before subjecting the same specimen to another creep test. This recovery time was selected based on a study conducted by Turner et al. [100] which was, however, on nonlinear viscoelastic synthetic polymers. Realistically, we could not have increased the recovery time among creep tests since the speckle pattern created on the specimen for DIC strain measurements would not have lasted longer. Although no statistical differences in the mean peak strains among the 1st, 2nd, and 3rd creep tests, along each loading direction and for each equi-biaxial load, were found (Figure 4.6), the mean normalized strain at $t = 1200$ s for the 1st and 3rd creep tests were statistically different. This indicated that, although the CL eventually reached comparable mean peak strain, in each loading direction and for each equi-biaxial load, it did not fully recover and thus was strained less after the 2nd recovery. Likely, the underlying microstructure of the ligament was altered during the 1st and 2nd creep tests and, as speculated above, water exudation and straightening of the collagen fibers may have occurred. No statistical differences were noted between the mean peak strains or normalized strains at $t = 0$, 100, 600, 1200 s along each direction during the 2nd and 3rd creep tests suggesting that, after the 2nd creep, the specimen microstructure was not altered significantly.

Isochronal stress-strain curves were generated by using only stress strain data at four time points. The nonlinearities of these curves suggested that the CL are nonlinear viscoelastic (Figure 4.11). As the number of creep tests increased, the change in strain over time decreased and the mean strain at the selected four time points became more comparable for each stress. Since there was less variation in mean strain for the 2nd and 3rd creep tests compared to the 1st creep test for each specimen group, the isochronal data from the 2nd and 3rd creep tests should be used to ascertain the nonlinear viscoelasticity of CL. More data need to be collected to draw definite conclusions on the nonlinearities of these liga-

ments. Ideally, in order to investigate the nonlinear viscoelasticity of these and other soft tissues, one should perform creep tests at different stress levels on the same specimens to minimize inter-specimen variability. This is, however, challenging because, as showed in this study, the 1st creep was always the highest, even when the magnitude of the subsequent equi-biaxial loads was not changed. It would also be important to determine the effect that the order of creep tests at different stress levels has on the changes in strain over time. Since no significant differences were observed between the 2nd and 3rd creep tests, one should maybe consider performing multiple creep tests at various stress levels starting from the 2nd creep.

In addition to the work published by our lab [41, 50, 51], a few other studies were published on the mechanical behavior of pelvic floor ligaments [44, 46–49], as summarized in Figure 4.1. Our study is, however, the first that aimed at characterizing the creep response of the CL under repeated equi-biaxial loads. Because the CL is attached to the USL at the cervix, typically both ligaments have been investigated together and have been referred to as the USL/CL complex. However, the CL is structurally and mechanically quite different from the USL [41], providing lateral support within the USL/CL complex [31, 93]. In a recent anatomical study, three (distal, intermediate, proximal) sections of the CL were detected in humans, and the distal and intermediate sections were determined to be safe for surgical use as found for the USL [28, 105]. Together with the knowledge about the anatomy, histology, and micro-structure of the CL, a better understanding of the time dependent properties of the CL can provide valuable insights into the development of effective treatment techniques for pelvic floor diseases such as POP and cervical cancer. For example, for milder cases of POP, stretching routines that control the tension/length of the ligaments and, ultimately, the support of the organs can be better designed. For invasive approaches, such as surgery, knowledge of the time-dependent properties of these ligaments may allow surgeons to establish the magnitude of the tension or to fix the length of this CL during surgical reconstruction procedures. For example, a surgeon may fix the length of the CL by taking into account the changes that will occur to this length over time under tension. In radical hysterectomy

for cervical cancer, the CL is sometimes preserved since, together with its mechanical role, it offers a neural pathway to the bladder proper function. How the material behavior of CL changes with the onset of cervical cancer should be further explored to determine its role in the treatment of cervical cancer.

4.6 Conclusions

This experimental study presents the creep properties of the swine CL subjected to repeated equi-biaxial loads. The mean pre-creep and peak strains of the CL were found to be different in the main *in vivo* and perpendicular loading directions indicating that the collagen fibers or/and other micro-structural components are oriented differently within the CL specimens or respond differently to equi-biaxial loads of different magnitude. Along each loading direction, the mean peak strains resulting from the 1 N, 2 N, or 3 N equi-biaxial loads were comparable during the 1st, 2nd, and 3rd creep tests. By the end of the 3rd creep test, no statistical differences were found in the relative increase in strain over time between the main *in vivo* and perpendicular directions. Moreover, the relative increase in strain over time during the 1st creep was always the largest (although not always significantly the largest), regardless of the loading direction and load magnitude. Some nonlinearities in the viscoelastic behavior were also observed from isochronal stress-strain data. The time-dependent response of the CL and other pelvic supportive ligaments to repeated biaxial loads should be further analyzed since these ligaments are subjected to multiple constant loads *in vivo*, especially when the muscles of the pelvic floors are damaged. Effective treatment for PFDs and cervical cancer that involve the CLs can benefit from new knowledge about the viscoelasticity of these ligaments.

5 Conclusions and Future Work

5.1 Conclusions

A direct comparison the structural and planar equi-biaxial viscoelastic properties between swine and human USL, a major suspensory ligament, were presented in Chapter 3. From the histological analysis, both swine and human USLs have similar components, with comparable collagen content, which was deduced from two different types of histological stains. While investigating the planar equi-biaxial viscoelastic behavior, no statistical differences were noted in the the Lagrangian strain achieved between the two species along both loading directions during cyclic loading, at the end of the elastic ramp, and during creep. The findings validate the use of swine as an appropriate animal model for the characterization of the USL. Since both human and swine tissues are subjected to repeated loads of different magnitudes *in vivo*, it is important to investigate this phenomena as it may affect the creep properties of these pelvic supportive ligaments.

Now having validated the use of swine as an appropriate animal model for the study of the mechanical behavior of pelvic supportive ligaments, the effects of repeated biaxial loads on the creep properties of the CL was presented in Chapter 4. The results indicate that the swine CL is anisotropic and exhibits nonlinear viscoelastic creep behavior. Also, the first creep was always the largest regardless of the loading direction and load magnitude, which was possibly due to exudation of water from the specimens during the 1st creep test. This study helps provide a better understanding of the time-dependent viscoelastic behavior of the CL and other pelvic supportive ligaments to multiple loads, as these ligaments are subjected to constant loads *in vivo*.

A better understanding of the viscoelastic behavior of the USL and CL will greatly help in the development of treatment options for POP. Now that swine has been validated as appropriate large scale animal model, further analysis can be conducted, such as more structural analysis of these ligaments or even *in vivo* mechanical characterization. Below is a description of immediate future work that could be conducted to further the knowledge of these ligaments.

5.2 Future Work

5.2.a 3D Visualization of USL and CL via Confocal Microscopy

While some work has been done to visualize the structure of these ligaments, a 3D visualization of these ligaments would give better insight into the organization and dispersion of the components within the tissue. Rezakhaniha et al. visualized collagen waviness and orientation in the arterial adventitia using confocal laser scanning microscopy [106]. Using similar methods, we will conduct immunofluorescence confocal microscopy of the USL and CL to visualize the collagen fibers and the smooth muscle cells. Figure 5.1 is a preliminary micrograph showing stained collagen fibers and nuclei in the USL. Immunofluorescence images will be taken using a confocal microscope to produce 2D images and to create a 3D reconstruction of the specimen. Using Image J, the number of smooth muscle cells will be counted and the cell density for the given volume will be calculated. Images will also be analyzed using Neuron J, a plugin in Image J, to determine the straightness of the collagen fibers within the tissue and fiber orientation with respect to the main *in vivo* loading direction as described in a previous study [51]. A straightness parameter will be defined as the ratio of the end to end distance of the fiber (L_0) and the length of the fiber (L_f).

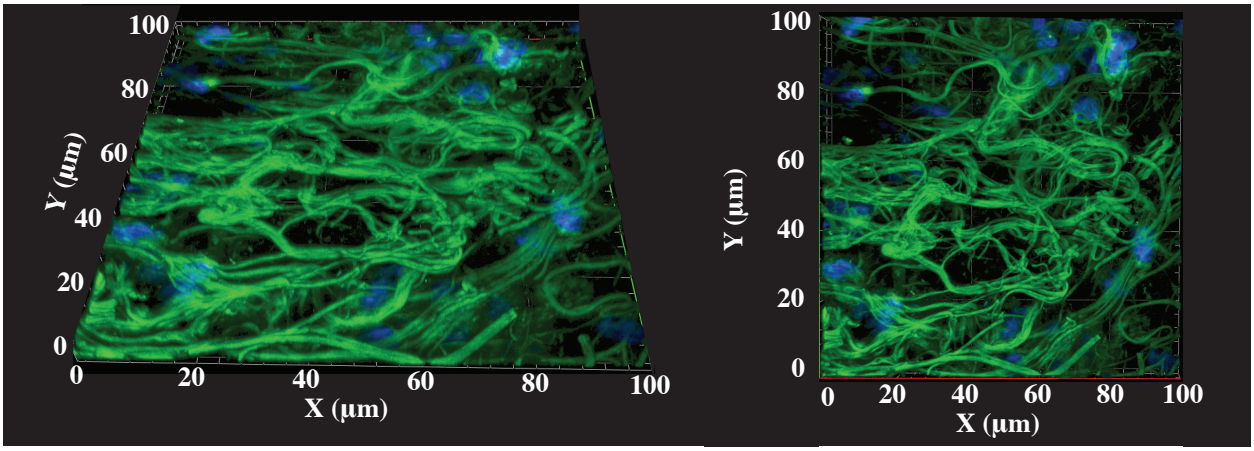

Figure 5.1: Preliminary staining of collagen and elastin fibers using Col-F binding stain, cell nuclei were stained with DAPI.

5.2.b Active Testing

Using histological analysis (Chapter 3), we have identified that the swine USL contains approximately 16 % - 35% smooth muscle. All of the mechanical tests performed in this dissertation were conducted in the passive state. With the knowledge of the smooth muscle content, future studies can be conducted with the USL in the activated state. Isometric and isotonic biaxial testing will be performed on specimens as shown in Figure 5.2 to test the USL and CL in the active state. In isometric testing, the specimen is maintained at a fixed displacement/stretch value while observing the changes in the force (Figure 5.2a). Isotonic testing consists of fixed forces being applied to the specimen while observing the change/decrease in stretch (Figure 5.2b). Isometric tests will be conducted first to determine the maximal contraction force generated by the ligaments, and that force will be taken into consideration for isotonic tests. Contraction will be induced by exposing specimens to an oxygenated Krebs solution (95% O_2 with 5% CO_2) that will be dosed with potassium chloride (KCl) to simulate different levels of contraction.

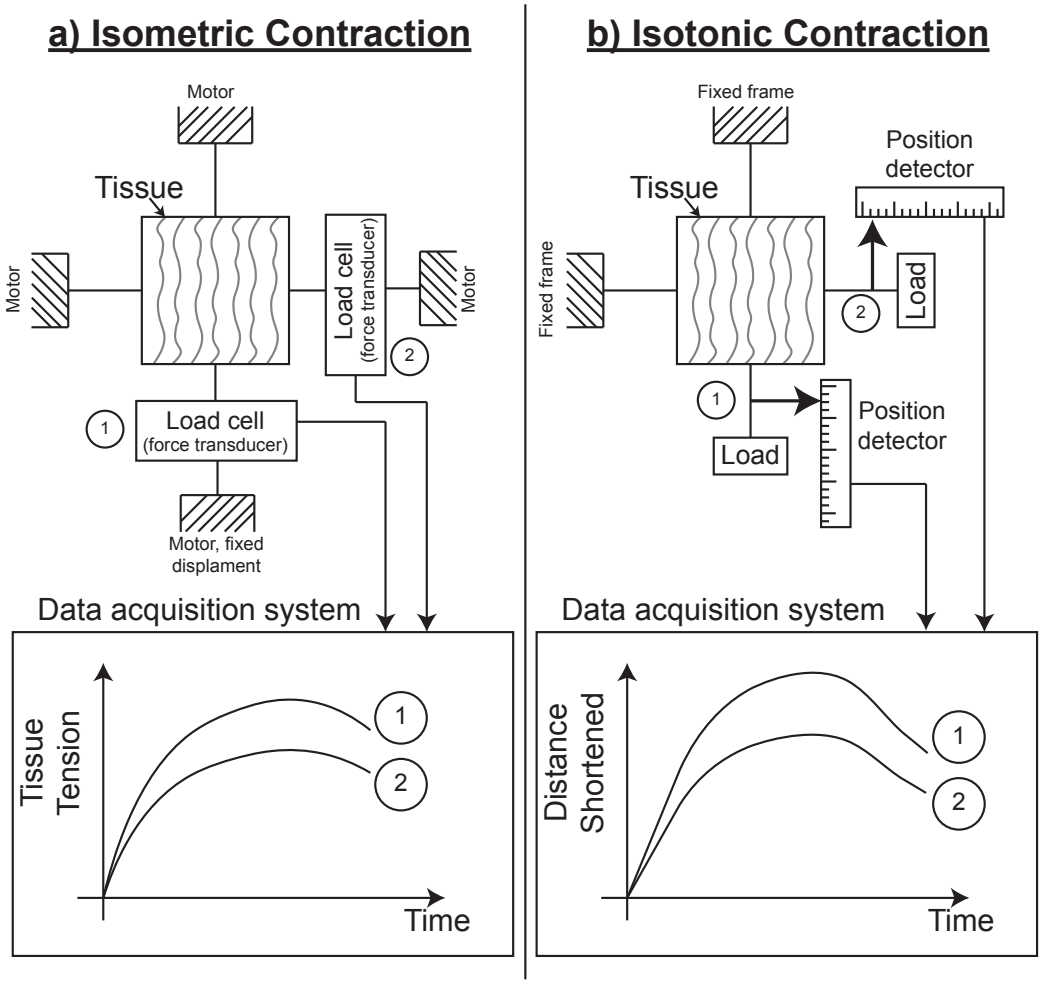

Figure 5.2: Schematic of isotonic and isometric testing in planar biaxial system. During isometric testing, displacement in 2 directions is held constant and the tension experienced in the tissue is recorded over time. During isotonic testing constant forces are applied in 2 directions and the shortened distance due to contraction is recorded over time.

Bibliography

[1] Nygaard, I., Barber, M. D., Burgio, K. L., Kenton, K., Meikle, S., Schaffer, J., Spino, C., Whitehead, W. E., Wu, J., Brody, D. J., et al., 2008. "Prevalence of symptomatic pelvic floor disorders in US women". *JAMA,* **300**(11), pp. 1311–1316.

[2] Hendrix, S. L., Clark, A., Nygaard, I., Aragaki, A., Barnabei, V., and McTiernan, A., 2002. "Pelvic organ prolapse in the women's health initiative: Gravity and gravidity". *American Journal of Obstetrics and Gynecology,* **186**(6), pp. 1160–1166.

[3] Swift, S., Woodman, P., O'boyle, A., Kahn, M., Valley, M., Bland, D., Wang, W., and Schaffer, J., 2005. "Pelvic organ support study (posst): The distribution, clinical definition, and epidemiologic condition of pelvic organ support defects". *American Journal of Obstetrics and Gynecology,* **192**(3), pp. 795–806.

[4] Wu, J. M., Vaughan, C. P., Goode, P. S., Redden, D. T., Burgio, K. L., Richter, H. E., and Markland, A. D., 2014. "Prevalence and trends of symptomatic pelvic floor disorders in us women". *Obstetrics and Gynecology,* **123**(1), p. 141.

[5] Haylen, B. T., De Ridder, D., Freeman, R. M., Swift, S. E., Berghmans, B., Lee, J., Monga, A., Petri, E., Rizk, D. E., Sand, P. K., et al., 2010. "An international urogynecological association (iuga)/international continence society (ics) joint report on the terminology for female pelvic floor dysfunction". *International Urogynecology Journal,* **21**(1), pp. 5–26.

[6] Price, D. M., Lane, F. L., Craig, J. B., Nistor, G., Motakef, S., Pham, Q.-A., and Keirstead, H., 2014. "The effect of age and medical comorbidities on in vitro myoblast expansion in women with and without pelvic organ prolapse". *Female Pelvic Medicine & Reconstructive Surgery,* **20**(5), pp. 281–286.

[7] Lukacz, E. S., Lawrence, J. M., Contreras, R., Nager, C. W., and Luber, K. M., 2006. "Parity, mode of delivery, and pelvic floor disorders". *Obstetrics & Gynecology,* **107**(6), pp. 1253–1260.

[8] Kasturi, S., Bentley-Taylor, M., Woodman, P. J., Terry, C. L., and Hale, D. S., 2012. "High uterosacral ligament vaginal vault suspension: Comparison of absorbable vs. permanent suture for apical fixation". *International Urogynecology Journal,* **23**(7), pp. 941–945.

[9] Jeffery, S. T., Doumouchtsis, S. K., Franco, A. V., and Fynes, M. M., 2009. "High uterosacral ligament vault suspension at vaginal hysterectomy: Objective and subjective outcomes of a modified technique". *Journal of Obstetrics and Gynaecology Research,* **35**(3), pp. 539–544.

[10] Edenfield, A. L., Amundsen, C. L., Weidner, A. C., Wu, J. M., George, A., and Siddiqui, N. Y., 2013. "Vaginal prolapse recurrence after uterosacral ligament suspension in normal-weight compared with overweight and obese women". *Obstetrics & Gynecology,* **121**(3), pp. 554–559.

[11] Frankman, E. A., Alperin, M., Sutkin, G., Meyn, L., and Zyczynski, H. M., 2013. "Mesh exposure and associated risk factors in women undergoing transvaginal prolapse repair with mesh". *Obstetrics and Gynecology International,* **2013**.

[12] Collinet, P., Belot, F., Debodinance, P., Duc, E. H., Lucot, J.-P., and Cosson, M., 2006. "Transvaginal mesh technique for pelvic organ prolapse repair: mesh exposure management and risk factors". *International Urogynecology Journal,* **17**(4), pp. 315–

320.

[13] Maher, C. M., Feiner, B., Baessler, K., and Glazener, C. M., 2011. "Surgical management of pelvic organ prolapse in women: The updated summary version cochrane review". *International Urogynecology Journal,* **22**(11), pp. 1445–1457.

[14] Heinonen, P., Aaltonen, R., Joronen, K., and Ala-Nissilä, S., 2016. "Long-term outcome after transvaginal mesh repair of pelvic organ prolapse". *International Urogynecology Journal,* **27**(7), pp. 1069–1074.

[15] Ellington, D. R., and Richter, H. E., 2013. "Indications, contraindications, and complications of mesh in surgical treatment of pelvic organ prolapse". *Clinical Obstetrics and Gynecology,* **56**(2), p. 276.

[16] Zuckerman, D. M., Brown, P., and Nissen, S. E., 2011. "Medical device recalls and the fda approval process". *Archives of Internal Medicine,* **171**(11), pp. 1006–1011.

[17] Ostergard, D. R., 2007. "Lessons from the past: directions for the future". *International Urogynecology Journal,* **18**(6), pp. 591–598.

[18] DeLancey, J. O., 1992. "Anatomie aspects of vaginal eversion after hysterectomy". *American Journal of Obstetrics and Gynecology,* **166**(6), pp. 1717–1728.

[19] Wei, J. T., and De Lancey, J. O., 2004. "Functional anatomy of the pelvic floor and lower urinary tract". *Clinical Obstetrics and Gynecology,* **47**(1), pp. 3–17.

[20] Drews, U., Renz, M., Busch, C., and Reisenauer, C., 2012. "Ex vivo pharmacology of surgical samples of the uterosacral ligament. part i: Effects of carbachol and oxytocin on smooth muscle". *Neurourology and Urodynamics,* **31**(8), pp. 1294–1299.

[21] Reisenauer, C., Shiozawa, T., Oppitz, M., Busch, C., Kirschniak, A., Fehm, T., and Drews, U., 2008. "The role of smooth muscle in the pathogenesis of pelvic organ prolapse?an immunohistochemical and morphometric analysis of the cervical third of

the uterosacral ligament". *International Urogynecology Journal,* **19**(3), pp. 383–389.

[22] Mei, S., Ye, M., Gil, L., Zhang, J., Zhang, Y., Candiotti, K., and Takacs, P., 2013. "The role of smooth muscle cells in the pathophysiology of pelvic organ prolapse". *Female Pelvic Medicine & Reconstructive Surgery,* **19**(5), pp. 254–259.

[23] Takacs, P., Nassiri, M., Gualtieri, M., Candiotti, K., and Medina, C. A., 2009. "Uterosacral ligament smooth muscle cell apoptosis is increased in women with uterine prolapse". *Reproductive Sciences,* **16**(5), pp. 447–452.

[24] Ramanah, R., Berger, M. B., Parratte, B. M., and DeLancey, J. O., 2012. "Anatomy and histology of apical support: A literature review concerning cardinal and uterosacral ligaments". *International Urogynecology Journal,* **23**(11), pp. 1483–1494.

[25] Blaisdell, F. E., 1917. "The anatomy of the sacro-uterine ligaments". *The Anatomical Record,* **12**(1), pp. 1–42.

[26] Fothergill, W. E., 1908. "The supports of the pelvic viscera: a review of some recent contributions to pelvic anatomy, with a clinical introduction.". *BJOG: An International Journal of Obstetrics & Gynaecology,* **13**(1), pp. 18–28.

[27] Campbell, R. M., 1950. "The anatomy and histology of the sacrouterine ligaments". *American Journal of Obstetrics and Gynecology,* **59**(1), pp. 1–12.

[28] Buller, J. L., Thompson, J. R., Cundiff, G. W., Sullivan, L. K., Ybarra, M. A. S., and Bent, A. E., 2001. "Uterosacral ligament: Description of anatomic relationships to optimize surgical safety". *Obstetrics & Gynecology,* **97**(6), pp. 873–879.

[29] Mackenrodt, A., 1895. "Ueber die ursachen der normalen und pathologischen lagen des uterus". *Archives of Gynecology and Obstetrics,* **48**(3), pp. 393–421.

[30] Range, R. L., and Woodburne, R. T., 1964. "The gross and microscopic anatomy of the transverse cervical ligament". *American Journal of Obstetrics and Gynecology,*

90(4), pp. 460–467.

[31] Samaan, A., Vu, D., Haylen, B. T., and Tse, K., 2014. "Cardinal ligament surgical anatomy: Cardinal points at hysterectomy". *International Urogynecology Journal,* **25**(2), pp. 189–195.

[32] Cole, E. E., Leu, P. B., Gomelsky, A., Revelo, P., Shappell, H., Scarpero, H. M., and Dmochowski, R. R., 2006. "Histopathological evaluation of the uterosacral ligament: is this a dependable structure for pelvic reconstruction?". *BJU International,* **97**(2), pp. 345–348.

[33] Kato, T., Murakami, G., and Yabuki, Y., 2002. "Does the cardinal ligament of the uterus contain a nerve that should be preserved in radical hysterectomy?". *Anatomical Science International,* **77**(3), pp. 161–168.

[34] Butler-Manuel, S. A., Buttery, L. D., A'Hern, R. P., Polak, J. M., and Barton, D. P., 2000. "Pelvic nerve plexus trauma at radical hysterectomy and simple hysterectomy". *Cancer,* **89**(4), pp. 834–841.

[35] Butler-Manuel, S. A., Buttery, L. D., Polak, J. M., A'Hern, R., and Barton, D. P., 2008. "Autonomic nerve trauma at radical hysterectomy: The nerve content and subtypes within the superficial and deep uterosacral ligaments". *Reproductive Sciences,* **15**(1), pp. 91–96.

[36] Gabriel, B., Denschlag, D., Göbel, H., Fittkow, C., Werner, M., Gitsch, G., and Watermann, D., 2005. "Uterosacral ligament in postmenopausal women with or without pelvic organ prolapse". *International Urogynecology Journal,* **16**(6), pp. 475–479.

[37] Gabriel, B., Watermann, D., Hancke, K., Gitsch, G., Werner, M., Tempfer, C., and Zur Hausen, A., 2006. "Increased expression of matrix metalloproteinase 2 in uterosacral ligaments is associated with pelvic organ prolapse". *International Urogynecology Journal,* **17**(5), pp. 478–482.

[38] Ewies, A. A., Al-Azzawi, F., and Thompson, J., 2003. "Changes in extracellular matrix proteins in the cardinal ligaments of post-menopausal women with or without prolapse: a computerized immunohistomorphometric analysis". *Human Reproduction,* **18**(10), pp. 2189–2195.

[39] Ewies, A. A., Thompson, J., and Al-Azzawi, F., 2004. "Changes in gonadal steroid receptors in the cardinal ligaments of prolapsed uteri: Immunohistomorphometric data". *Human Reproduction,* **19**(7), pp. 1622–1628.

[40] Gruber, D. D., Warner, W. B., Lombardini, E. D., Zahn, C. M., and Buller, J. L., 2011. "Anatomical and histological examination of the porcine vagina and supportive structures: In search of an ideal model for pelvic floor disorder evaluation and management". *Female Pelvic Medicine & Reconstructive Surgery,* **17**(3), pp. 110–114.

[41] Tan, T., Davis, F. M., Gruber, D. D., Massengill, J. C., Robertson, J. L., and De Vita, R., 2015. "Histo-mechanical properties of the swine cardinal and uterosacral ligaments". *Journal of the Mechanical Behavior of Biomedical Materials,* **42**, pp. 129–137.

[42] Iwanaga, R., Orlicky, D. J., Arnett, J., Guess, M. K., Hurt, K. J., and Connell, K. A., 2016. "Comparative histology of mouse, rat, and human pelvic ligaments". *International Urogynecology Journal*, pp. 1–8.

[43] Cosson, M., Boukerrou, M., Lacaze, S., Lambaudie, E., Fasel, J., Mesdagh, H., Lobry, P., and Ego, A., 2003. "A study of pelvic ligament strength". *European Journal of Obstetrics & Gynecology and Reproductive Biology,* **109**(1), pp. 80–87.

[44] Reay Jones, N. H. J., Healy, J. C., King, L. J., Saini, S., Shousha, S., and Allen-Mersh, T. G., 2003. "Pelvic connective tissue resilience decreases with vaginal delivery, menopause and uterine prolapse". *British Journal of Surgery,* **90**(4), pp. 466–472.

[45] Moalli, P. A., Howden, N. S., Lowder, J. L., Navarro, J., Debes, K. M., Abramowitch, S. D., and Woo, S. L., 2005. "A rat model to study the structural properties of the

vagina and its supportive tissues". *American Journal of Obstetrics and Gynecology,* **192**(1), pp. 80–88.

[46] Vardy, M. D., Gardner, T. R., Cosman, F., Scotti, R. J., Mikhail, M. S., Preiss-Bloom, A. O., Williams, J. K., Cline, J. M., and Lindsay, R., 2005. "The effects of hormone replacement on the biomechanical properties of the uterosacral and round ligaments in the monkey model". *American Journal of Obstetrics and Gynecology,* **192**(5), pp. 1741–1751.

[47] Rivaux, G., Rubod, C., Dedet, B., Brieu, M., Gabriel, B., and Cosson, M., 2013. "Comparative analysis of pelvic ligaments: A biomechanics study". *International Urogynecology Journal,* **24**(1), pp. 135–139.

[48] Martins, P., Silva-Filho, A. L., Fonseca, A. M., Santos, A., Santos, L., Mascarenhas, T., Jorge, R. M., and Ferreira, A. M., 2013. "Strength of round and uterosacral ligaments: A biomechanical study". *Archives of Gynecology and Obstetrics,* **287**(2), pp. 313–318.

[49] Chantereau, P., Brieu, M., Kammal, M., Farthmann, J., Gabriel, B., and Cosson, M., 2014. "Mechanical properties of pelvic soft tissue of young women and impact of aging". *International Urogynecology Journal,* **25**(11), pp. 1547–1553.

[50] Becker, W. R., and De Vita, R., 2015. "Biaxial mechanical properties of swine uterosacral and cardinal ligaments". *Biomechanics and Modeling in Mechanobiology,* **14**(3), pp. 549–560.

[51] Tan, T., Cholewa, N. M., Case, S. W., and De Vita, R., 2016. "Micro-structural and biaxial creep properties of the swine uterosacral–cardinal ligament complex". *Annals of Biomedical Engineering,* **44**(11), pp. 3225–3237.

[52] Couri, B. M., Lenis, A. T., Borazjani, A., Paraiso, M. F. R., and Damaser, M. S., 2012. "Animal models of female pelvic organ prolapse: Lessons learned". *Expert Review of Obstetrics & Gynecology,* **7**(3), pp. 249–260.

[53] Smith, T. M., Luo, J., Hsu, Y., Ashton-Miller, J., and Delancey, J. O., 2013. "A novel technique to measure in vivo uterine suspensory ligament stiffness". *American Journal of Obstetrics and Gynecology,* **209**(5), pp. 484–e1.

[54] Luo, J., Smith, T. M., Ashton-Miller, J. A., and DeLancey, J. O., 2014. "In vivo properties of uterine suspensory tissue in pelvic organ prolapse". *Journal of Biomechanical Engineering,* **136**(2), p. 021016.

[55] Samuelsson, E. C., Victor, F. A., Tibblin, G., and Svärdsudd, K. F., 1999. "Signs of genital prolapse in a swedish population of women 20 to 59 years of age and possible related factors". *American Journal of Obstetrics and Gynecology,* **180**(2), pp. 299–305.

[56] Wu, J. M., Hundley, A. F., Fulton, R. G., and Myers, E. R., 2009. "Forecasting the prevalence of pelvic floor disorders in US women: 2010 to 2050". *Obstetrics & Gynecology,* **114**(6), pp. 1278–1283.

[57] Jelovsek, J. E., and Barber, M. D., 2006. "Women seeking treatment for advanced pelvic organ prolapse have decreased body image and quality of life". *American Journal of Obstetrics and Gynecology,* **194**(5), pp. 1455–1461.

[58] Lowder, J. L., Ghetti, C., Nikolajski, C., Oliphant, S. S., and Zyczynski, H. M., 2011. "Body image perceptions in women with pelvic organ prolapse: a qualitative study". *American Journal of Obstetrics and Gynecology,* **204**(5), pp. 441–e1.

[59] Olsen, A. L., Smith, V. J., Bergstrom, J. O., Colling, J. C., and Clark, A. L., 1997. "Epidemiology of surgically managed pelvic organ prolapse and urinary incontinence". *Obstetrics & Gynecology,* **89**(4), pp. 501–506.

[60] Togami, J. M., Brown, E., and Winters, J. C., 2012. "Vaginal mesh–the controversy". *F1000 medicine reports,* **4**.

[61] Feiner, B., Jelovsek, J., and Maher, C., 2009. "Efficacy and safety of transvaginal mesh

kits in the treatment of prolapse of the vaginal apex: a systematic review". *BJOG: An International Journal of Obstetrics & Gynaecology,* **116**(1), pp. 15–24.

[62] Baah-Dwomoh, A., McGuire, J., Tan, T., and De Vita, R., 2016. "Mechanical properties of female reproductive organs and supporting connective tissues: A review of the current state of knowledge". *Applied Mechanics Reviews,* **68**(6), p. 060801.

[63] Baah-Dwomoh, A., and De Vita, R., 2017. "Effects of repeated biaxial loads on the creep properties of cardinal ligaments". *Journal of the Mechanical Behavior of Biomedical Materials,* **74**, pp. 128–141.

[64] Lehr, H.-A., van der Loss, C. M., Teeling, P., and Gown, A. M., 1999. "Complete chromogen separation and analysis in double immunohistochemical stains using photoshop-based image analysis". *Journal of Histochemistry & Cytochemistry,* **47**(1), pp. 119–125.

[65] Lionello, G., Sirieix, C., and Baleani, M., 2014. "An effective procedure to create a speckle pattern on biological soft tissue for digital image correlation measurements". *Journal of the Mechanical Behavior of Biomedical Materials,* **39**, pp. 1–8.

[66] Hingorani, R. V., Provenzano, P. P., Lakes, R. S., Escarcega, A., and Vanderby Jr, R., 2004. "Nonlinear viscoelasticity in rabbit medial collateral ligament". *Annals of Biomedical Engineering,* **32**(2), pp. 306–312.

[67] Bancroft, J. D., and Gamble, M., 2008. *Theory and Practice of Histological Techniques.* Elsevier Health Sciences.

[68] Kielty, C. M., Sherratt, M. J., and Shuttleworth, C. A., 2002. "Elastic fibres". *Journal of cell science,* **115**(14), pp. 2817–2828.

[69] Fung, Y.-c., 1993. *Biomechanics: Mechanical Properties of Living Tissues.* Springer Science & Business Media.

[70] Fung, Y., 1967. "Elasticity of soft tissues in simple elongation". *American Journal of*

Physiology–Legacy Content, **213**(6), pp. 1532–1544.

[71] Fung, Y.-C. B., 1973. "Biorheology of soft tissues 1". *Biorheology,* **10**(2), pp. 139–155.

[72] Pinto, J., and Patitucci, P., 1980. "Visco-elasticity of passive cardiac muscle". *Journal of Biomechanical Engineering,* **102**(1), pp. 57–61.

[73] Woo, S., 1982. "Mechanical properties of tendons and ligaments. i. quasi-static and nonlinear viscoelastic properties.". *Biorheology,* **19**(3), p. 385.

[74] Cheng, S., Clarke, E. C., and Bilston, L. E., 2009. "The effects of preconditioning strain on measured tissue properties". *Journal of Biomechanics,* **42**(9), pp. 1360–1362.

[75] Carew, E. O., Barber, J., and Vesely, I., 2000. "Role of preconditioning and recovery time in repeated testing of aortic valve tissues: validation through quasilinear viscoelastic theory". *Annals of Biomedical Engineering,* **28**(9), pp. 1093–1100.

[76] Carew, E. O., Garg, A., Barber, J. E., and Vesely, I., 2004. "Stress relaxation preconditioning of porcine aortic valves". *Annals of Biomedical Engineering,* **32**(4), pp. 563–572.

[77] Bate-Smith, E., and Bendall, J., 1949. "Factors determining the time course of rigor mortis". *The Journal of Physiology,* **110**(1-2), pp. 47–65.

[78] Bate-Smith, E., and Bendall, J., 1956. "Changes in muscle after death". *British Medical Bulletin,* **12**(3), pp. 230–235.

[79] Ota, S., Furuya, Y., and Shintaku, K., 1973. "Studies on rigor mortis". *Forensic Science,* **2**, pp. 207–219.

[80] Krompecher, T., 1981. "Experimental evaluation of rigor mortis v. effect of various temperatures on the evolution of rigor mortis". *Forensic Science International,* **17**(1), pp. 19–26.

[81] Kobayashi, M., Takatori, T., Iwadate, K., and Nakajima, M., 1996. "Reconsideration of the sequence of rigor mortis through postmortem changes in adenosine nucleotides and lactic acid in different rat muscles". *Forensic Science International,* **82**(3), pp. 243–253.

[82] Kobayashi, M., Takatori, T., Nakajima, M., Saka, K., Iwase, H., Nagao, M., Niijima, H., and Matsuda, Y., 1999. "Does the sequence of onset of rigor mortis depend on the proportion of muscle fibre types and on intra-muscular glycogen content?". *International Journal of Legal Medicine,* **112**(3), pp. 167–171.

[83] Giles, J. M., Black, A. E., and Bischoff, J. E., 2007. "Anomalous rate dependence of the preconditioned response of soft tissue during load controlled deformation". *Journal of Biomechanics,* **40**(4), pp. 777–785.

[84] Waldman, S. D., and Lee, J. M., 2002. "Boundary conditions during biaxial testing of planar connective tissues. Part I: Dynamic behavior". *Journal of Materials Science: Materials in Medicine,* **13**(10), pp. 933–938.

[85] Waldman, S., Sacks, M., and Lee, J., 2002. "Boundary conditions during biaxial testing of planar connective tissues. Part II: Fiber orientation". *Journal of Materials Science Letters,* **21**(15), pp. 1215–1221.

[86] Sun, W., Sacks, M. S., and Scott, M. J., 2005. "Effects of boundary conditions on the estimation of the planar biaxial mechanical properties of soft tissues". *Journal of Biomechanical Engineering,* **127**(4), pp. 709–715.

[87] Eilaghi, A., Flanagan, J. G., Brodland, G. W., and Ethier, C. R., 2009. "Strain uniformity in biaxial specimens is highly sensitive to attachment details". *Journal of Biomechanical Engineering,* **131**(9), p. 091003.

[88] Jacobs, N. T., Cortes, D. H., Vresilovic, E. J., and Elliott, D. M., 2013. "Biaxial tension of fibrous tissue: using finite element methods to address experimental challenges arising from boundary conditions and anisotropy". *Journal of Biomechanical*

Engineering, **135**(2), p. 021004.

[89] MacLennan, A. H., Taylor, A. W., Wilson, D. H., and Wilson, D., 2000. "The prevalence of pelvic floor disorders and their relationship to gender, age, parity and mode of delivery". *BJOG: An International Journal of Obstetrics & Gynaecology,* **107**(12), pp. 1460–1470.

[90] Wu, J. M., Kawasaki, A., Hundley, A. F., Dieter, A. A., Myers, E. R., and Sung, V. W., 2011. "Predicting the number of women who will undergo incontinence and prolapse surgery, 2010 to 2050". *American Journal of Obstetrics and Gynecology,* **205**(3), pp. 230–e1.

[91] Dwyer, P. L., and Fatton, B., 2008. "Bilateral extraperitoneal uterosacral suspension: A new approach to correct posthysterectomy vaginal vault prolapse". *International Urogynecology Journal,* **19**(2), pp. 283–292.

[92] Ramanah, R., Parratte, B., Arbez-Gindre, F., Maillet, R., and Riethmuller, D., 2008. "The uterosacral complex: ligament or neurovascular pathway? Anatomical and histological study of fetuses and adults". *International Urogynecology Journal,* **19**(11), pp. 1565–1570.

[93] Chen, L., Ramanah, R., Hsu, Y., Ashton-Miller, J. A., and DeLancey, J. O., 2013. "Cardinal and deep uterosacral ligament lines of action: MRI based 3D technique development and preliminary findings in normal women". *International Urogynecology Journal,* **24**(1), pp. 37–45.

[94] Latzko, W., and Shiffmann, J., 1919. "Zur klinik and anatomie der erweiterten abdominallen operation des gebarmutter-krebses". *Zentralb Gynaekol,* **34**, pp. 715–9.

[95] Okabayashi, H., 1921. "Radical abdominal hysterectomy for cancer of the cervix uteri". *Surgery, Gynecology & Obstetrics,* **33**(4), pp. 335–41.

[96] Yabuki, Y., Asamoto, A., Hoshiba, T., Nishimoto, H., and Kitamura, S., 1991. "Dissection of the cardinal ligament in radical hysterectomy for cervical cancer with emphasis on the lateral ligament". *American Journal of Obstetrics and Gynecology,* **164**(1), pp. 7–14.

[97] Yabuki, Y., Asamoto, A., Hoshiba, T., Nishimoto, H., and Satou, N., 1996. "A new proposal for radical hysterectomy". *Gynecologic Oncology,* **62**(3), pp. 370–378.

[98] Yabuki, Y., Sasaki, H., Hatakeyama, N., and Murakami, G., 2005. "Discrepancies between classic anatomy and modern gynecologic surgery on pelvic connective tissue structure: Harmonization of those concepts by collaborative cadaver dissection". *American Journal of Obstetrics and Gynecology,* **193**(1), pp. 7–15.

[99] Luo, J., Betschart, C., Chen, L., Ashton-Miller, J. A., and DeLancey, J. O., 2014. "Using stress MRI to analyze the 3D changes in apical ligament geometry from rest to maximal valsalva: A pilot study". *International Urogynecology Journal,* **25**(2), pp. 197–203.

[100] Turner, S., 1973. "Creep in glassy polymers". In *The Physics of Glassy Polymers*. Springer, pp. 223–278.

[101] Provenzano, P. P., Heisey, D., Hayashi, K., Lakes, R., and Vanderby, R., 2002. "Subfailure damage in ligament: A structural and cellular evaluation". *Journal of Applied Physiology,* **92**(1), pp. 362–371.

[102] Thornton, G. M., Shrive, N. G., and Frank, C. B., 2001. "Altering ligament water content affects ligament pre-stress and creep behavior". *Journal of Orthopaedic Research,* **19**(5), pp. 845–851.

[103] Thornton, G., Oliynyk, A., Frank, C., and Shrive, N., 1997. "Ligament creep cannot be predicted from stress relaxation at low stress: A biomechanical study of the rabbit medial collateral ligament". *Journal of Orthopaedic Research,* **15**(5), pp. 652–656.

[104] Thornton, G. M., Shrive, N. G., and Frank, C. B., 2002. "Ligament creep recruits fibres at low stresses and can lead to modulus-reducing fibre damage at higher creep stresses: A study in rabbit medial collateral ligament model". *Journal of Orthopaedic Research,* **20**(5), pp. 967–974.

[105] Vu, D., Haylen, B. T., Tse, K., and Farnsworth, A., 2010. "Surgical anatomy of the uterosacral ligament". *International Urogynecology Journal,* **21**(9), pp. 1123–1128.

[106] Rezakhaniha, R., Agianniotis, A., Schrauwen, J. T. C., Griffa, A., Sage, D., Bouten, C., Van de Vosse, F., Unser, M., and Stergiopulos, N., 2012. "Experimental investigation of collagen waviness and orientation in the arterial adventitia using confocal laser scanning microscopy". *Biomechanics and Modeling in Mechanobiology,* **11**(3-4), pp. 461–473.